UNIVERSITAT POLITÈCNICA
DE CATALUNYA
BARCELONATECH

Programmable DSP-enabled multi-adaptive optical transceivers based on OFDM technology for Software Defined Networks

Ph.D. Dissertation

Author

Laura Martín González

Advisors

Dr. Michela Svaluto Moreolo

Dr. Josep Maria Fàbrega

Tutor

Prof. Gabriel Junyent Giralt

Barcelona, March 2019

Abstract

The dynamic behavior of the traffic demand, due to the advent of technologies such as cloud services or Internet of Things, is increasing. In fact, heterogeneous connections with different characteristics such as bandwidth or bit rate are expected that coexist in the optical networks. An evolution of the optical networks is crucial to face the new claims. In this respect, Elastic Optical Networks (EONs) emerge as a cost-effective, flexible and dynamic solution. The main idea is the efficient utilization of the optical spectrum by combining flexible transceivers, flexi-grid and flexible optical switching. Including the principles of Software Defined Network (SDN) paradigm further flexibility and adaptability can be achieved. The adoption of the SDN architecture involves the separation of the control plane and data plane enabling the programmability of the network in a dynamic way.

The Sliceable Bandwidth Variable Transceiver (S-BVT), as a key element in EONs, provides flexibility and adaptability to the optical networks. It is able to dynamically tune the optical bandwidth or bit rate changing parameters such as the modulation format, bandwidth or (Forward Error Correction) FEC coding, among others, to find a trade-off between transmission reach and spectral efficiency, serving multiples destinations. The combination of programmable Digital Signal Processing (DSP) modules with advanced transmission techniques based on Orthogonal Frequency Division Multiplexing (OFDM) technology using Direct Detection (DD) or COherent (CO) detection are proposed to be implemented at the S-BVT, making it suitable for elastic optical metro/regional networks.

Furthermore, the envisioned migration from fixed-grid to flexi-grid, in order to exploit the fine granularity of 12.5 GHz, can benefit from the use of S-BVTs since they are able to generate or receive multiple channels and slicing the aggregated flow into multiples flows with different capacities and destinations. In this respect, we propose the use of S-BVTs based on multi-band OFDM signals combined in the electrical domain in order to limit the optoelectronic resources and relax the Digital to Analog Converter (DAC) or Analog to Digital Converter (ADC) requirements. In particular, we focus on the the-

oretical model of an advanced transmission technique based on OFDM technology with DD. Then we evaluate the system for a realistic optical metro network. In the context of flexi-grid optical metro/regional networks, as well as the sliceability of the channels, the reduction of channel width for low bit rate connections can be envisioned. It involves that the signal traverses several nodes with the corresponding filtering elements, causing a substantially decrease and distortion of the signal bandwidth. This phenomenon known as filter narrowing effect has been also studied in this thesis, by simulations and experimentally for an adaptive cost-effective OFDM system using DD and for a standard OOK system. DD-OFDM system has turned out to be a good candidate providing the increase of flexibility and robustness against transmission impairments without dispersion compensation.

Apart from adaptive, flexible and programmable transceivers, metro optical networks have to be equipped with flexible optical switching systems at the node level. In this respect, we propose the adoption of adaptive S-BVTs based on advanced transmission techniques using DD with Discrete MultiTone (DMT) modulation and adaptive capabilities in combination with Semiconductor Optical Amplifier (SOA)-based switching nodes. SOAs can be conveniently used for optical switching in metro networks because of their low cost or low power consumption, among others relevant characteristics. The system has been experimentally analyzed with and without considering filtering elements. Thanks to the combination of adaptive DMT modulation and SOA-based switching nodes, impairments due to the fiber links and the filtering elements can be compensated. Finally, to enhance the transmission distance and data rate, we propose the combination of multidimensional constellations implemented at the DSP modules of the S-BVT with CO detection and OFDM technology. In fact, CO-OFDM systems have a 4D signal space (two quadratures and two polarizations), which can be used with multidimensional constellations than can be more efficient than conventional ones, such as Binary Phase-Shift Keying (BPSK) or Quadrature Phase-Shift Keying (QPSK). Thus, the deployed infrastructure is more efficiently exploited since the quadrature and polarization dimensions are used to transmit the signal. Additionally, CO-OFDM systems can recover the amplitude and the phase of the signal at the receiver, mitigating the fiber effects and therefore, increasing the transmission distance. CO-OFDM system using Dual Polarization Quadrature Phase Shift Keying (DPQPSK) constellation format and transmitting the signal over the time in the optical domain have been demonstrated to be a promising solution.

Resumen

El comportamiento dinámico de la demanda de tráfico, debido a la llegada de tecnologías como los servicios en la nube o el Internet of Things (IoT), está aumentando. De hecho, se espera que coexistan en las redes ópticas conexiones heterogéneas con características diferentes, tales como ancho de banda o tasa de bits. Para hacer frente a estas demandas es crucial una evolución de las redes ópticas. En este sentido, las Elastic Optical Networks (EONs) emergen como una solución rentable, flexible y dinámica. La idea principal se basa en la utilización eficiente del espectro óptico mediante la combinación de trasceptores flexibles, redes flexibles y conmutación óptica flexible. Una mayor flexibilidad y adaptabilidad se puede conseguir incluyendo los principios del paradigma conocido como Software Defined Network (SDN). La adopción de la arquitectura SDN implica la separación del plano de control y de datos, permitiendo la programabilidad dinámica de la red.

Un elemento clave en las EONs es el Sliceable Bandwidth Variable Transceiver (S-BVT), ya que prové de flexibilidad y adaptabilidad a las redes ópticas. El S-BVT es capaz de cambiar el ancho de banda o la tasa de bits modificando parámetros como el formato de modulación, el ancho de banda o la codificación de Forward Error Correction (FEC), entre otros, para encontrar un equilibrio entre el alcance de la transmisión y la eficiencia espectral, sirviendo múltiples destinos. La combinación de módulos programables de Digital Signal Processing (DSP) con técnicas de transmisión avanzadas, basadas en la tecnología Orthogonal Frequency Division Multiplexing (OFDM) con detección directa o detección coherent, se han propuesto para ser implementadas en el S-BVT, haciéndolo adecuado para su uso en redes ópticas elásticas metropolitanas y regionales.

Además, la migración prevista de las redes fijas a las redes flexibles, con el fin de explotar la granualidad de 12.5 GHz, puede beneficiarse del uso de S-BVTs ya que son capaces de generar y recibir múliples canales y dividir el flujo agregado en múltiples flujos con diferentes capacidades y destinos. A este respecto, proponemos el uso de S-BVTs basados en señales OFDM multi banda combinadas en el dominio eléctrico con el fin de limitar los recursos optoelectrónicos y relajar los requerimientos de los convertidores

digitales analógicos y analógicos digitales. En particular, nos centramos en el modelo teórico de una técnica de transmisión avanzada basada en la tecnología OFDM con detección directa. A continuación, evaluamos el sistema para una red metropolitana óptica realista. En el contexto de redes metropolitanas y regionales flexibles, además de la capacidad de división de los canales, se puede prever una posible reducción del ancho de canal para las conexiones de baja tasa de bits. Esto implica que la señal atraviese varios nodos con los correspondientes elementos filtrantes causando un substancial decremento y distorsión del ancho de banda de la señal. Este fenómeno conocido como el efecto de estrechamiento de filtrado ha sido también estudiado en esta tesis, mediante simulaciones y de manera experimental para un sistema OFDM rentable y adaptativo usando detección directa y un sistema estándar On-Off Keying (OOK). El sistema OFDM de detección directa ha resultado ser un buen candidato para aumentar la flexibilidad y la robustez frente a las deficiencias de transmisión sin necesidad de compensar la dispersión.

Aparte de los transceptores adaptables, flexibles y programables, las redes ópticas metropolitanas deben estar equipadas con sistemas de conmutación óptica flexible a nivel de nodo. En este sentido, proponemos la adopción de S-BVTs adaptativos basados en técnicas de transmisión avanzadas usando detección directa con modulación Discrete MultiTone (DMT) y capacidades adaptativas, adoptando nodos de conmutación basados en Semiconductor Optical Amplifier (SOA). Los SOAs pueden ser utilizados para la conmutación óptica en redes metropolitanas debido a su bajo coste o bajo consumo de energía, entre otras características relevantes. El sistema ha sido analizado experimentalmente considerando y sin considerar la presencia de elementos filtrantes. Gracias a la combinación de la modulación DMT adaptativa y los nodos de conmutación basados en SOA, las degradaciones debidas a los enlaces de fibra y a los elementos filtrantes se pueden compensar. Finalmente, para mejorar la distancia de transmisión y la tasa de datos, proponemos la combinación de constelaciones multidimensionales implementadas en los módulos DSP del S-BVT utilizando detectión coherente y la technología OFDM. De hecho, los sistemas OFDM coherentes tienen un espacio de señal 4D (dos cuadraturas y dos polarizaciones), que puede ser utilizado con constelaciones multidimensionales, pudiendo éstas ser mas eficientes que las convencionales Binary Phase-Shift Keying (BPSK) o Quadrature Phase-Shift Keying (QPSK). De este modo, la infraestructura desplegada se explota de manera más eficiente, ya que tanto la dimensión de cuadratura como de polarización se utilizan para transmitir la señal. Además, los sistemas OFDM coherentes pueden recuperar la amplitud y la fase de la señal en el receptor, mitigando los efectos de la fibra aumentando, de esta forma, la distancia de transmisión. El sistema OFDM coherente que utiliza el formato de constelación Dual Polarization Quadrature Phase Shift Keying (DPQPSK) y que transmite la señal a lo largo del tiempo ha demostrado ser una solución prometedora.

Resum

El comportament dinàmic de la demanda de trànsit, a causa de l'arribada de tecnologies, com poden ser els serveis al núvol o l'Internet of Things (IoT), està creixent. De fet, s'espera que coexisteixin a les xarxes òptiques connexions heterogènies amb característiques diferents, tal com l'ample de banda o la taxa de bits. Per a fer front a aquestes demandes és crucial una revolució de les xarxes òptiques. En aquest sentit, les Elastic Optical Networks (EONs) emergeixen com una solució rendible, flexible i dinàmica. La idea principal es basa en la utilització eficient de l'espectre òptic mitjançant la combinació de transceptors flexibles, xarxes flexibles i commutació òptica flexible. Una major flexibilitat i adaptabilitat es pot aconseguir incloent els principis del paradigma conegut com a Software Defined Networks (SDN). L'adopció de l'arquitectura SDN implica la separació del plànol de control i de dades permetent la programabilitat de la xarxa d'una forma dinàmica.

Un element clau en les EONs és l' Sliceable Bandwith Variable Transceiver (S-BVT), ja que aporta flexibilitat i adaptabilitat a les xarxes òptiques. L' S-BVT és capaç de canviar l'ample de banda o la taxa de bits modificant paràmetres com el format de modulació, l'ample de banda o la codificació del Forward Error Correction (FEC), entre altres, per a trobar un equilibri entre l'aistència assolida i l'eficiència espectral, servint múltiples destinacions. La combinació de mòduls de Digital Signal Processing (DSP) amb tècniques de transmissió avançades basades en la tecnologia Orthogonal Frequency Division Multiplexing (OFDM) i detecció directa o detecció coherent s'han proposat per a ser implementades en l'S-BVT, fent-lo adient per a les xarxes òptiques elàstiques metropolitanes i regionals.

A més, la migració prevista des de les xarxes fixes a les xarxes flexibles, amb el fi d'explotar la granualitat de 12.5GHz, pot beneficiar-se de l'ús d'S-BVTs ja que són capaços de generar i rebre múltiples canals i dividir el flux agregat en múltiples fluxos amb diferents capacitats i destinacions. Per aquest motiu, proposem l'ús d'S-BVTs basats en senyals OFDM multi banda combinats en el domini elèctric amb el fi de limitar els recursos optoelectrònics i relaxar els requeriments dels convertidors digitals analògics

i analògics digitals. Particularment, ens centrem en el model teòric d'una tècnica de transmissió avançada basada en la tecnologia OFDM amb detecció directa. A continuació, avaluem el sistema per a una xarxa metropolitana òptica realista. En el context de xarxes metropolitanes i regionals flexibles, a més de la propietat de divisió dels canals, es pot preveure una possible reducció de l'ample de canal per a les connexions de baixa taxa de bits. Això implica que el senyal travessi diversos nodes amb els corresponents elements filtrants causant un substancial decrement i distorsió de l'ample de banda del senyal. Aquest fenomen conegut com l'efecte d'estretament de filtrat ha sigut també estudiat en aquesta tesi, mitjançant simulacions i de manera experimental en el cas d'un sistema OFDM rendible i adaptatiu utilitzant detecció directa i un sistema estàndard On-Off Keying (OOK). El sistema OFDM de detecció directa ha resultat ser un bon candidat per augmentar la flexibilitat i la robustesa front a les deficiències de transmissió sense necessitat de compensar la dispersió.

A part dels transceptors adaptables, flexibles i programables, les xarxes òptiques metropolitanes han d'estar equipades amb sistemes de commutació òptica flexible a nivell de node. En aquest sentit, proposem l'adopció d'un S-BVT adaptatiu basat en tècniques de transmissió avançades i utilitzant detecció directa amb modulació Discrete MultiTone (DMT) i capacitats adaptatives, adoptant nodes de comunicació basats en Semi-conductor Optical Amplifier (SOA). Els SOAs poden ser utilitzats per la commutació òptica en xarxes metropolitanes degut al seu baix cost o baix consum d'energia, entre altres característiques rellevants. El sistema ha sigut analitzat experimentalment considerant i sense considerar la presència d'elements filtrants. Gràcies a la combinació de la modulació DMT adaptativa i dels nodes de commutació basats en SOA, les degradacions degudes als enllaços de fibra i als elements filtrants es poden compensar. Finalment, per a millorar la distància de transmissió i la taxa de dades, proposem la combinació de constel·lacions multidimensionals implementades als mòduls DSP de l'S-BVT utilitzant detecció coherent i la tecnologia OFDM. De fet, els sistemes coeherents OFDM tenen un espai de senyal 4D (dues quadratures i dues polaritzacions), que pot ser utilitzat amb constel·lacions multidimensionals, arribant a ser més eficients que les modulacions convencionals Binary Phase-Shift Keying (BPSK) o Quadrature Phase-Shift Keying (QPSK). D'aquesta manera, la infraestructura desplegada s'explota de forma més eficient, ja que tant la dimensió de quadratura com de polarització s'utilitzen per transmetre el senyal. A més, els sistemes coherents basats en OFDM poden recuperar l'amplitud i la fase del senyal en el receptor, mitigant els efectes de la fibra i d'aquesta forma augmentant la distància de transmissió. El sistema OFDM coherent que utilitza el format de constel·lació Dual Polarization Quadrature Phase Shift Keying (DPQPSK) i que transmet el senyal al llarg del temps ha demostrat ser una solució prometedora.

Acknowledgements

First of all, I would like to express my gratitude to my advisors Josep M. Fàbrega and Michela Svaluto Moreolo and my tutor Gabriel Junyent for giving me the opportunity to work at CTTC and develop my thesis at UPC. I would particularly like to thank my advisors Josep M. Fàbrega and Michela Svaluto Moreolo for their guidance, comments and suggestions to the successful development of this thesis. In addition, I would like to extend my gratitude to Laia Nadal for her support and advice.

My sincere thanks also to Nicola Calabretta, Chigo Okonkwo, Sjoerd van der Heide, X. (Xuwei) Xue, John van Weerdenburg, who gave me the opportunity to join their team during my research stay at TU/e (Netherlands).

Further, I would like to extend my gratitude to Dr. Albert Rafel, Prof. Alberto Gatto for reviewing this thesis. Also, I would like to thank Dr. Albert Rafel, Prof. Alberto Gatto and Prof. Salvatore Spadaro for agreeing to serve in this thesis' committee. My gratitude also extends to Dr. Ana González and Jaume Comellas, for fulfilling the role of substitute members of the committee.

I am deeply grateful to all the people from CTTC both at a professional and a personal level. In particular, I would like to express my sincere gratitude to my friends and collegues Laia Nadal, Maria Gregori, Jessica Moysen, Miguel Ángel Vázquez, Miquel Calvo, Luis Carlos Buelga and Jesús Soriano.

I would also like to thank the rest of my friends who have always been by my side during this period. I thank you very much for having given me all the support, collaboration, encouragement and especially affection and friendship.

Por último, pero no menos importante, me gustaría agradecer a mi familia por todo su apoyo incondicional en el desarollo de la tesis y en mi vida en general.

Laura Martín González, Barcelona, March 2019

ADC	Analog-to-Digital Converter
ASE	Amplified Spontaneous Emission
AWG	Arrayed Waveguide Grating
AWGN	Additive white Gaussian Noise
B2B	Back-to-Back
BER	Bit Error Rate
BPSK	Binary Phase-Shift Keying
BRAS	Broadband Remote Access Server
CapEx	CAPital EXpenditure
CD	Chromatic Dispersion
CO	Coherent
CP	Cyclic Prefix
CW	Continuous Wave
CWDM	Coarse Wavelength Division Multiplexing
DAC	Digital-to-Analog Converter
DC	Direct Current
DD	Direct Detection
DD-MZM	Dual Drive Mach-Zhender Modulator
DEMAP	Demapping
DHT	Discrete Hartley Transform
DMT	Discrete MultiTone
DP	Dual Polarization
DRS	Dual-Ring Structure
DSB	Double Side Band
DSP	Digital Signal Processing
DWDM	Dense Wavelength Division Multiplexing
EDFA	Erbium Doped Fiber Amplifier
EON	Elastic Optical Network
ETDM	Electrical Time Division Multiplexing
FP	Fabry-Perot
FDM	Frequency Division Multiplexing
FEC	Forward Error Correction
FFT	Fast Fourier Transform

FFT2D	Fast Fourier Transform 2 Dimensions
FMF	Few Mode Fibers
H	Horizontal
HD	Hard-Decision
HS	Hermitian symmetry
ICI	Inter-Carrier Interference
IF	Intermediate Frequency
IFFT	Inverse Fast Fourier Transform
IFFT2D	Inverse Fast Fourier Transform 2 Dimensions
IM	Intensity Modulation
I/Q	Inphase/Quadrature
ISI	Inter-Symbol Interference
ITU	International Telecommunication Union
LCoS	Liquid Cristal on Silicon
LO	Local Oscilator
LPF	Low Pass Filter
MA	Margin Adaptive
MCF	Multi-Core Fiber
MCM	MultiCarrier Modulation
MEMS	Micro-Electro-Mechanical Systems
MIMO	Multiple-Input Multiple-Output
M-PSK	M-Phase Shift Keying
M-QAM	M-ary Quadrature Amplitude Modulation
MTU	MultiTenant Units
MZM	Mach-Zehnder Modulator
NWDM	Nyquist Wavelength-Division Multiplexing
NRZ	Non Return Zero
OAD	Optical Add Drop
OFDM	Orthogonal Frequency Division Multiplexing
OM	Optical Monitoring
OOK	On-Off Keying
OSA	Optical Spectral Analyzer
OSNR	Optical Signal to Noise Rate

OTDM	Optical Time Division Multiplexing
PAM	Pulse Amplitude-Modulation
PAPR	Peak-to-Average Power Ratio
PBS	Polarization Beam Splitter
PC	Polarization Controller
PD	Polarization Diversity
PDI	Propagation-Direction Interleaving
P/S	Parallel-to-Serial
PS	Polarization Switched
QPSK	Quadrature Phase Shift Keying
RA	Rate Adaptive
RF	Radio Frequency
ROADM	Reconfigurable Optical Add/Drop Multiplexer
Rx	Receiver
S-BVT	Sliceable-Bandwidth Variable transceiver
SCM	SubCarrier Multiplexing
SD	Soft-Decision
SDM	Spatial Division Multiplexing
SDN	Software Defined Network
SE	Spectral Efficiency
SG	Spectral Gap
SNR	Signal-to-Noise Ratio
SOA	Semiconductor Optical Amplifier
SOP	State Of Polarization
SSB	Single Side Band
SSMF	Standard Single Mode Fiber
TD	Time Diversity
TDM	Time division multiplexing
TFP	Time-Frequency Packing
TLS	Tunable Laser Source
TRX	Transceiver
TS	Training Symbols
TSW	Total Size Window

Tx	Transmitter
TW	Traveling Wavelength
V	Vertical
VOA	Variable Optical Attenuator
VSB	Vestigial Side Band
WDM	Wavelength-Division Multiplexing
WS	Window Size
WSS	Wavelength Selective Switches
ZP	Zero Padding

List of publications

List of publications associated with this thesis, divided into journals and international conferences in inverse chronological order.

Journals

- **L. Martín,** S. van der Heide, X. (Xuwei) Xue, J. van Weerdenburg, N. Calabretta, C. Okonkwo, J. M. Fàbrega, M. S. Moreolo, "Programmable Adaptive BVT for Future Optical Metro Networks adopting SOA-based Switching Nodes", Photonics 2018, 5(3), 24. (Special Issue: Lightwave Communications and Optical Networks).

- **L. Martín,** J. M. Fàbrega and M. S. Moreolo, "Experimental Assessment of Filter Narrowing Effect for Low Bandwidth Connections in EON", in IEEE Photonics Technology Letters, vol. 29, no. 23, pp. 2027-2030, Dec.1, 1 2017.

- J. M. Fàbrega, M. S. Moreolo, **L. Martín**, A. Chiadò Piat, E. Riccardi, D. Roccato, N. Sambo, F. Cugini, L. PotFì, S. Yan, E. Hugues-Salas, D. Simeonidou, M. Gunkel, R. Palmer, S. Fedderwitz, D. Rafique, T. Rahman, Huug de Waardt, A. Napoli , "On the Filter Narrowing Issues in Elastic Optical Networks," *Journal of Optical Communications and Networking*, 8(7):A23–A33, 2016.

- M. S. Moreolo, J. M. Fàbrega, **L. Martín**, K. Christodoulopoulos, E. Varvarigos, J. P. Fernández-Palacios ,, "Flexgrid Technologies Enabling BRAS Centralization in MANs ," *Journal of Optical Communications and Networking*, 8(7):A64–A75, 2016.

International conferences

- M. S. Moreolo, J. M. Fàbrega, L. Nadal and **L. Martín**, "Optical technology options for programmable S-BVT." *Proceedings of Internation Conference on Transparent Optical Networks (ICTON)*, 1-5 July 2018 (Bucarest).

- **L. Martín**, J. M. Fàbrega, L. Nadal, and M. S. Moreolo, "Performance analysis of CO-OFDM schemes based on multidimensional constellations for long-haul transmission." *Proceedings of Internation Conference on Transparent Optical Networks (ICTON)*, Tu.D1.5., July 2017 (Girona). **Best Ph.D. student paper in the category of networking.**

- J. M. Fàbrega, **L. Martín** and M. Svaluto Moreolo,"Data Plane Alternatives based on Sliceable Transceivers for Optical Aggregation Networks." *Proceedings of Internation Conference on Transparent Optical Networks (ICTON)*, We.A1.4, 5-9 July 2015 (Budapest).

Contents

List of Figures

List of Tables

Chapter 1

Introduction

1.1 Motivation

The bandwidth demand is increasing and becoming more dynamic due to the advent of technologies such as Internet of Things and/or cloud-based services. In fact, the increase of Internet traffic is estimated to be threefold in the next 5 years and it is expected to reach an annual global IP traffic of 3.3 ZB per year by 2021 according to CISCO forecast [1].

The majority of current deployed Dense Wavelength Division Multiplexing (DWDM) techology is able to transmit 10 Gb/s per wavelength channel. Considering 80 wavelenghts as the maximum link limit, a total of 800 Gb/s can be transmitted. However, 800 Gb/s are insufficient to cope with the actual traffic demand. Thus, efforts have been carried on to develop transceivers that support 40 Gb/s, 100 Gb/s and beyond per channel [2]. Furthermore, it is expected that heterogeneous connections through the network, with different bandwidth demands, can coexist. A crucial aspect to be considered to cope with these demands is an efficient use of the optical spectrum. Thus, an evolution towards more flexible and dynamic solutions are expected. In this context, Elastic Optical Network (EON) paradigm emerges [3,4]. The key enablers to be considered in EONs are flexible transceivers, flexi-grid and switching technologies.

Flexible transceivers allow to adjust the bandwidth, modulation format or bit rate increasing the capacity of the network. These kind of transceivers are known as Bandwidth Variable Transceiver (BVT) [5]. Further flexibility is obtained if the sliceability concept is introduced. Sliceable (S) BVT involves the splitting of several optical flows to different destinations, each of them adjusted according to their specific characteristics (e.g bandwidth or modulation format, etc) [3,4]. The S-BVTs can be remotely programmed, adapted and reconfigured following the Software Defined Network (SDN) paradigm, enabling further flexibility and adaptability for the effective use of the resources [3, 6].

In order to exploit the flexibility at the BVTs, MultiCarrier Modulation (MCM)

and particularly Orthogonal Frequency Division Multiplexing (OFDM) is gaining special attention, since it allows the manipulation of individual subcarriers [4, 7–9]. Adaptive Digital Signal Processing (DSP) based on OFDM is considered for the implementation of programmable multi-adaptive optical transceivers for metro/regional EONs. For a cost-effective solution, OFDM based on Direct Detection (DD) is usually considered. However, COherent (CO) OFDM is also a suitable candidate due to its robustness to transmission impairments but, in contrast, the system complexity and cost increase.

In addition to flexible transceivers, an improvement of the overall optical spectrum efficiency is needed. In this respect, an evolution from the fixed grid to flexible grid is envisioned. International Telecommunication Union (ITU) has standarized a finer grid with frequency slots of 12.5 GHz, avoiding the restrictions of typical 50 GHz or 100 GHz [10]. Thus, the channels can be adjusted to the specific grid according to the bandwidth requirements. As an example, superchannels containing multiple subchannels can be performed, thanks to the combination of different frequency slots. A key element of flexi-grid is the Wavelength Selective Switch (WSS) based on Liquid-Crystal-On-Silicon (LCoS) technology [11]. It provides functionalities such as routing, switching and variable passband filtering, being this latter point of great importance in the context of flexi-grid paradigm. WSS are widely used components of Reconfigurable Optical Add and Drop Multiplexer (ROADM) architecture. ROADMs are optical network devices that allow to dinamically add or drop different wavelengths at the network nodes [12]. Novel ROADMs use WSS with $\leq$ 12.5 GHz granularity [3]. Thus, the bandwidth allocation within the networks is optimized. However, the evolution towards flexi-grid envisions a cascade of filtering elements, which can involve the degradation of the optical channel, entailing spectral distortions and an Optical Signal to Noise Rate (OSNR) penalty [13].

In this thesis, we focus on the implementation and design of programmable multi-adaptive optical transceivers following the SDN paradigm. Particularly, we focus our work on optical transceivers based on OFDM technology for both Direct Detection (DD) and COherent (CO) detection. As it is well-known, OFDM is a multiplexing technique that uses the frequency domain to transmit the information. Particularly, in this case, the information is transmited over orthogonal subcarriers. Multiple multiplexing and modulation techniques based on different dimensions can be also exploited at the transceivers, in order to increase the adaptability and enhance the capacity in EONs. As an example, adaptive modulation algorithms such as bit and power loading can be implemented at the transceivers, to adapt the data rate to the traffic demand. Hence, different modulation formats are used, based on the channel profile previously obtained, increasing the spectral efficiency and overcoming fiber impairments such as Chromatic Dispersion (CD) [8,14]. Multiplexing techniques based on different dimensions as time, polarization or space can be also exploited. In the case of polarization multiplexing, the signal is transmitted over two orthogonal polarization doubling the capacity of the fiber. Using

the time domain, different signals can be transmitted over different time slots through the same frequency. However, despite the development of these advanced techniques, conventional single mode fiber is reaching the nonlinear Shannon limit [14, 15]. Hence, Space Division Multiplexing (SDM) based on few-mode or multi-core fibers are reaching great relevance for the propagation of the optical signals. In future optical networks, SDM could then be envisioned as a solution to the saturation of Standar Single Mode Fibers (SSMF) [14].

1.2 Objectives

This section presents the general and specific objectives addressed in this thesis.

As mentioned above, the dynamic behavior of the traffic requires the flexibility and adaptability of the optical networks. In this thesis, we mainly focus on the metro/regional network segment, which is considered one of the most challenging. In fact, metro networks has to be able to support heterogeneous traffic, addressing the anticipated capacity increase and its specific characteristics, at low cost. Thus, flexible and cost-effective metro networks technologies must be deployed. The main goal of this thesis is the implementation of flexible and multi-adaptive transceivers capable to face the metro networks requirements.

As specific objectives we can point out the following:

- Study of the SDN paradigm combined with EONs supporting the innovative concepts of S-BVT, flexi-grid and flexible switching for flexible programmability of the metro network elements.

- Study of the OFDM technology as advanced transmission technology suitable to cope with the specific requirements of metro/regional networks. Identification of the strong and weak points of DD and CO detection OFDM systems.

- Analysis of the applicability of different multi-adaptive transceivers to be implemented, in order to exploit more efficiently the EONs' capabilities, taking into account different multiplexing techniques, based on different physical dimensions, advanced and adaptive modulation formats and the combination of them.

- Assessment of different options of multi-adaptive optical transceivers using advanced transmission techniques based on OFDM technology. Selection of the most appropriate multi-adaptive technique and OFDM system according to the specific envisioned scenario.

- Implementation of cost-effective OFDM systems based on DD as suitable transmission technique to be implemented in flex-grid scenario for low bit rate connections.

- Study of the filter narrowing effect as a critical point to be overcome in the context of flexi-grid metro networks. Implementation and design of flexible transceivers with adaptive capabilities, to adapt the transmission according to the impairments resulting from the filter narrowing effect, and combined with cost-effective OFDM systems using DD, in order to meet the metro networks requirements.

- Assessment of the maximum attainable distance with and without considering filtering elements in a metro optical network, using advanced transmission techniques based on DMT modulation with DD, with adaptive capabilities, combined with Semiconductor Optical Amplifier (SOA)-based switching nodes.

- Implementation of advanced transmission systems based on CO detection to enhance impairments tolerance and the attainable reach with respect to DD-OFDM systems. Study and design of multi-adaptive techniques based on multidimensional constellation formats, as the most appropriated technique to increase the data rate and transmission distance, at the expense of increasing the system complexity.

1.3 Thesis overview

In this section, we present the topic of each chapter and outline the contributions that are included in the present dissertation.

In chapter 2, the state of the art is introduced. Firstly, a brief historical perspective of optical communications is presented. After that, an overview of the SDN paradigm and EON concept is shown. Then, OFDM technology as a key element in EONs an its application in optical communications is studied. Different OFDM schemes based on DD and CO detection are compared in terms of cost-efficiency and performance. Finally, several multi-adaptive transceivers based on different physical dimensions are discussed.

In chapter 3, a multi-band system with DD-OFDM technology is assessed. A theoretical model of the multi-band system is presented and then the system is simulated for a realistic regional network. Finally, the performance analysis is provided. The contribution of this chapter are published in the following paper:

- M. S. Moreolo, J. M. Fábrega, **L. Martín**, K. Christodoulopoulos, E. Varvarigos, J. P. Fernández-Palacios, "Flexgrid Technologies Enabling BRAS Centralization in MANs ," *Journal of Optical Communications and Networking*, 8(7):A64–A75, 2016.

In chapter 4, the problematic of filter narrowing effect is presented. A DD-OFDM system with adaptive capabilities and legacy On Off Keying (OOK) approach has been assessed by simulations and experimentally in the laboratory. Performance analysis is provided for comparison. The contributions corresponding to this chapter are listed below:

- **L. Martín,** J. M. Fàbrega and M. S. Moreolo, "Experimental Assessment of Filter Narrowing Effect for Low Bandwidth Connections in EON", in IEEE Photonics Technology Letters, vol. 29, no. 23, pp. 2027-2030, Dec.1, 1 2017.

- J. M. Fàbrega, M. S. Moreolo, **L. Martín**, A. Chiadò Piat, E. Riccardi, D. Roccato, N. Sambo, F. Cugini, L. Potì, S. Yan, E. Hugues-Salas, D. Simeonidou, M. Gunkel, R. Palmer, S. Fedderwitz, D. Rafique, T. Rahman, Huug de Waardt, A. Napoli , "On the Filter Narrowing Issues in Elastic Optical Networks," *Journal of Optical Communications and Networking*, 8(7):A23–A33, 2016.

- J. M. Fàbrega, **L. Martín** and M. S. Moreolo,"Data Plane Alternatives based on Sliceable Transceivers for Optical Aggregation Networks." *Proceedings of Internation Conference on Transparent Optical Networks (ICTON)*, We.A1.4, 5-9 July 2015 (Budapest).

In chapter 5, the study and experimental assessment of the adoption of adaptive transceivers based on Discrete MultiTone (DMT)/OFDM in optical networks, using SOA-based switching nodes, is presented. The contributions related to this chapter are published in the following papers.

- **L. Martín,** S. van der Heide, X. (Xuwei) Xue, J. van Weerdenburg, N. Calabretta, C. Okonkwo, J. M. Fàbrega, M. S. Moreolo, "Programmable Adaptive BVT for Future Optical Metro Networks adopting SOA-based Switching Nodes", Photonics 2018, 5(3), 24. (Special Issue: Lightwave Communications and Optical Networks).

- M. S. Moreolo, J. M. Fàbrega, L. Nadal and **L. Martín**, "Optical Technology Options for Programmable S-BVT." *Proceedings of Internation Conference on Transparent Optical Networks (ICTON)*, 1-5 July 2018 (Bucarest).

In chapter 6, transceivers using multidimensional constellation formats based on quadrature and polarization dimensions have been studied. Then, two transmission schemes using DPQPSK constellation formats considering CO-OFDM systems have been proposed. Finally, a performance analysis is provided by means of numerical simulations. The publication reporting results described in this chapter is listed here:

- **L. Martín**, J. M. Fàbrega, L. Nadal, and M. S. Moreolo, "Performance Analysis of CO-OFDM Schemes based on Multidimensional Constellations for Long-Haul Transmission." *Proceedings of International Conference on Transparent Optical Networks (ICTON)*, Tu.D1.5., July 2017 (Girona).

Finally, in Chapter 7, the final conclusions of the current thesis and future work are discussed.

Chapter 2

State of the art

2.1 Brief perspective of optical communications

Optical communications uses the light to carry the information and the optical fiber to transport the light. The first optical communication system proving service, was the optical telegraph in 1794 in Paris. In 1830, it was extended throughout Europe. Nonetheless, the advent of electrical telecommunications due to the telegraph and the invention of the telephone in 1876, dominated the communication systems. In fact, the development of telephone networks was increasing and enhancing. In 1940 transmission cables evolved from wire pairs to coaxial cables, reaching 3 MHz of bandwidth, improving significantly the capacity [16]. The most advanced coaxial system reached 274 Mb/s in 1948 but it needed repeater spacing of 1 km, increasing the cost of the system.

In 1960 the laser light started to be considered in several fields of knowledge including optical communications. Charles Kao was the poineer to combine glass optical fibers and lasers for optical communications [17]. In fact, in 2009 he won the nobel prize for the achievements concerning the transmission of light in fibers.

The main limitation of the transmission over optical fiber was the high losses (around 1000 dB/km) [18]. By 1970, Corning laboratory, an American company, demonstrated a optical fiber wire capable of transmistting 65.000 times more information than copper wire, reducing the fiber losses to below 20 dB/km in the region near 630 nm [16, 18]. In 1979, a Japanese scientific group achieved an attenuation of 0.2 dB/km in the infrared wavelength region near 1550 nm [18].

In addition to the optical fiber improvements, lasers also evolved. First lightwave systems used GaAs semiconductor lasers in the region near 830 nm [16]. Later, InGaAsP semiconductor lasers were developed to operate at 1550 nm wavelength region. In 1990, thanks to the combination of InGaAsP semiconductor lasers and Dispersion Shifted Fibers (DSFs), introduced in 1985, 10 Gb/s of bit rate were achieved [18].

Although first commercial systems were installed in 1980, it was with the advent

of Internet, in the 1990s decade when the new era of optical communications began to become evident. On one hand, the emergence of optical amplifiers in 1990s allowed to increase the repeater spacing. On the other hand, thanks to the Wavelength Division Multiplexing (WDM) technology, the capacity of the system grew doubling every 6 months.

As a result of these progess, optical communications systems became the communication system able to cope with the requirements of the traffic demand [19]. Indeed, the intense growth of internet in the 1990s, prompted to considerable progress in 2000s in advanced optical communication systems, making WDM more spectrally efficient and using coherent receivers or advanced modulation formats [18].

Despite all the advances in optical communication technologies, conventional single-mode fiber is limited by Shannon's nonlinear limit [14]. In order to enhance the capacity of the optical fiber and in response of the internet traffic demand, SDM technique is expected around 2020 [14, 18].

The evolution of the different technologies is illustrated in Figure 2.1 (source: [16]). A common figure of merit in optical communications is the BL product, where B is the bit rate and L is the repeater spacing [19]. Figure 2.1 (source: [16]) illustrates the representation of the BL product versus the year, for the different technologies. It is important to note that there is a significant increase of the BL product around 1980, when optical fibers started to be used for optical communications [19]. After 1980, there is an accelerated growth supported by the introduction of advanced technologies such as WDM.

In order to delay the capacity crunch, more efficient use of the deployed infrastructure need to be exploited, overcoming the new traffic demands. In this respect, flexible, dynamic and adaptive solutions would be an atractive alternative. In this context, significant research is directed towards EONs following the SDN paradigm [20,21]. SDN capabilities and EONs can be exploited thanks to next generation transceivers that enables flexible and adaptive modulation formats, bit rate or reach for a given traffic demand. These transceivers are known as BVT [5]. In the following section SDN paradigm, EONs and BVTs will be deeply addressed.

2.2 Envisioned EONs following the SDN paradigm

Optical communication networks are composed by a large number of routers or switches, among others devices, with complex protocols implemented on them. Networks operators have to cope with low-level configuration commands to implement complex hig-level policies, which involves the reduction of the flexibility and the hindering of the development towards innovative networking infrastructures [6, 21, 22].

Software Define Networks (SDN) paradigm has emerged as a promising architecture

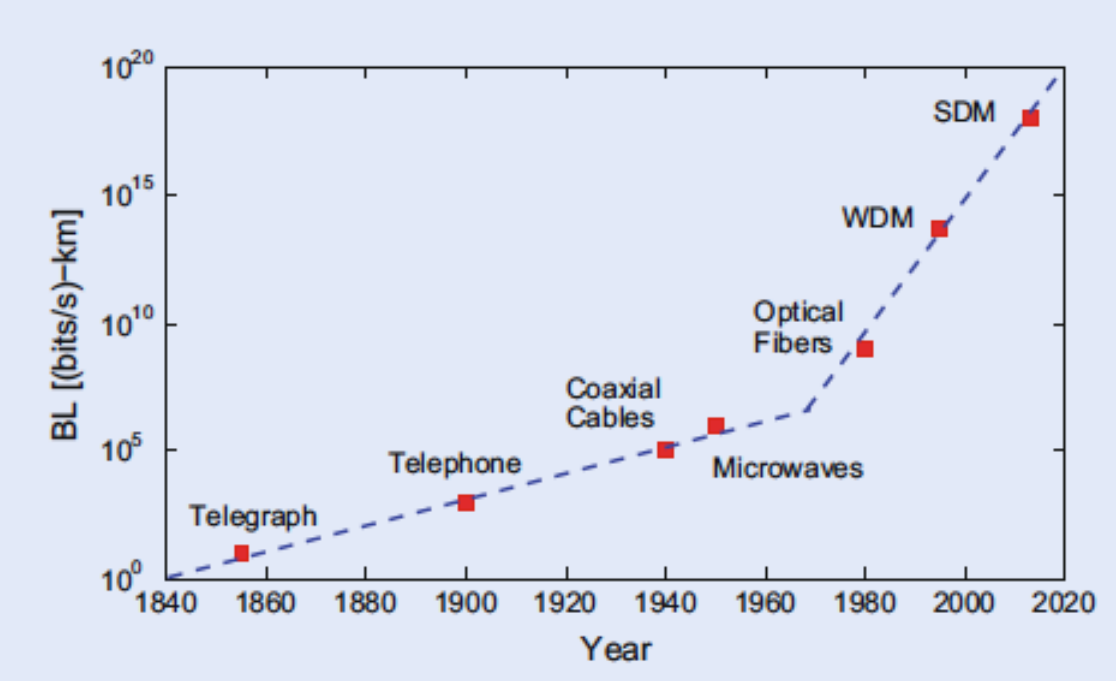

Figure 2.1: BL product during the period 1840–2015. The emergence of new technologies is marked by red squares (source: [16]).

to face with these limitations [6]. Following the Open Networking Foundation (ONF) definition, SDN architecture can be summarized in three main points: the control and data planes are decoupled, the network view is centralized in a network controller and the network infrastructrure is abstracted from the applications [23]. This implies that the network can be programmed and controlled on demand obtaining a more flexible, scalable and adaptive networks [21–23]. The separation of the control and data plane allows the deployment of new protocols and applications. The first standard communication interface between the control and data plane was OpenFlow in 2008 [23]. It consists on flow tables with flow entries containing information about how the different flows have to be processed and forwarded [6, 21, 23].

On the other hand, the increasing demand for new services are driving the development of novel EONs. Flexible transceivers, that are a key element in EONs, provide adaptability in terms of bit rate, modulation format or bandwidth [20]. These flexible transceivers, also known as BVT, increase the flexiblility and dynamicy overcoming the traffic demand [5]. The traffic demand may come from heterogeneous resources, thus, different transmission techniques have to coexist on the same network increasing the need of the automatic control and monitoring [4]. According to the SDN principles, adaptive parameters such as modulation format or bit rate, can be controlled by the SDN controllers so that the optical networks would be exploited more efficiently. Thus, SDN paradigm combined with EONs enable to customize the infrastructure and reduce

costs.

Further adaptability, flexibility and programmability can be dealt with S-BVT [5]. In fact, S-BVT is an evolution of BVT which enhances BVT functionalities. BVT serves one fixed flow with a specific traffic demand adapting the modulation format, bandwidth or bit rate, considering a trade-off between reach and espectral efficiency [4,5]. Hence, S-BVT allows to dinamically serve multiple flows with different destinations, each of them with different parameters such as bit rate, Forward Error Correction (FEC) coding, modulation format or bandwidth [20]. Furthermore, the electronic and optical resources can be flexible divided for each flow. Thus, the S-BVT can be considered as a combination of several low-capacity BVTs.

S-BVT technology can support several transceivers implementation, such as Nyquist Wavelength Division Multiplexing (NWDM), OFDM or Time-Frequency Packing (TFP). NWDM uses optical pulses with an almost rectangular spectrum [24]. In OFDM sinc pulses with orthogonal signaling are employed [7]. On the other hand, TFP consists in sending pulses that are strongly overlapped in time, frequency or both [25]. The selection of one of these transmission techniques depends on the spectral efficiency, the complexity, the cost and the optical reach required. This thesis is focused on OFDM implementation considering DD or CO detection depending on the given traffic scenario. In fact, next section presents different implementations of OFDM systems.

An example of a generic SDN architecture considering different S-BVTs located at the nodes, is illustrated in Figure 2.2. It can be oberved that the SDN architecture is divided into three main layers: application layer, control layer and data layer. In general terms, the application layer is where the applications and services define the network behavior. The control layer receives instructions from the application layer and relays them to the network components [6]. The data plane is comprised of the network elements (routers, switches, optical nodes, etc.) that can include the S-BVTs. The S-BVTs can be remotely programmed by the SDN controller as well as the network devices. Parameters such as the modulation format, target performance, bit rate or bandwidth, as well as the selection of the BVT slice or the operating wavelength, among others, can be configured on-demand by the SDN controller by means of the DSP modules and the BVT front-ends.

In Figure 2.3 the block diagram of a generic S-BVT, is illustrated. It is mainly composed of two blocks, the S-BVT at the transmitter (BVTx) and the S-BVT at the receiver (BVRx). The digital signals after the DSP blocks are converted to analog by a DAC array. The S-BVTx optoelectronic front-end converts the signal to optical domain. The aggregated flow can be further sliced into data flows with less capacity, concurrently serving multiple destination nodes at variable rate. Then the signal goes through the optical network. At the S-BVRx, the received flow is distributed and the optical front-end converts the traffic into electrical domain adopting either DD or CO detection. After

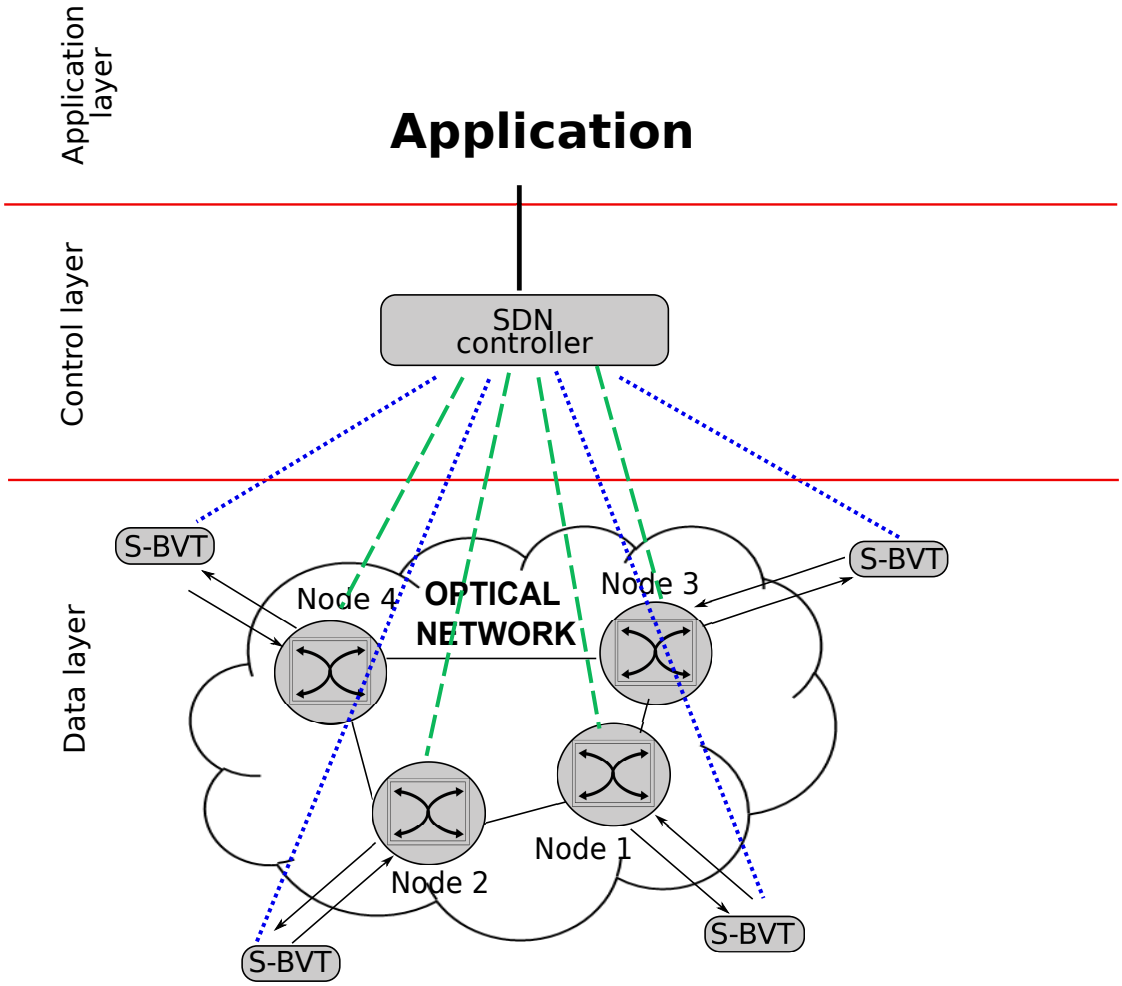

Figure 2.2: Generic Software Defined Network (SDN) architecture. S-BVT: Sliceable-Bandwidth Variable Transceiver.

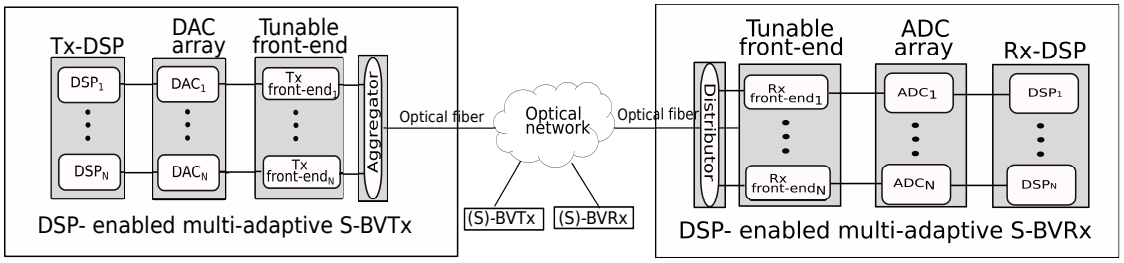

Figure 2.3: Generic S-BVT architecture. DSP: Digital Signal Processing, DAC: Digital to Analog Converter, ADC: Analog to Digital Converter, SNR: Signal to Noise Rate, Tx: Transmitter, Rx: Receiver.

the detection, ADC is implemented by an ADC array. Then the signal is processed by the DSP blocks at the receiver.

The future adoption of EON involves that the optical spectrum need be used in a

more flexible way. Then, the evolution of fixed-grid towards flexi-grid networks is envisioned [20]. In fact, a coexistence of fixed and flexi-grid networks is expected according to recent studies [3, 13]. In a flexi-grid scenario, channels with different bandwidths can go through the same fiber enhancing the flexibility. This granularity enables the reduction of the channel width. Traditionally, fixed-grid is based on 100 GHz or 50 GHz grid standardized by the ITU [10]. When the optical spectrum, corresponding to the standardized slots, is underutilized, the networks resources are inefficiently exploited. ITU has standardized a flexible WDM grid, using variable bandwidths in steps of 12.5 GHz [26]. As a consequence, programmable filters, using proper technologies as LCoS [11], are employed for flexible optical spectrum switching, avoiding the restrictions of typical 50 GHz or 100 GHz channel spacing of fixed-grid. ROADMs are also key elements to increase the flexibility and the scalability in EONs to support this evolutionary approach. In fact, ROADMs allow dynamically drop and add any wavelength to remotely switch traffic. Third generation of ROADMs are mainly based on LCoS-based WSS [27].

Although these flexi-grid elastic networks have been studied for core scenarios, they are also proposed for metro/regional area networks [6, 15]. The main objective is that future metro architectures integrate different optical technologies controlled by the SDN control plane. Thus, it is expected that the data plane, optical switching and transmission technologies, among others, can be adapted dynamically, according to the traffic needs.

2.3 Orthogonal Frequency Division Multiplexing (OFDM)

In 1957, the kineplex system developed by Collins Radio Co. proposed the idea of transmitting parallel bit streams of data and use them to modulate several carriers [28]. This kind of modulation was called Frequency Division Multiplexing (FDM) or more generic as MultiCarrier Modulation (MCM) [29]. Robert W. Chang was the first who proposed the orthogonal multiplexing avoiding the interchannel and intersymbol interferences and maximizing the spectral efficiency [30]. As a consequence, OFDM received considerable research interest. Firstly, it was considered in wireless and mobile communications [31] and later, in wireless local areas, fixed wireless, television and radio broadcasting [32, 33]. The applications of OFDM in optical communications started thanks to Pan and Roger in 1996 [34]. Few years later, Dixon confirmed the advantage of using OFDM against optical channel dispersion in optical communications [35]. Another advantage of applying OFDM is its easy phase and channel estimation in a time varying environment. However, there are some disadvantages to overcome such as the Peak-to-Average Power Ratio (PAPR) and the high sensitivity to frequency and phase noise [7].

As mentioned before, OFDM is a MCM that divides the data rate in a large number of orthogonal parallel narrowband subcarriers. The mathematical formulation of the transmitted signal is:

$$s(t) = \sum_{i=-\infty}^{\infty} \sum_{k=1}^{N_{sc}} c_{ki} s_k(t - iT_s) \tag{2.1}$$

$$S_k(t) = \Pi(t) e^{j2\pi f_k t} \tag{2.2}$$

$$\Pi(t) = \begin{cases} 1, (0 < t \leq T_s) \\ 0, (t \leq 0, t > T_s) \end{cases} \tag{2.3}$$

where c_{ki} is the ith information symbol at the kth subcarrier, s_k is the waveform for the kth subcarrier, N_{sc} is the number of subcarriers, f_k is the frequency of the subcarrier, T_s is the symbol period and $\Pi(t)$ is the pulse shaping function [7]. The fundamental elements of an OFDM system are illustrated in Figure 2.4.

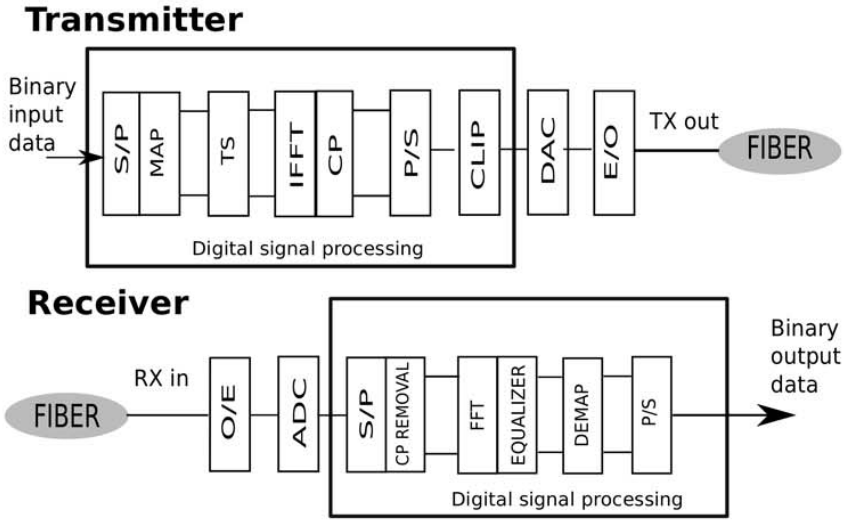

Figure 2.4: Conceptual diagram of a generic OFDM system. S/P:Serial to Parallel, MAP: MAPping, TS: Training Symibols, IFFT: Inverse Fast Fourier Transform, CP: Cyclic Prefix, P/S: Parallel to Serial, CLIP: CLIPing, DAC: Digital to Analog Converter, E/O: Electrical to Optical, O/E: Optical to Electrical, ADC: Analog to Digital Converter, S/P: Serial to Parallel, FFT: Fast Fourier Transform, DEMAP: DEMAPping, P/S: Parallel to Serial.

At the OFDM transmitter the input data is converted from serial to parallel. This information is mapped into different constellations depending on the specific implementation. OFDM allows to use high order modulation formats to increase the spectral efficiency. Then, the Training Symbols (TS) are inserted. The resulting signal is the input of the Inverse Fast Fourier Transfer (IFFT) block. At the output of the IFFT block, the time domain OFDM is obtained. The transmitted signal is a sequence of

these OFDM symbols. In order to avoid the InterSymbol Interference (ISI) and Inter-Carrier Interference (ICI) caused by Chromatic Dispersion (CD), a Cyclic Prefix (CP) is added. The CP is a copy of the last samples of the IFFT output. It is similar as a guard band between OFDM symbols. The following step is the conversion of the signal from digital to analog by means of a DAC. The dynamic range of the converters must be adjusted in order to accommodate the signal. This signal usually presents notably increasing of the PAPR, that limits the performance of the system. A possible way to mitigate this problem is to clip the signal [36–38]. The analog OFDM signal is modulated from electrical to optical domain. Then, the signal is transmitted over a fiber link.

At the receiver side, the signal is converted from optical to electrical domain. Afterwards, the signal is digitized by means of an ADC. The resulting signal is parallelized and the CP is removed. Finally, the Fast Fourier Transform (FFT) is implemented, the equalization is performed and the signal is demapped.

There are several ways to classify optical OFDM systems. One of them is considering the type of detection. In this respect, the optical OFDM systems can be divided into two groups: optical OFDM systems that use DD and optical OFDM systems that use CO detection. In DD-OFDM systems, direct laser modulation is possible and no laser is needed at the receiver [7]. So, the cost and the complexity at both, transmitter and receiver sides are low. Moreover, it allows a better recovery of the signal even in long links and the improvement of the performance. On the other hand, CO-OFDM systems are more robust against CD in long haul transmission and present better performance in terms of bandwidth efficiency, robustness against fiber dispersion and receiver sensitivity. It can recover full information of the received optical signal in terms of phase, amplitude and polarization. The main drawbacks of CO-OFDM systems are the complexity, required in transceivers with respect to DD-OFDM systems, and the effects caused by fiber nonlinearities [39].

2.3.1 DD-OFDM systems

In DD-OFDM systems there are many alternative transmitter designs. The main difference between transmitters is the way the input vector of the IFFT is mapped. As it was mentioned above, after the IFFT block the CP is added and the data is converted from parallel to serial. Then, the signal is converted from electrical to optical domain. There are different kinds of optical modulators. The semiconductor laser is commonly biased at constant current to provide Continuous Wave (CW) output, and external modulators are used to impose the information signal to be transmitted [7]. The most popular external electro-optical modulator is the Mach-Zehnder Modulator (MZM). The main parameters of a MZM are the bias voltage (V_{bias}) and the switching voltage (V_{π}). The power transfer characteristic is given by the expression $\cos^2[\frac{\pi}{2}\frac{s(t)+V_{bias}}{V_{\pi}}]$, being $s(t)$ the signal that is going to be modulated [40]. The characteristic could operate in the nonlinear

regime resulting in signal distortion when the standard deviation (σ_s) of the transmitted signal is high enough. In order to avoid this problem the signal before modulation is multiplied by a scale factor. On the other hand, the selection of the bias has also significance. The optimal bias for optical intensity modulation is the quadrature point (V_{bias}=$V_\pi/2$), whereas the optimal bias for optical field modulation is near the null point ($V_{bias} \approx V_\pi$) [7], [40]. At the output of a MZM a Double Side Band (DSB) signal with respect to the optical carrier (f_c) is created. DSB transmission is very sensitive to CD due to the interactions of the two side bands of the modulated optical signal. To solve this problem, one of the two sides can be suppressed, generating a Single Side Band (SSB) signal.

There are many techniques to suppress one of the side bands [41]. Several approaches are shown in Figure 2.5. The most common transmitter is presented in Figure 2.5 a). The output of the IFFT is converted from parallel to serial. Then, the real and imaginary parts of the signal are converted to analog domain by two DACs. These signals are then upconverted to a Radio Frequency (RF) carrier. The width of the guard band between optical carrier and the OFDM signal is determined by the value of the RF carrier. Finally, the signal is modulated and filtered with an optical SSB filter.

Another scheme is based on using the Hilbert transform. The block diagram is presented in Figure 2.5 b). In order to get the Hilbert transform, half of the IFFT input carriers are set to zero. The guard band is created including zeros in the other half of the IFFT input carriers. The remaining subcarriers are filled with data. As a result, two outputs are obtained from the IFFT. The first output is the OFDM signal and the second is its Hilbert transform. These two outputs are converted from digital to analog domain and drive an optical Inphase/Quadrature (I/Q) modulator. Therefore, the resulting optical signal is a SSB signal. This design doesn't require an optical filter but it requires two DACs and an expensive modulator [41].

In the design of Figure 2.5 c) the mapping of the IFFT input is done in different way. In this OFDM transmitter, Hermitian symmetry (HS) is forced at the input of the IFFT in order to obtain a real valued signal at the output of the transform. This means that half of the input vector of IFFT block is the data vector and the other half is the complex conjugate of the same vector. The guard band is determined by the zeros included at the first part of the data vector. So, the resulting signal after the DAC is a real signal. Then, the signal is modulated and finally filtered by an optical SSB filter. This transmitter design saves one DAC whereas the design presented in Figure 2.5 b) saves the optical SSB filter.

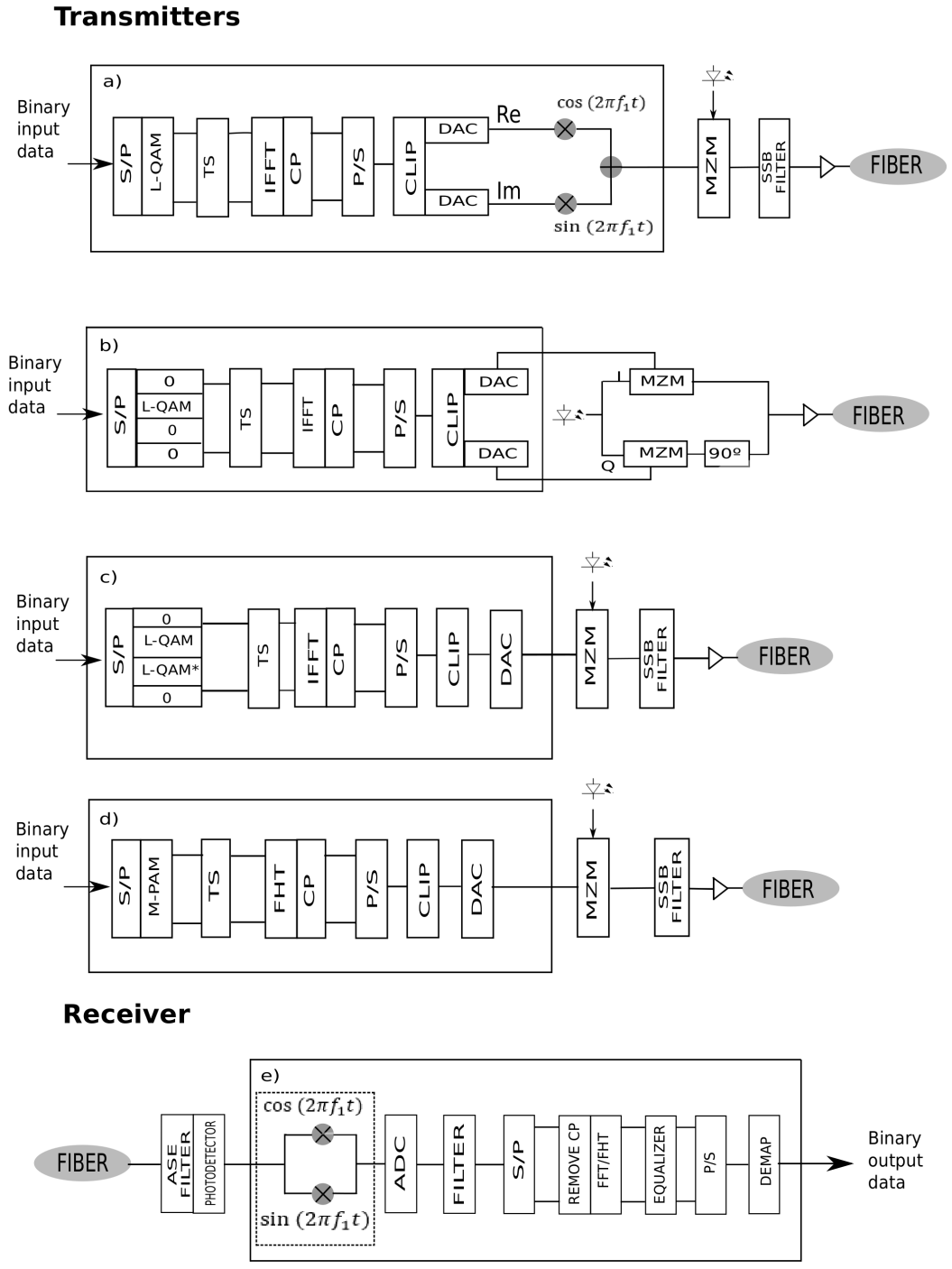

Figure 2.5: DD-OFDM transmitters using a) RF upconverter and optical SSB filter, b) frequency domain Hilbert transform, c) Hermitian symmetry and an optical SSB filter, d) real transform (DHT) and an optical SSB filter and e) DD-OFDM receiver. SSB:Single Side Band, MZM: Mach-Zhender Modulator, ASE: Amplified Spontaneous Emission.

It can be seen that the spectral efficiency in Figures 2.5 b) and c) is lower compared to Figure 2.5 a). This is because in Figure 2.5 a) all subcarriers except DC are used to carry data. In contrast, for this design two DACs and a RF converter are required.

An alternative design has been proposed in [42]. The block diagram is illustrated in Figure 2.5 d). They use a real trigonometric transform to directly deal with real signal. This real trigonometric transform is the Discrete Hartley Transform (DHT). It generates real data when the input signal is mapped into a real constellation such as Binary Phase-Shift Keying (BPSK) or Pulse Amplitude-Modulation (PAM) [42, 43].

When the output signal after the IFFT block is real-valued, the OFDM can be also referred to as DMT. DMT is considered as a subclass of OFDM. The transmitter of Figure 2.5 c) and Figure 2.5 d) are two examples of this kind of modulation. Comparing both systems, it can be seen that using FFT of order N_{sc} with HS, the information data is transmitted over N_{sc} subcarriers. However, using DHT the information data is transmitted over N_{sc} subcarriers. Therefore, to transmit the same information for both systems, the input data has to be mapped in different ways [43]. The relation between modulation formats is $M = \sqrt{L}$, being $M = 2^{bps}$ the levels of the real constellations for DHT and bits per symbol, and being $L = 2^{bps}$ the levels of the complex constellations for FFT.

At the receiver side of a DD-OFDM system a simple photodetector is used after noise filtering. The block diagram is presented in Figure 2.5 e). It can be modeled as a square law detector. The RF downconversion is needed only for the transmitter of Figure 2.5 a) (dotted line).

2.3.2 CO-OFDM systems

CO-OFDM system was proposed by W. Shieh *et al.* in [44] and [45] as another optical configuration due to its robustness against CD and polarization mode dispersion [7]. The block diagram of a CO-OFDM system is depicted in Figure 2.6. Input data is mapped onto the corresponding information symbols of the subcarriers and the digital time domain signal is obtained by using IFFT. Then, the OFDM in-phase and quadrature components of the OFDM complex signal are modulated by using an I/Q optical modulator. In order to achieve a linear conversion between the RF signal and optical field, the MZM must be biased close to the null point [7]. Then, the modulated signal is transmitted to the optical channel. At the receiver side, a local laser, a 90^{o} hybrid and 2 pairs of balanced photodetectors are needed to recover the signal. Finally, I/Q components are demodulated.

Although OFDM has emerged as the leading modulation technique, advanced multiplexing and modulation techniques based on available physical dimensions and a combination of them, has to be addressed, to meet the future network challenge and requirements. In the next section, different multi-adaptive transceivers based on different

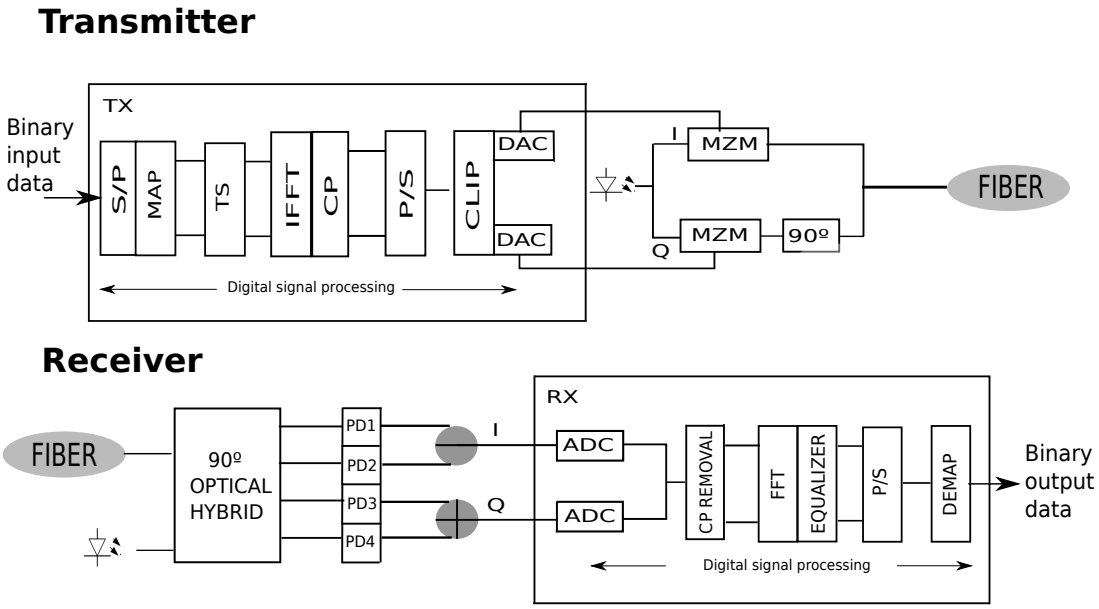

Figure 2.6: CO-OFDM transmitter and receiver.

dimensions are dealt.

2.4 Multi-adaptive optical transceivers for Elastic Optical Networks

As it was mentioned above, the information is rapidly growing. In order to overcome this demand, some progress are carrying out in component technology, either in the electronic or in the optical part, as well as in the transmission technologies. In this thesis, we focus on the transmission technology development.

SDN architectures combined with EONs, paying special attention to the development of S-BVTs for the envisioned flexi-grid networks, have been introduced in the previous sections. The S-BVT technology is programmable, reconfigurable and adaptive in order to support the on-demand configuration of programmable network functions [4, 5]. The key component for the programmability of a multi-adaptive S-BVT is the DSP module, where different parameters such as modulation format, bit rate, bandwidth, wavelength, among others, can be selected. Furthermore, making use of the physical dimensions of the electromagnetic waves, multi-adaptive optical transceivers, based on modulation and multiplexing techniques, can be implemented, further increasing the flexibility and adaptability of the optical networks [14].

Adaptive modulation, and multiplexing techniques in time, frequency, quadrature and polarization are the first options to be exploited in order to take full advantage of the deployed optical infrastructure. However, the achievable capacity per fiber may

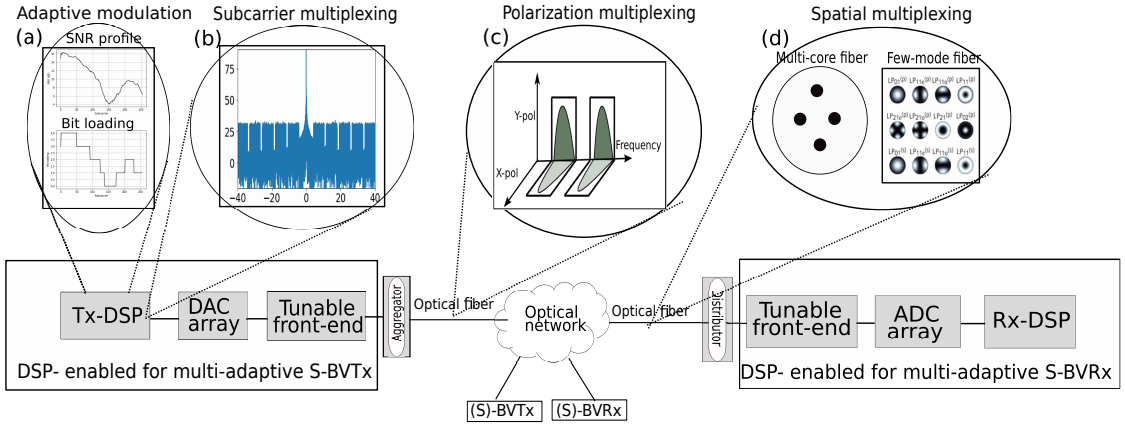

Figure 2.7: Multi-adaptive optical transceivers based on a) adaptive modulation, b) subcarrier multiplexing, c) polarization multiplexing and d) space division multiplexing (multi-core and few-mode fibers).

become a bottleneck because of the nonlinear Shannon limit [14,15]. In order to overcome this issue, spatial dimension is also being considered for the deployment of future optical networks [14].

In this section, different modulation and multiplexing techniques based on physical dimensions that can be implemented at the S-BVT, are introduced. In Figure 2.7 some examples of multi-adaptive transceivers are illustrated.

2.4.1 Advanced and adaptive modulation formats

The most common modulation formats in OFDM systems are M-Quadrature Amplitude Modulation (M-QAM) and M-Phase Shift Keying (M-PSK). In QAM, information is encoded on both amplitude and phase and symbols have different energy levels, whereas in PSK, the information is encoded only on phase and symbols are distributed in a circle of unitary energy. For high constellation sizes, the symbols in QAM are sufficiently separated from each others so, there will be less errors at the receiver. In contrast, more power is needed to transmit them. In PSK, the distance between symbols is low and the transmission without errors is more difficult.

Recent studies uses 512QAM [46], 256QAM [47], 64QAM [48], 16QAM [49], Quadrature Phase Shift Keying (QPSK) [50] modulation formats. In general terms , when we consider a fixed channel capacity, if we increase the constellation size (bits per pulse), both the symbol rate and the required optical bandwidth decrease and therefore, spectral efficiency improves.

More efficient modulation formats, are Dual Polarization (DP)QPSK or Polarization Switched (PS)QPSK. DPQPSK constellation takes advantage of the 4 degrees of freedom of the electromagnetic field using both quadrature and polarization components.

DPQPSK can be seen as four parallel and independent BPSK channels or as two independent QPSK in each polarization. Thus, this constellation have the same Bit Error Rate (BER) performance as BPSK [39, 51]. In the case of PSQPSK, that can be considered as a subset with respect to the DPQPSK modulation format, the BER performance improves with respect to the BSPK, as it can be seen in [51]. Recent studies have extended the dimensionality to 8 as in [52].

On the other hand, adapting modulation algorithms such as bit loading or power loading have been proposed to adapt the data rate to the current demand and network conditions overcoming the CD and maximizing the spectral efficiency. In this case, the different subcarriers are mapped with different modulation formats providing greater flexibility to the system [8]. An example of bit loading implementation according to the channel profile is shown in Figure 2.7 (a). Depending on the maximization function, these algorithms can be classified under two criterion, Rate Adaptive (RA) or Margin Adaptive (MA) algorithms. MA criterion considers energy minimization at a given data rate and RA considers rate maximization for a fixed energy constraint [8, 53].

2.4.2 Subcarrier multiplexing

Multi-band is also referred to as SubCarrier Multiplexing (SCM) [54]. It consists on the multiplexing and transmission of multiple signals by a single wave. These systems achieve high degree of flexibility due to the possibility of playing with the modulation format and bandwidth, or being combined with WDM technology, enhancing the spectral efficiency [46, 54, 55]. Thus, the capacity of each band could be adapted to the traffic demand. Furthermore, using multi-band systems, high data rates are divided in low data rates, thereby, relaxing the DAC and ADC requirements. If we compare SCM techniques with WDM systems, more optical spectral efficiency can be obtained with SCM because much narrower channel is allowed.

The combination of the different bands can be realized in the electrical domain using In-phase and Quadrature (I/Q) mixers at different intermediate frequencies, in the optical domain using optical I/Q mixers or in electrical hybrid domain with optical I/Q mixers [56]. In Figure 2.8 an example of the combination in the electrical and optical domain are illustrated (based on Figure 5 of [56]). In electrical domain, IQ mixers are employed to upconvert the OFDM bands onto an intermediate frequency. Then, the OFDM bands are combined and a MZM is used for the optical modulation as it can be seen in Figure 2.8 (a). An example of a multi-band signal spectrum using I/Q mixers in electrical domain is shown in Figure 2.7 (b). In optical domain, the OFDM bands are optically modulated by means of optical I/Q mixers and the resulting optical OFDM bands are combined as it is observed in Figure 2.8 (b). If a hybrid electrical and optical I/Q mixer is used, both schemes are mixed. Similar to the transmitters, the receiver can be realized with either electrical or optical IQ mixers [56].

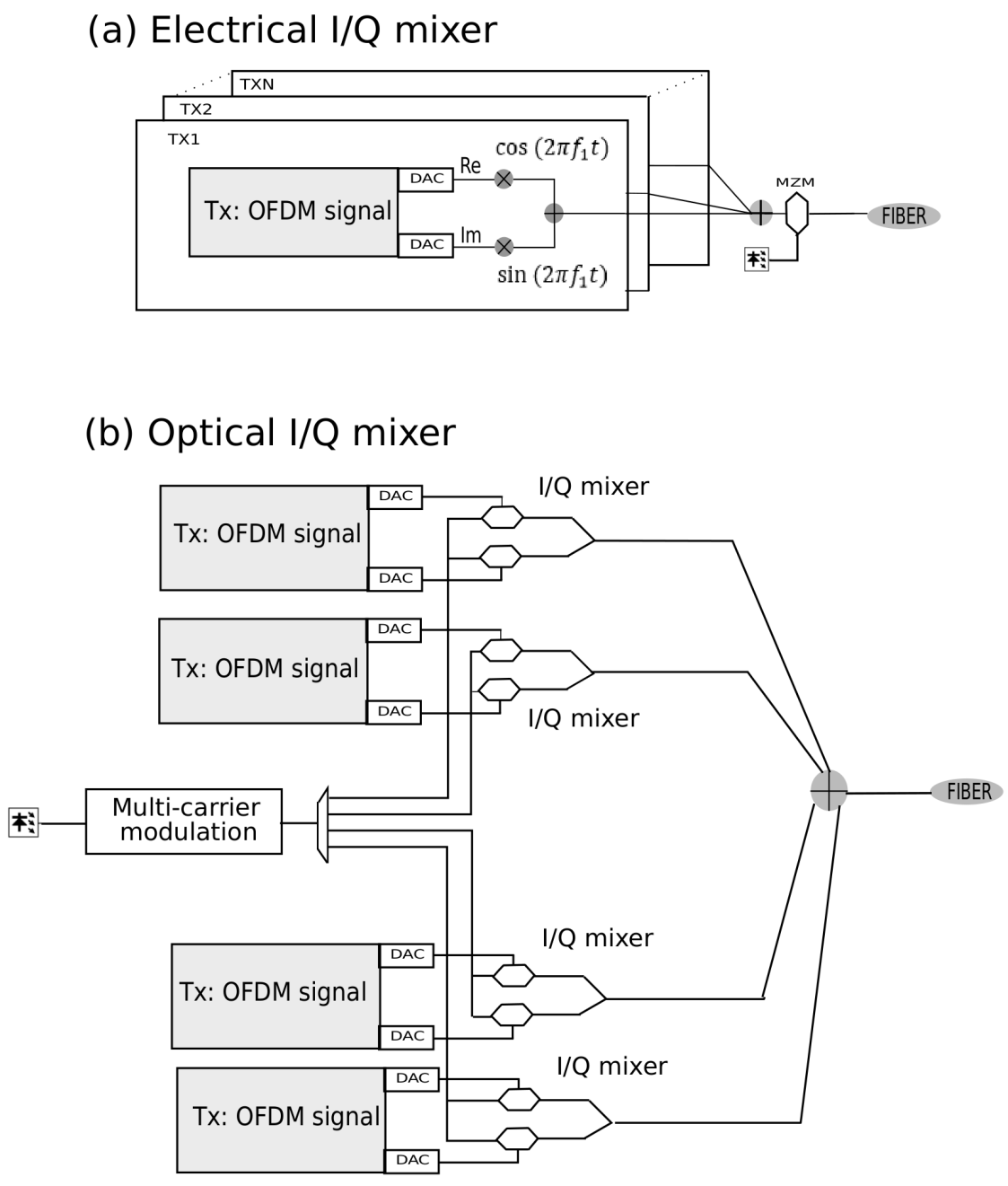

Figure 2.8: Multi-band OFDM transmitter based on (a) electrical I/Q Mixers and in (b) optical I/Q mixers.

Some examples of multi-band systems, for long-haul transmission, are presented in [56], [57] and [58]. In [56] the authors use DP transmission. Thus, the channel capacity doubles. In this case, they use electrical I/Q mixers obtaining a transmission of 121.9 Gb/s over 1000 km of Standard Single Mode Fiber (SSMF) using coherent receiver.

Coherent detection and DP transmission is also used in [57] but, in this case, the electrical to optical conversion is done by means of optical I/Q mixers. They demonstrate 100 Gb/s over 1000 km of transmission line.

As it was presented, a multi-band OFDM signal can be detected employing CO-OFDM detection. However, due to the requirements that CO-OFDM detection involves, recent studies are focusing on DD-OFDM such as in [54, 58, 59]. In [58] the authors propose a multi-band system using optical I/Q mixers with the bands aligned in the same polarization. They achieve to transmit more than 100 Gb/s over 720 km SSMF using DD. In [54] the authors study the optimization of system performance considering tradeoffs as data rate per subcarrier, modulation format, channel spacing between bands, optical power, etc. A novel double-sided multiband OFDM system using DD is demonstrated in [59]. For the [54] and [59] studies multi-band systems are generated in the electrical domain.

2.4.3 Polarization division multiplexing

Polarization Division Multiplexing, refered as DP in this thesis, is an approach that offers the opportunity to double the capacity, exploiting the polarization physical dimension. It consists on the transmission of two independent signals on both orthogonal polarization states in a single-mode fiber. With the increase of the fiber links, power fading can occurs due to the polarization mode dispersion effect producing the rotation of the State Of Polarization (SOP) [60, 61]. This rotation must be corrected in order to avoid misalignment penalties at the receiver. Some solutions to mitigate this effect has been proposed in both electrical or optical domain. Electrical solutions based on Multiple-Input Multiple-Output (MIMO) processing at the receiver can be adopted as in [62] and [63]. In [64], the authors demonstrate the transmission of 160 Gb/s using DP over 214 km using automatic polarization control. In Figure 2.7 (c) an example of polarization multiplexing is shown. Here, we can see that one signal is trasmitted over the horizontal axes and the other signal is trasmitted over the vertical axes carrying both different information, over the frequency dimension.

DP can be used in combination with DD or CO detection systems. Qian [65] and Lin [66] evaluate the BER performance based on DP for DD systems. They demonstrate the possibility to transmit 40 Gb/s over 20 km of fiber. Recently, an advanced programmable S-BVT with DP capabilities, also using DD receiver for metro networks, have been demonstrated [60]. In this case, Polarization Beam Splitters (PBSs) and polarization controlers are included at the transceivers, enabling to change the polarization arbitrarily. CO detection in combination with DP for long-haul optical transmission systems, are presented in [61, 67]. They show that using CO detection the polarization can be demultiplexed electronically demonstrating to be a potential commercial viable technology.

2.4.4 Time and frequency division multiplexing

Time division multiplexing (TDM) is a method to increase data transmission rate, multiplexing independent signals, over a common signal. It is performed by dividing the time domain in time slots of fixed lengths, one for each independent signal. Thus, all signals operate with the same frequency at different times. The transmission using the time dimension can be performed in the electrical or in the optical domain. Electrical Time Division Multiplexing (ETDM) transmission implies signal processing in electrical domain. In contrast, Optical Time Division Multiplexing (OTDM) involves signal processing in the optical domain. In OTDM there are some transmission limits related to the impairments of the fiber, such as CD or PD, whereas in ETDM the limitations come from the electrical signal processing at the required data rate.

In recent studies, techniques of OTDM with DP have been combined resulting in 1.28 Tb/s transmission over 240 km and 2.56 Tb/s over 160 km [68]. Continuous progress has been made to reach 5.1 Tb/s in a Back to Back (B2B) system using 1.28 Tbaud OTDM, Differential (D)QPSK as data format and DP, as it is demonstrated in [69].

Due to the progress in electronic components, recent advances in ETDM transmission have been performed trying to reduce the power consumption and system complexity of OTDM [70]. Some of these advances are shown in [71–73]. Lee *et al.* propose a ETDM optical transmitter operating at 80 Gb/s [71]. In [72,73], Winzer *et al.* have demonstrated 107 Gb/s transmission data rate using ETDM transmitter in order to reach 1 Tb/s by combining ten 107 Gb/s ETDM signals with WDM transmission over 400 km system and in a 1000 km recirculating loop.

When FDM techniques are used, the frequency spectrum is divided into several independent frequency signals. All signals operate at independent frequency at the same time. If the frequencies are orthogonal between them, the transmission technique is known as OFDM (It was already introduced in previous sections). WDM is the same concept as FDM but, in this case, using different wavelengths onto the fiber simultaneaously, increasing the capacity. Each of the channels of the WDM system transmits independent information. WDM systems can be divided into two categories: Coarse Wavelength Division Multiplexing (CWDM) and DWDM. The main diference is the associated spacing between channels. In case of CWDM the spacing is 20 nm and it is convenient for short distances (up to a maximum of 70 km). In contrast, in DWDM the spacing is 0.8 nm and it supports longer distances. WDM systems were applied together with ETDM in [72,73]. In Lowery *et al.*, authors focus on the combination of OFDM with SSB and WDM systems in order to compensate CD [74, 75]. They explore the effects of fiber nonlinarities design rules based on the number of channels, spacing between them, fiber dispersion or the maximum power per channel for transmission distances between 800 km and 4000 km in steps 800 km. Furthermore, OFDM system is compared with Non Return to Zero (NRZ) systems obtaining a 0.5 dB power sensitivity advantage in

OFDM with respect to NRZ, for long-haul optical transmission.

2.4.5 Space division multiplexing

As it was previously mentioned, in order to overcome the demand of high capacity technologies due to the growth of broadband services, advanced modulation formats and different multiplexing techniques are being exploited, to maximize the use of the deployed optical fiber infrastructure. However, single mode fiber is reaching its limit capacity. This capacity barrier is known as the nonlinear Shannon limit [15, 76]. Thus, SDM is becoming more important in optical communications. It consists on sending information over parallel spatial paths. This information can be transmitted by multiples cores, Multi-Core Fibers (MCF), in the same cladding or in multiple modes, Few-Mode Fibers (FMF), across the core area [14, 77, 78]. In Figure 2.7 (d) a MCF and the signal modes for a FMF are illustrated.

In both, the main obstacle to overcome is the crosstalk. Crosstalk appears because of the coupling between signals propagating through parallel paths. In MCF tranmission, some parameters such as the effective area of each core, the number of cores, the propagation direction of the closest core or the Propagation-Direction Interleaving (PDI) and the spatial distribution of the cores within the fiber, must be considered in order to reduce the crosstalk. A. Sano *et al.* summarized and detailed the parameters used in recent transmission experiments for high capacity long-haul transmission through MCF focusing on crosstalk suppression [77]. They have shown how increasing the number of cores and considering PDI and a Dual-Ring Structure (DRS), the transmission distance increases by reducing the crosstalk. On the other hand, in FMF transmission is very common to use MIMO DSP techniques to compensate the crosstalk between modes. Some studies such as [79] proposes a FMF system with six spatial and polarization modes and a MIMO DSP to recover the transmitted signal. A FM-MCF has been proposed enabling dense SDM. In [80], three mode 12 core fiber have been used, reaching 500 km of transmission distance. The main problems to address in these systems were the inter-core crosstalk, the inter-mode crosstalk and the dispersion mode delay.

Some efforts have been recently done in the SDM technology including SDM amplifiers or switching and routing functionalities. Flexible optical routing is being contemplated with the aim that spatial superchannels where subchannels with the same wavelength can be transmitted on separate modes but route together [76]. The main problem to overcome for the deployment of these systems is the transition from systems based on single mode fiber in terms of cost and flexibility.

Chapter 3

Multi-band OFDM systems with DD

3.1 Introduction

Due to the increment of the traffic demand, the current technology is becoming limited [1, 59, 81]. As in section 2 was introduced, a possible solution is to use multi-adaptive transceivers that can fit to the actual traffic needs. Particularly, in section 2.4.2 multi-band systems were presented as a possible solution to increase flexibility and capacity since these systems allow to multiplex and transmit multiple low bit rates signals by a single wave [54].

Recently, multi-band systems have been considered for the envisioned flexi-grid scenarios [55]. Although flexi-grid technologies have been mainly studied for core network scenarios, they are also considered as a candidate solution for the metro/regional area network segment, due to the high bandwidth pressure. In this context, high bit rate connections can be replaced by flexible low bit rate connection each of them with different transmission requirements.

We propose the implementation of a multi-band system based on OFDM technology for optical metro networks. Particularly, the multi-band OFDM using DD is considered to maintain low complexity at the receiver, improving the optical spectrum efficiency while reducing Capital Expenditure (CapEx) investment.

The simplest system considers one photodetector, therefore all the bands are photodetected at the same time. In this case, the electrical bandwidth of the photodetector has to include all the OFDM signal bandwidths as well as the guard band with respect to the optical carrier as it is shown in [82]. Alternative solution consists on detecting the OFDM bands separately. For example, using a dual band optical filter that allows to filter the optical carrier and the OFDM band. The main disadvantage of this kind of detection is the high cost of the dual band filters. Recent studies propose the use of

virtual carriers generated in electrical domain together with the OFDM band as in [83] or [84]. This allows to detect separately the OFDM band reducing the photodetector bandwidth. In contrast, we need as many photodetectors as OFDM bands.

Hence, the specific implementation has to be carefully selected according to the particular application, feasibility, technological limitations or cost. In the context of EONs, multi-band systems can be integrated at the S-BVT architectures improving the spectral efficiency allowing to use 12.5 GHz frequency slot of the envisioned flexi-grid [85,86]. The creation of low bit rate connections find application in metro area networks, as we presented in section 2.4.2., since allow to enhance the transceiver capacity, flexibility and reduce optoelectronic devices for cost-effective applications. Particularly, we propose to use a single optoelectronic front-end in order to limit the number of optoelectronic blocks, thus reducing the cost. Furthermore, thanks to its simplicity at both transmitter and receiver, we propose OFDM systems using DD. The combination of the signals in a single electrical wave, is made in the analog domain by means of an electrical I/Q mixer [39,56]. Then, the signal is optically modulated by a simple external optical modulator. At the receiver, we use a common photodetector. DD is combined with SSB OFDM tranmission enhancing the robustness to the CD effect on long-haul transmission [41]. This implementation requires adding an optical filter at the transmitter. On the other hand, in DD-OFDM systems a guard band between the optical carrier and the OFDM signal is required, to avoid the mixing products generated at the photodetector [7]. The spectral efficiency can be enhanced by minimizing the guard band and using higher size constellations in the subcarrier loading.

A general aspect to be consider in an optical communication system is the nonlinearities due to optoelectronics modulators characteristics. As it is well-known, the ratio between the power of the optical carrier and the OFDM signal provides relevant information about the efficiency at the detection. In [88], the authors analize the influence of the MZM bias point and the receiver sensitivity. By biasing the MZM at quadrature point the power of the optical carrier increases with respect to the power of the OFDM signal, the nonlinearities distortions due to the MZM are reduced but, in contrast, the receiver sensitivity is degraded. However, if the MZM is biased near the null point, the power of the optical carrier decreases with respect to the power of the OFDM signal and the OFDM signal is less influenced by noise distortions improving the sensitivity at the receiver. These nonlinearities impact has been also studied in [87] using a DSB with subcarrier supression modulation scheme. In a multi-band OFDM system, in addition to these nonlinearities, inter-bands effects appear.

In this section, we present a theoretical model of the resulting photodetected signal in a multi-band DD-OFDM system, assuming that the MZM is biased near the null point in order to improve the receiver sensitivity. Based on this model, we analyze the nonlinearities due to the optoelectronic modulator and we identify the inter-band effects.

The proposed solution is simulated for a realistic regional network.

Therefore, the main contributions of the thesis are listed below.

- We propose a cost-efficient multi-band DD-OFDM system with SSB combining the different OFDM bands in the analog domain by an electrical I/Q mixer [39, 56]. The main concept is the division of high data rate in low data rates, enabling the relaxation of DAC and ADC bandwidth requirements [56].

- A theoretical model of the resulting photodetected signal of a generic multi-band system is presented, assuming that the MZM is biased near the null point. Thanks to this model, we identify the mixing products due to the interaction of different bands after the photodetection.

- Then, a multi-band system consisting on five bands is validated by numerical simulations and the mixing products and the inter-band effects are identified. After that, we assess the relation between them and the number of bands as well as the impact of the MZM bias point.

- Finally, the multi-band system model is validated for a realistic regional network by numerical simulations. Thus, different transmission distances have been assessed for the first, the third and the fifth band.

3.2 Transmission scheme for a multi-band DD-OFDM system

The multi-band DD-OFDM system proposed is illustrated in Figure 3.1. At the transmitter, the binary input data is converted from serial to parallel. Then, this information is mapped into M-QAM and the TS are inserted. The resulting signal is the input of the IFFT block. In order to limit the ISI and ICI caused by CD, a CP is added. The resulting OFDM symbol is serialized and clipped. The next step is the upsampling of the OFDM symbols to emulate an ideal DAC assumed to have the same bandwidth as the OFDM signal (6.25 GHz in our case). The described process is the same for each band of the multi-band DD-OFDM system. Afterwards, the analog signal of each band is upconverted to an intermediate frequency by an I/Q mixer. This intermediate frequency is different for each band in order to avoid overlaps. Subsequently, the bands are combined in the electrical domain and converted to optical. The optical conversion is made by means of a MZM with a linear driver, which is modeled as ideal. The MZM creates a DSB signal with respect to the optical carrier. In order to mitigate the CD effect, one of the side bands is suppressed by a SSB filter [41]. After that, the resulting signal is sent through the channel. At the receiver side, a noise filter and a photodetector

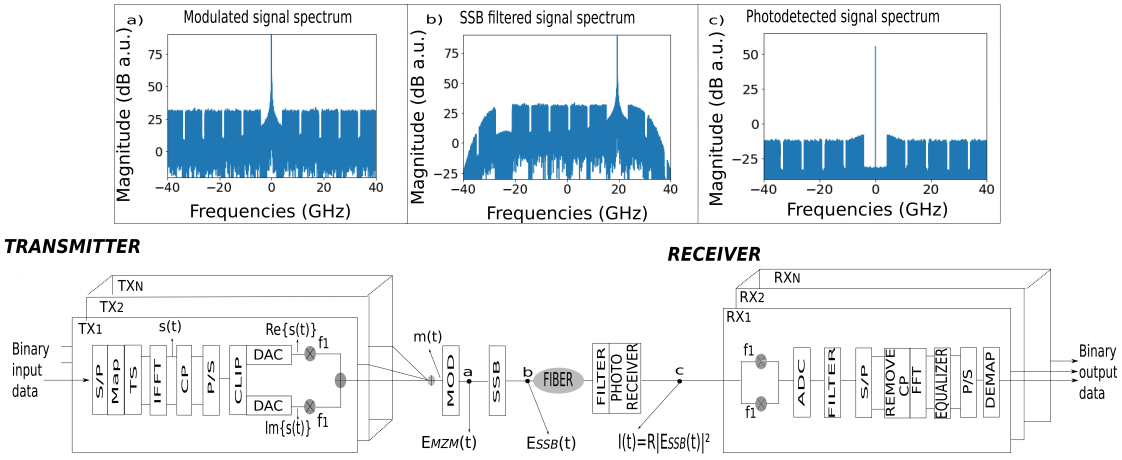

Figure 3.1: Multi-band DD-OFDM scheme. TX: Transmitter, RX: Receiver, S/P: Serial to Parallel, CP: Cyclic Prefix, DAC: Digital to Analog Converter, Map: Mapping, IFFT: Inverse Fast Fourier Transform, P/S: Parallel to Serial, CLIP: Clipping, MOD: Modulator, E_{MZM}: Signal after the Mach Zehnder Modulator (MZM), SSB: Single Side Band, E_{SSB}: Signal after the SSB filter, I: Photodetetectd signal, R: Responsivity, ADC: Analog to Digital Converter, FFT: Fast Fourier Transform, DEMAP: Demapping.

are required. Then, each band is downconverted to the corresponding intermediate frequency. The resulting signal is converted to digital, filtered and parallelized. Finally, the CP is removed, the FFT is implemented, the equalization is performed and the signal is demapped in order to recover the original bit stream.

It is important to note that the extinction ratio is a MZM limitation. In our case study, we consider an ideal MZM because the typical extinction ratio value of a commercial MZM is 20 dB, as it can be seen in [89]. For this value, the effect that the extinction ratio could produce to the overall performance of the system is minimum. In case of considering the finite extinction ratio, the generation of additional orthogonal terms would occur. In this case, after the photodetection (without considering transmission over fiber), these additional orthogonal terms would not imply any significant adverse effects as it is analyzed in [87].

The corresponding spectra for the modulated signal, the SSB filtered signal and the photodetected signal for five bands are presented in Figure 3.1 a), b) and c). In Figure 3.1 a) we can observe that the modulated signal is composed of five bands at each side of the optical carrier. Then, after the SSB filter, in Figure 3.1 b), we can observe that one of the sides of the modulated signal is suppressed. The photoreceiver is modeled as a square law detector obtaining the photodetected signal spectra shown in Figure 3.1 c). We can clearly distinguish the different OFDM bands in Figures 3.1 a)-c).

3.3 Theoretical model

After performing the IFFT transform and the digital to analog conversion, the baseband OFDM signal can be described as

$$s(t) = \sum_{k=-\frac{1}{2}N_{sc}+1}^{\frac{1}{2}N_{sc}} c_k e^{(j2\pi f_k t)}, \tag{3.1}$$

where c_k is the OFDM information symbol normalized to the number of subcarriers, N_{sc}, of the k-th subcarrier and f_k is the frequency of the k-th subcarrier.

Then, the resulting signal after the upconversion to intermediate frequencies, $\bar{f}_b$, can be described as

$$m(t) = \sum_{b=1}^{N_B} \{s_{r_b}(t)\cos(2\pi \bar{f}_b t) + s_{i_b}(t)\sin(2\pi \bar{f}_b t)\}, \tag{3.2}$$

where N_B is the total number of bands, $s_{r_b}(t) = \mathrm{Re}\{s_b(t)\}$ and $s_{i_b}(t) = \mathrm{Im}\{s_b(t)\}$.

Next, the electrical signal is modulated into the optical domain by means of a MZM. The power transfer characteristic of a MZM is given by the expression $\cos^2[\frac{\pi}{2}\frac{m(t)+V_{bias}}{V_\pi}]$ [40], where V_{bias} is the bias voltage and V_π is the switching voltage. The optical field at the output of the MZM can be expressed as

$$E_{MZM}(t) = \sqrt{P_s}\cos\left(\frac{\pi m(t)}{2V_\pi} + \frac{\pi V_{bias}}{2V_\pi}\right) e^{(j2\pi f_o t)}, \tag{3.3}$$

being P_s the maximum optical power at the output of the modulator and f_o the optical carrier frequency.

Then, we apply the cosine of sum identity in (3.3) and the expression results in

$$E_{MZM}(t) = \sqrt{P_s}\Bigg(\underbrace{\cos\left(\frac{\pi m(t)}{2V_\pi}\right)\cos(\alpha)}_{A} - \underbrace{\sin\left(\frac{\pi m(t)}{2V_\pi}\right)\sin(\alpha)}_{B}\Bigg) e^{(j2\pi f_o t)}, \tag{3.4}$$

where we define $\alpha = \frac{\pi V_{bias}}{2V_\pi}$. The $E_{MZM}(t)$ expression is composed by two terms. They are marked in the expression (3.4) as A and B. First, we will focus on A. We replace the $m(t)$ signal (see equation (3.2)) and we apply the cosine of sum identity. First of all, as can be seen in [90], the maximum peak-to-peak amplitude that the driving signal, $m(t)$, can take is V_π. Therefore, the maximum amplitude that $m(t)$ can take is $V_\pi/2$. Thus, we can do the following approximations

$$\max\{m_r(t)\} = \max\Big\{\sum_{b=1}^{N_B} s_{r_b}(t)\cos(2\pi \bar{f}_b t)\Big\} \leq \sum_{b=1}^{N_B} \max\{s_{r_b}(t)\} \triangleq s_r \tag{3.5}$$

$$\max\{m_i(t)\} = \max\left\{\sum_{b=1}^{N_B} s_{i_b}(t)\sin(2\pi\bar{f}_b t)\right\} \leq \sum_{b=1}^{N_B}\max\{s_{i_b}(t)\} \triangleq s_i \tag{3.6}$$

being $m_r(t)$ the corresponding $m(t)$ signal that depends on $s_{r_b}(t,)$ and $m_i(t)$ the corresponding $m(t)$ signal that depends on $s_{i_b}(t)$. On the other hand, s_r and s_i are the maximum value that the $m_r(t)$ and $m_i(t)$ signals can take, respectively. We assume that the OFDM bands are loaded with the same modulation format. Therefore, the maximum amplitude that each OFDM band can take is $\frac{s_r}{N_B}$ and $\frac{s_i}{N_B}$. Thus, the $m(t)$ expression can be written as

$$m(t) \leq \frac{s_r}{N_B}\sum_{b=1}^{N_B}\cos(2\pi\bar{f}_b t) + \frac{s_i}{N_B}\sum_{b=1}^{N_B}\sin(2\pi\bar{f}_b t) \tag{3.7}$$

Then, the resulting expression can be rewritten as

$$\begin{aligned} A &= \cos\left(\beta_r\sum_{b=1}^{N_B}\cos(\omega_b t) + \beta_i\sum_{b=1}^{N_B}\sin(\omega_b t)\right)\cos(\alpha) \\ &= \left[\cos\left(\beta_r\sum_{b=1}^{N_B}\cos(\omega_b t)\right)\cos\left(\beta_i\sum_{b=1}^{N_B}\sin(\omega_b t)\right)\right. \\ &\quad \left.-\sin\left(\beta_r\sum_{b=1}^{N_B}\cos(\omega_b t)\right)\sin\left(\beta_i\sum_{b=1}^{N_B}\sin(\omega_b t)\right)\right]\cos(\alpha), \end{aligned} \tag{3.8}$$

where we define $\beta_r = \pi s_r/(2V_\pi N_B)$ and $\beta_i = \pi s_i/(2V_\pi N_B)$. For compactness, we replace $\omega_b = 2\pi\bar{f}_b$.

After that, we use the cosine and sine of sum identities (i.e $\cos(p \pm q) = \cos(p)\cos(q) \mp \sin(p)\sin(q)$), for each factor of the expression in (3.8) that depends on N_B sum. These terms can then be developed resulting in an expression composed of terms as $\cos(z\cos(\theta))$, $\sin(z\cos(\theta))$, $\cos(z\sin(\theta))$ or $\sin(z\sin(\theta))$. Then, we can apply the Jacobi-Anger expansion and the Bessel functions of the first kind [91] for each of them.

The argument of the Bessel functions is given by β_r or β_i. In order to determine these arguments, some considerations must be taken into account. As it was aforementioned, the maximum amplitude that $m(t)$ can take is $V_\pi/2$, therefore, $\max\{m_r(t)\} = \max\{m_i(t)\} = V_\pi/2$. Hence, $\max\{\beta_r\} = \max\{\beta_i\} = \beta = \pi/(4N_B)$.

On the other hand, the Bessel functions amplitude, $J_n(\theta)$, being θ a generic argument, decreases with the increase of the order n of the function [91]. Moreover, as the number of bands increases the contribution of the non-zero Bessel functions decreases. Hence, we consider for the approximation the worst case, that is when $N_B = 1$. In this case $\beta = \pi/4$, and the even order Bessel functions are $J_0(\pi/4) = 0.881$, $J_2(\pi/4) = 0.059$, $J_4(\pi/4) = 0.001$ while the odd order are $J_1(\pi/4) = 0.329$ or $J_3(\pi/4) = 0.007$. It can be

observed that the 2^{nd} harmonic of even Bessel functions is only the 6.69% of the $J_0(\pi/4)$ harmonic and $J_4(\pi/4)$ is only the 0.11% of the $J_0(\pi/4)$ harmonic. As a result, only the $J_0(\pi/4)$ harmonic contributes. Similarly, for the odd order Bessel functions, the 3^{rd} harmonic is only 2.13% of the $J_1(\pi/4)$ harmonic. According to that, the most relevant terms considered are $J_0(\pi/4) = 0.881$ for the even terms and $J_1(\pi/4) = 0.329$ for the odd terms.

Keeping in mind these considerations, we can do the following approximations

$$\begin{aligned}
\cos\Big(\beta_r \cos(\omega_b t)\Big) &\approx J_0(\beta_r) \\
\cos\Big(\beta_i \sin(\omega_b t)\Big) &\approx J_0(\beta_i) \\
\sin\Big(\beta_r \cos(\omega_b t)\Big) &\approx 2J_1(\beta_r)\cos(\omega_b t) \\
\sin\Big(\beta_i \sin(\omega_b t)\Big) &\approx 2J_1(\beta_i)\sin(\omega_b t)
\end{aligned} \tag{3.9}$$

After that, we assume that the MZM is biased near the null point, ($V_{bias} \approx V_\pi$) in order to consider the best receiver sensitivity. For this value, $\cos(\alpha)$ in (3.8) is close to 0. By replacing the approximations of (3.9) in the expression (3.8) some crossed terms appear. We only consider those terms that fall inside our spectrum of interest. Nevertheless, near the null point of the MZM bias, these crossed terms decrease and can be neglected. As a consequence, the term that only depends on $J_0(\beta_r)$ and $J_0(\beta_i)$ adds relevant information. We consider the maximum value of the argument θ of $J_0(\theta)$ previously analyzed, that is $\pi/4$. Then, we have $J_0(\max\{\beta_r\}) = J_0(\max\{\beta_i\}) = J_0(\beta)$ and the expression in (3.8) becomes

$$A \approx J_0(\beta)^{2N_B} \cdot \cos(\alpha) \tag{3.10}$$

To derive the term B in (3.4) the procedure is similar. We replace the $m(t)$ signal in B and then apply the sine of sum identity, giving the following expression

$$\begin{aligned}
B &= \sin\left(\beta_r \sum_{b=1}^{N_B} \cos(\omega_b t) + \beta_i \sum_{b=1}^{N_B} \sin(\omega_b t)\right)\sin(\alpha) \\
&= \left[\sin\left(\beta_r \sum_{b=1}^{N_B} \cos(\omega_b t)\right)\cos\left(\beta_i \sum_{b=1}^{N_B} \sin(\omega_b t)\right)\right. \\
&\quad \left. + \cos\left(\beta_r \sum_{b=1}^{N_B} \cos(\omega_b t)\right)\sin\left(\beta_i \sum_{b=1}^{N_B} \sin(\omega_b t)\right)\sin(\alpha)\right],
\end{aligned} \tag{3.11}$$

After that, we use the cosine and sine of sum identities again, for each factor that depends on the N_B sum. The Jacobi-Anger expansion and the Bessel functions of the

first kind are applied to the resulting factors as in the case of the A term. Then, we use the approaches shown in (3.9). The resulting signal is composed of the terms that are related to the OFDM subcarriers centered at $\bar{f}_b$ each one and the terms that are related to the crossed terms after the optical modulation. As we assumed previously, the MZM bias point is near the null point, therefore $\sin(\alpha)$ will be near one. By developing the product-to-sum identities, it can be seen that the terms related to the OFDM subcarriers centered at $\bar{f}_b$ dominate over the crossed terms. Considering the maximum value that the argument θ of $J_0(\theta)$ can take, that is $\pi/4$, we have $J_0(\max\{\beta_r\}) = J_0(\max\{\beta_i\}) = J_0(\beta)$ as in the previous case. Thus, the expression (3.11) can be written as

$$B \approx \left(2J_0(\beta)^{2N_B-1} J_1(\beta_r) \sum_{b=1}^{N_B} \cos(\omega_b t) + 2J_0(\beta)^{2N_B-1} J_1(\beta_i) \sum_{b=1}^{N_B} sin(\omega_b t) \right) \sin(\alpha), \tag{3.12}$$

In order to express (3.12) as a function of the baseband OFDM signal of each band $s_b(t)$, we replace in $J_1(\beta_r)$ and $J_1(\beta_i)$, the Bessel approximation of $J_v(\theta) \sim (\frac{1}{2}\theta)^v / v!$ for $v = 1$. Taking into account that $s_b(t) = s_{r_b}(t) + j s_{i_b}(t)$, the resulting signal after the SSB filter can be expressed as

$$B \approx \frac{J_0(\beta)^{2N_B-1}\pi}{4V_\pi} \sum_{b=1}^{N_B} s_b(t) e^{-j\omega_b t} \sin(\alpha), \tag{3.13}$$

Hence, if we replace the expressions of (3.10) and (3.13) in (3.4), we can see that the signal after the SSB filter can be modelled as:

$$E_{SSB}(t) \approx \lambda \cdot e^{(j\omega_o t)} - \mu \cdot \sum_{b=1}^{N_B} s_b(t) e^{(j(\omega_o - \omega_b)t)}, \tag{3.14}$$

where $\omega_o = 2\pi f_o$, $\lambda = \sqrt{Ps} J_0(\beta)^{2N_B} \cos(\alpha)$ and $\mu = \sqrt{Ps} \frac{J_0(\beta)^{2N_B-1}\pi}{4V_\pi} \sin(\alpha)$.

At the receiver, the photodetector can be modeled by the square law detector. The general expression is given by $I(t) = R|E_{SSB}(t)|^2$, where $I(t)$ is the photocurrent and R is the diode responsivity. In (3.16) we can observe the resulted photocurrent, being $\mathcal{K}_l = \{-\frac{1}{2}N_{sc_l}+1, \ldots, \frac{1}{2}N_{sc_l}\}$ the subcarrier index set of the l-th band. It is comprised of four terms. The first term of the equation is the Direct Current (DC) component. The second is the fundamental term consisting of the linear OFDM subcarriers displaced at $\bar{f}_b$ frequency. The $\bar{f}_b$ frequency is defined by

$$\bar{f}_b = \begin{cases} GB + \frac{B_b}{2}, & \text{if } b = 1 \\ GB + \frac{B_b}{2} + \sum_{i=1}^{b-1} B_i + \sum_{i=1}^{b-1} B_{i|i+1}, & \text{if } b > 1 \end{cases} \tag{3.15}$$

where GB is the guard band between the optical carrier and the first OFDM band, B_b is the bandwidth of the band b, B_i is the bandwidth of the $(b-1)$ OFDM bands and $B_{i|i+1}$ is the guard band between two consecutive OFDM bands. The third term in (3.16) is related to the second-order nonlinearity term due to the mixing products of each band with itself. This contribution is distributed within frequencies $(f_{k_1} - f_{k_2})$ corresponding with the frequencies between the DC component and the first OFDM band, namely at the GB. Finally, the last term is the result of the interaction of two different bands displaced at two different frequencies, named as $\bar{f}_{b_m}$ and $\bar{f}_{b_n}$ in order to distinguish both. In this case, the interaction of two different bands appears at frequencies $(\bar{f}_{b_m} - \bar{f}_{b_n})$. The frequency distribution of the different terms in (3.16) will be further analysed in the Section 3.4. For our study, we have considered that the OFDM bands are loaded with the same modulation format.

$$
\begin{aligned}
I(t) = R \cdot |E_{SSB}(t)|^2 = R|\lambda^2| - 2R\lambda\mu \sum_{b=1}^{N_B} Re\left\{ e^{j2\pi\bar{f}_b t} \sum_{k\in\mathcal{K}_b} c_k e^{(j2\pi f_k t)} \right\} \\
+ R|\mu^2| \sum_{b=1}^{N_B} \sum_{k_1\in\mathcal{K}_b} \sum_{k_2\in\mathcal{K}_b} c_{k_1} c_{k_2}^* e^{(j2\pi(f_{k_1}-f_{k_2})t)} \\
+ 2R|\mu^2| \sum_{b_m=2}^{N_B} \sum_{b_n=1}^{b_m-1} Re\left\{ e^{j2\pi(\bar{f}_{b_m}-\bar{f}_{b_n})t} \sum_{k_1\in\mathcal{K}_{b_n}} \sum_{k_2\in\mathcal{K}_{b_m}} c_{k_1} c_{k_2}^* e^{(j2\pi(f_{k_1}-f_{k_2})t)} \right\}
\end{aligned} \tag{3.16}
$$

3.4 Simulation assessment

In order to assess the theoretical model proposed in (3.16), the multi-band DD-OFDM system described in Figure 3.1 is simulated. The total number of transmitted bits is 65536 per each band. We have analyzed the case of transmitting at a net bit rate of 10 Gb/s for each band (50 Gb/s for 5 bands in our case) using a 4QAM modulation format. The number of OFDM subcarriers is 512 and the total number of frames is 131 with the TS. The target BER is set to $2 \cdot 10^{-2}$, assuming an overhead of 20% due to the Soft-Decision Forward Error Correction code (SD-FEC). Thus, to support a net bit rate of 10 Gb/s, the bandwidth of each OFDM band is 6.25 GHz. This bandwidth includes the CP (1.9%) and TS (2.29%). The guard band between the optical carrier and the first band is 6.05 GHz. The guard band between two consecutive bands is 0.05 GHz. As the total number of bands considered is 5, the total optical bandwidth is 37.5 GHz, that corresponds to 3 frequency slots of 12.5 GHz in a flexi-grid network [26]. The frequencies where each band is centered are $\bar{f}_1 = 9.18$ GHz, $\bar{f}_2 = 15.48$ GHz, $\bar{f}_3 = 21.78$ GHz, $\bar{f}_4 = 28.08$ GHz and $\bar{f}_5 = 34.38$ GHz. The laser driving the MZM is modulated as a standard CW centered at a wavelength of $\lambda = 1550$ nm with output power 1 mW and 1 MHz linewidth. The receiver is modeled as a PIN photodiode with 0.7 A/W

responsivity, impedance of 50 Ω and dark current of 1 pA.

As it was presented on the section 3.3, in a multi-band DD-OFDM system, mixing products can appear due to the interaction of the bands [58], at the receiver. These impairments are related to the terms of the equation (3.16) and their impact depends on the MZM bias point.

By biasing the MZM near the null point, $\lambda < \mu$ in (3.16), the DC component and the second term which are the linear OFDM signals, decrease with respect to the third and the fourth terms, which represent the mixing products of the interaction between the bands. In Figure 3.2 (a) the spectrum of the received signal is shown. We can observe that the mixing products are concentrated at the guard band. The frequency distribution of each term in (3.16) is shown in Figure 3.2 (c) according to the theoretical model proposed. The DC component and third term in (3.16) are plotted in red, the second term in (3.16) is plotted in blue and the fourth term in (3.16) is plotted in green. We can confirm that the mixing products due to the interaction of each OFDM band with itself, plotted in red, are concentrated at the GB, and the mixing products due to the interaction of two different bands, plotted in green, are also at the guard band and decrease as the frequency increases. Therefore, the first OFDM band is the most affected.

However, if the MZM is biased near the quadrature point ($V_{bias}/V_{\pi} = 0.6$), $\lambda > \mu$, the first term, which is the DC component, and the second term, which is the linear OFDM subcarriers, become more relevant than the third and fourth terms. In Figure 3.2 (b), the simulation of the resulting signal spectrum after the photodetection is presented for this MZM bias point. It can be seen that the mixing products are lower and most of the transmitted power is collected by the optical carrier. The frequency distribution is presented in Figure 3.2 (d). As expected, the DC component increases but the mixing products plotted in green and red decrease substantially. In this case, the first OFDM is less affected by the mixing products.

In this research study, we have also analyzed how the mixing products affect to the performance of the system. To this end, we analyze by numerical simulations the relationship between the BER and MZM bias point for each band of the multi-band OFDM system. As it is shown in Table 3.1, the maximum BER values are obtained for a MZM bias point of 0.9 being the BER 0.016 for the first band, 0.010 for the second band, 0.0021 for the third band and $2.28 \cdot 10^{-2}$ for the fourth band. In the rest of the cases and MZM bias points, the BER values are lower than $< 2.28 \cdot 10^{-2}$. Then, the target BER of $2 \cdot 10^{-2}$ has not been exceeded for any of the bands and MZM bias point considered.

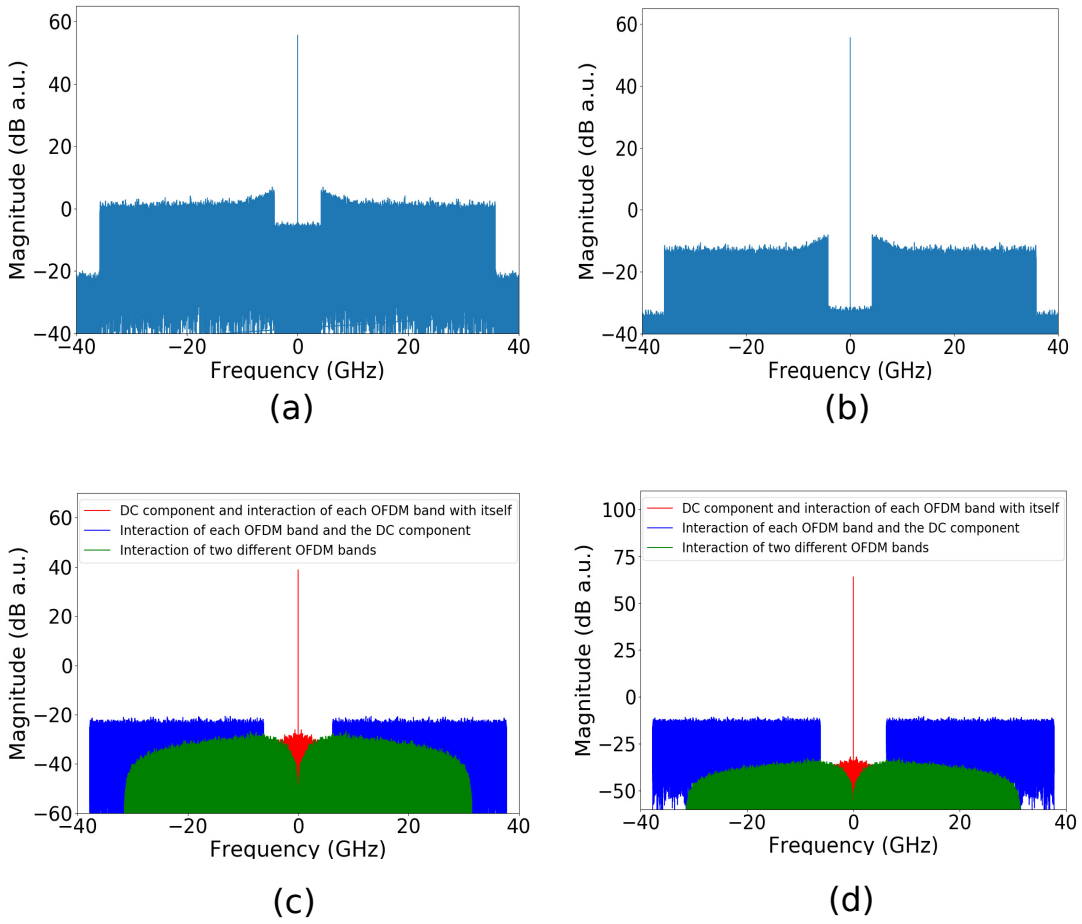

Figure 3.2: Signal spectrum after the photodetector with a MZM biased (a) near the null point ($V_{bias}/V_\pi = 0.9$) and (b) near the quadrature point ($V_{bias}/V_\pi = 0.6$) for a B2B system. Frequency distribution of the different contributions in (3.16) with the MZM biased (c) near the null point ($V_{bias}/V_\pi = 0.9$) and (d) near the quadrature point ($V_{bias}/V_\pi = 0.6$)

MZM bias	Band 1	Band 2	Band 3	Band 4	Band 5
0.9	0.016	0.010	0.0021	$2.28 \cdot 10^{-2}$	$< 2.28 \cdot 10^{-2}$
0.8	$< 2.28 \cdot 10^{-2}$	$< 2.28 \cdot 10^{-2}$	$< 2.28 \cdot 10^{-2}$	$< 2.28 \cdot 10^{-2}$	$< 2.28 \cdot 10^{-2}$
0.7	$< 2.28 \cdot 10^{-2}$	$< 2.28 \cdot 10^{-2}$	$< 2.28 \cdot 10^{-2}$	$< 2.28 \cdot 10^{-2}$	$< 2.28 \cdot 10^{-2}$
0.6	$< 2.28 \cdot 10^{-2}$	$< 2.28 \cdot 10^{-2}$	$< 2.28 \cdot 10^{-2}$	$< 2.28 \cdot 10^{-2}$	$< 2.28 \cdot 10^{-2}$

Table 3.1: BER performance for B2B transmission for each band and MZM bias point of the multi-band DD-OFDM system.

As a conclusion, we can observe that the BER performance is affected by the inter-band effects (fourth term in (3.16)) and also by the mixing products of each band with

itself (third term in (3.16)) when the MZM bias point is near the null point for a B2B transmission system. These nonlinearities are more relevant for the guard band and for the OFDM bands located close to the optical carrier.

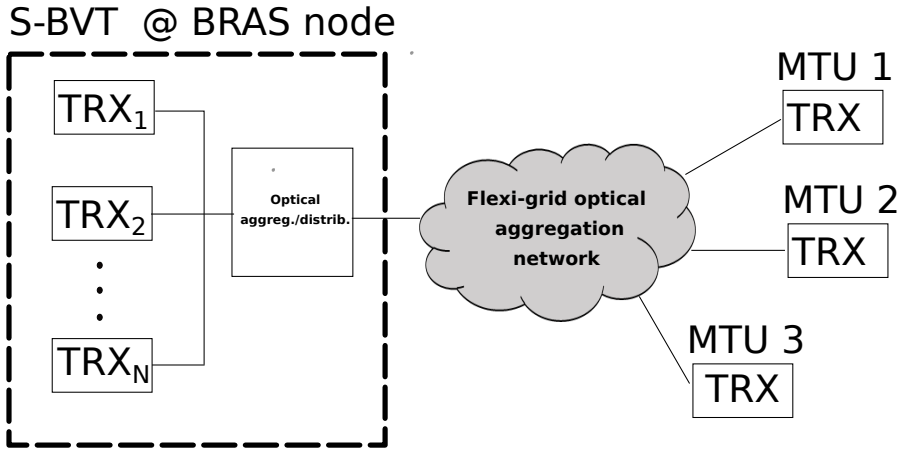

Figure 3.3: Generic architecture for BRAS-MTU connectivity. MTU: MultiTenant Unit, BRAS: Broadband Remote Access Server. S-BVT: Sliceable-Bandwidth Variable Transceiver, TRX- Transceiver.

3.5 Performance analysis in a realistic regional network

As it was introduced in section 3.1, flexi-grid involves the reduction of channel width and enables the creation of low bit rate connections, which may be used in metro area networks, leading to an evolutionary approach for this network segment [9, 55].

In this scenario, it is expected to have the Broadband Remote Access Server (BRAS) centralized and, consequently, a vast number of low bit rate connections from the virtual BRASes to the Multi-Tenant Units (MTUs) as it is shown in Figure 3.3. For BRAS centralization in a regional network, the S-BVT must be both cost-effective and robust against transmission impairments, in order to support multiple low bit rate connections over regional optical paths of hundreds of km. In this respect, advanced features of transmission technologies such as flexi-grid transponders can be exploited [55]. Within these flexi-grid transponders, the multi-band DD-OFDM system previously introduced, is considered.

The evolutionary metro/regional scenario is based on a cost-effective software-defined S-BVT. As shown in Figure 3.4, the S-BVT at the BRAS node consists of a set of virtual transceivers serving multiple MTUs located at different nodes of the network. The aggregated flow of high capacity can be opportunely sliced into N flows of lower capacity routed over different lightpaths. The bandwidth and bit rate of each flow can be varied at the DSP module by software, selecting the suitable modulation format and number of active OFDM subcarriers. Individual subcarrier bit and power loading can be performed

for optimal spectral usage and performance improvement, if specialized DSP modules based on adaptive modulation algorithms are included in the S-BVT architecture [8]. The wavelength of the flexi-grid channel is set at the Tunable Laser Source (TLS). In order to limit the array dimension and the number of optoelectronic blocks, each multi-band OFDM S-BVTx element serves a number (M) of MTUs with a single optoelectronic front-end. It uses only one laser source at the transmitter side (BVTx) and simple/cost-effective DD at the receiver side (BVRx).

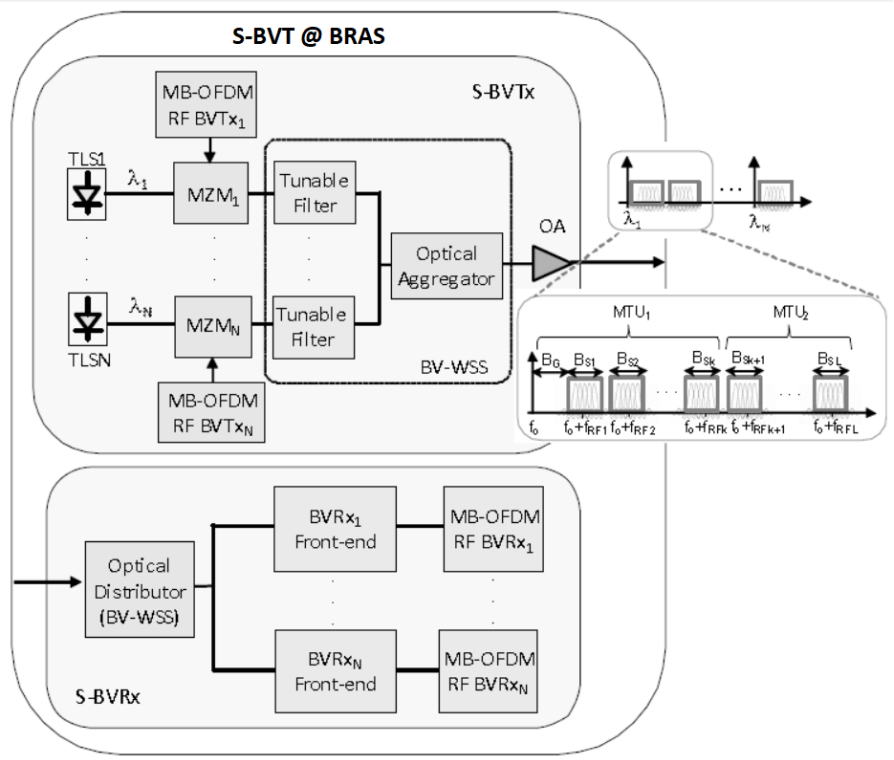

Figure 3.4: S-BVT sited at the BRAS. WSS: wavelength selective switch, MB: Multi-Band, S-BVTx: Sliceable-Bandwidth Transceiver at the transmitter. S-BVRx: Sliceable-bandwidth Transceiver at the Receiver. MTU: MultiTenant Unit.

Especially for cost-sensitive applications, a critical issue to take into account is the DAC as it was mentioned in section 3.1. The number (M) of MTUs per multi-band OFDM slice (corresponding to a single optical carrier λ_n) is limited by the DAC bandwidth and the optoelectronic components. In this analysis, we consider that the number of subbands coincides with the number of bands M, being M=5 for assuming the use of low-cost devices, a transmission bit rate of 10 Gb/s per each band using the 4-QAM format. The MZM modulator is biased at the quadrature point. The parameters used for the simulations are the same as were presented in section 3.4.

Thus, the BER performance has been analyzed for different optical paths considering the realistic regional network shown in Figure 3.5 where the region-A of the Telefonica

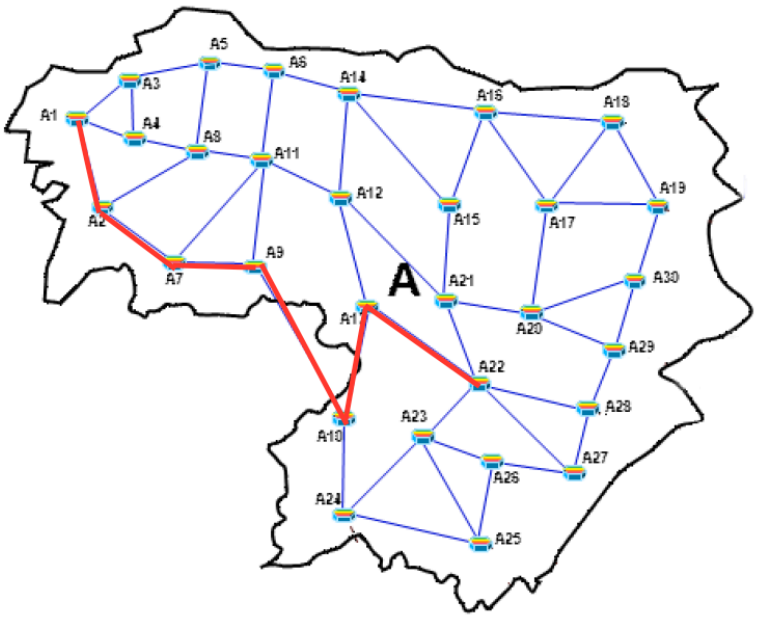

Figure 3.5: Region-A of the Telefonica Spanish network. The considered path traverses the nodes 1, 2, 7, 9, 10, 13 and 22 for a maximum length of 545km.

spanish network is illustrated. The considered path lengths cover up to 6 hops, traversing the nodes 1, 2, 7, 9, 10, 13 and 22, for a maximum length of 545 km as it is marked by the red colour in the Figure 3.5. The photodetected signal is affected by the second order nonlinear effects [7]. These effects appear mainly at the guard band and within the first band (the closest to the optical carrier) as expected according to the previous analysis. Furthermore, the path length also affects the performance of the system. As a consequence, the BER performance varies depending on the OFDM band number and the considered path.

In Figures 3.6, the BER performance of the first, third and last bands are shown, respectively. It can be observed that the results are below the target BER of $2{\cdot}10^{-2}$ (FEC threshold) for OSNR values ranging between 7 dB and 10 dB. Successful transmission is obtained for all the bands and all the paths including the worst case (corresponding to the first band and the maximum path length of 545 km). However, at the increase of the number of hops the influence of nonlinearities becomes more relevant leading to performance degradation. As expected, the first band is more affected by these effects. If a Hard-Decision FEC (HD-FEC) is considered with a target BER of 10^{-3}, the bandwidth occupancy slightly decreases due to the reduced overhead (7%). However, in none of the considered paths 10 Gb/s transmission can be supported by the first band. The third and fifth bands are less affected by nonlinearities, showing performance below the HD-FEC limit in case of few hops paths, as can be argued from Figures 3.6.

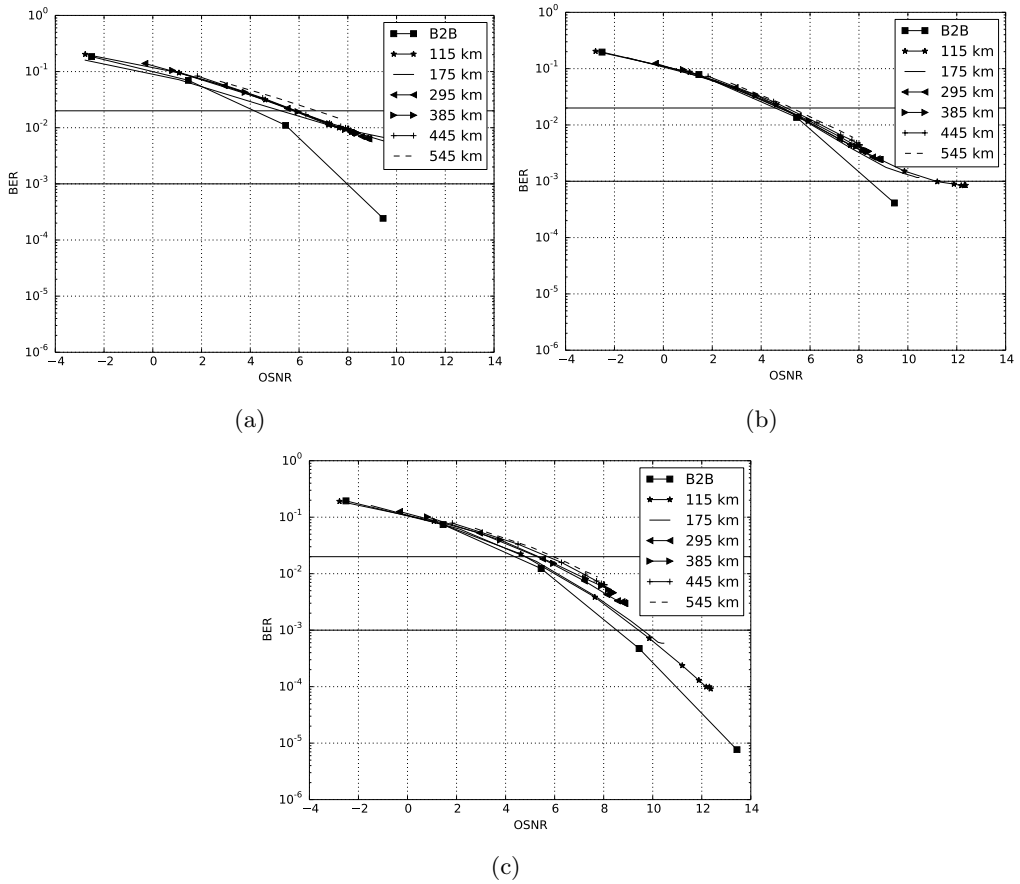

Figure 3.6: Performance BER for the (a) first, (b) third, and (c) fifth band for B2B and considering path lengths cover up to 6 hops.

3.6 Summary

In this section, we have presented a theoretical model for the photodetected signal of a multi-band DD-OFDM system. To this end, we have assumed that the MZM is biased near the null point. Based on this assumption, we have derived the theoretical photodetected expression. A multi-band DD-OFDM system based on 5 band has been proposed and simulated. The inter-band effects due to the interaction of the different bands have been studied theoretically and by the simulations, for different values of the MZM bias point.

Furthermore, a generic architecture for BRAS-MTU connectivity enabling the creation of low bit rate connections, which may be used in the metro/regional network segment, adopting flexi-grid transceivers, has been presented. The transceiver with flexible functionalities is based on the multi-band DD-OFDM technology previously introduced. The multi-band system has been validated by numerical simulations for a realistic regional network.

Some of the results are here summarized:

- The mixing products due to the inter-band effects, are located at the bands closer to the optical carrier. Thus, the performance of the system decreases for the bands that are centered at frequencies close to the optical carrier with respect to the bands centered at higher frequencies, as it was validated by numerical simulations.

- Furthermore, considering different values of the MZM bias point, we can conclude that the performance decrease is more relevant for values of $V_{bias}/V_{\pi} = 0.9$ (close to the null point), with respect to $V_{bias}/V_{\pi} = 0.6$ (close to the quadrature point).

- We have also demonstrated that with the adoption of cost-effective multi-band DD-OFDM, up to 5 bands with 50 Gb/s per flow (10 Gb/s per OFDM band) can be successfully transmitted. Particularly, a realistic regional network is analyzed considering 6 hops and the worst path (maximum length of 545km) and the multi-band DD-OFDM system proposed. We can conclude that the transmission over different paths and for all the bands has been successful. However, at the increase of the number of hops, the influence of nonlinearities becomes more relevant leading to performance degradation. This degradation is more significant for the bands that are closer to the optical carrier. In our particular case, the degradation is more obvious for the first band.

As it has been discussed in this chapter, in flexi-grid metro/regional networks, low bit rate connections can be expected (10 Gb/s). As a consequence, a cascade of several narrow bandwidth filters is envisioned, which results in a non-negligible effect, that can limit the system performance. This effect, known as filter narrowing effect, is analyzed experimentally and by numerical simulations in the next chapter, comparing On Off Keying (OOK) and advanced transmission schemes based on OFDM technology.

Chapter 4

Filter narrowing effect in EONs

4.1 Introduction

The advent of EONs and transmission techniques in terms of flexibility and capacity, has led to undertake new challenges and goals, enabling the introduction of the sliceable superchannels, as well as the reduction of channel width for low bit rate connections, outlined in section 3. This granularity is especially useful in the context of future flexi-grid optical aggregation networks, improving the spectrum utilization and network efficiency, while reducing CapEx investment.

In fact, ITU-T has standardized a flexible WDM grid, with a view to making the use of variable bandwidths in steps of 12.5 GHz possible [10], avoiding the restrictions of typical 50 GHz or 100 GHz channel spacing of fixed-grid. This allows, for example, a new 37.5 GHz slot size, providing an additional 33% of aggregated throughput when compared with the legacy 50 GHz networks [11]. To support the bandwidth elasticity, new flexi-WSSs with $\leq$ 12.5 GHz granularity at the network nodes are needed. These devices present enhanced performance and advanced features when compared with conventional WSSs [3]. Thanks to the flexible frequency slot, the transmission of superchannels can be supported, giving a further spectral efficiency.

Hence, in future flexi-grid optical networks, the wavelength allocation and channel bandwidth are variable, with bandwidth granularity of 12.5 GHz and nominal central frequency granularity of 6.25 GHz [10]. Thus, filters featuring small bandwidth are expected for low bit rate connections (e.g. 10 Gb/s). When cascading these narrow bandwidth filters, the resulting bandwidth of the optical path is substantially decreased and distorted. This can be a non-negligible effect, seriously limiting the transceiver performance. The consequent performance degradation is a concern in metro/regional networks where low bit rate connections can be expected. This reduction of the bandwidth is known as filter narrowing effect. Although this effect based mainly on Arrayed Waveguide Grating (AWG) mux/demux and Micro-Electro-Mechanical Systems (MEMS) switches or

ROADM nodes have been widely studied for architectures as in [92], it is also relevant in the context of future flexi-grid networks, where the cascade of filtering elements is envisioned [12].

In this section, the filter narrowing effect is evaluated for two approaches. The first option is a sliceable transceiver delivering flows that uses standard OOK transmission at 10 Gb/s. OOK option is heavily affected by the CD, needing compensation modules at the nodes.

The second option is based on OFDM, since it has emerged as a candidate in order to cope with elastic networking challenges [5]. Among all the OFDM possible implementations, an OFDM with SSB transmission and cost-effective DD is analysed, which is capable to cope with the targeted distances at 10 Gb/s. We have also implemented bit loading algorithms for the DD-OFDM alternative. The main advantage of using the OFDM option is that no dispersion compensation is needed at the expense of including the SSB filter at the transmitter side.

Thus, in this section, two potential candidates, that are standard OOK approach and cost-effective advanced transmission techniques based on OFDM technology, are proposed taking into account the trade-off between cost and flexibility.

The main contributions of the section are:

- The filter narrowing effect has been investigated in the context of flexi-grid optical aggregation networks, assuming narrow bandwidth connections.
- Two alternatives transmission approaches have been compared as potential candidates to investigate the optical filter narrowing effect. These alternatives are: the legacy OOK system and advanced transmission techniques based on OFDM technology.
- First of all, the concatenation of optical filters with nominal bandwidth of 12.5 GHz, 25 GHz and 50 GHz (ITU-T specifications) have been modelled according to [93]. Then, the optical filter narrowing effect have been studied and compared for both alternatives by numerical simulations using Python or Matlab software.
- Furthermore, the transmission schemes proposed have been also experimentally studied and compared in the laboratory. To do that, we have characterized the concatenation of the filters by a high resolution Optical Spectral Analizer (OSA) and then we set up the programmable filters with the obtained characterization, in order to emulate the filter concatenation impairments. Similarly to the simulation analysis, the optical filters have nominal bandwidths of 12.5 GHz, 25 GHz and 50 GHz. After that, the filter narrowing effect have been experimentally analyzed and compared for the two transmission schemes considered.
- Finally, the applicability in the metro/regional segment is evaluated.

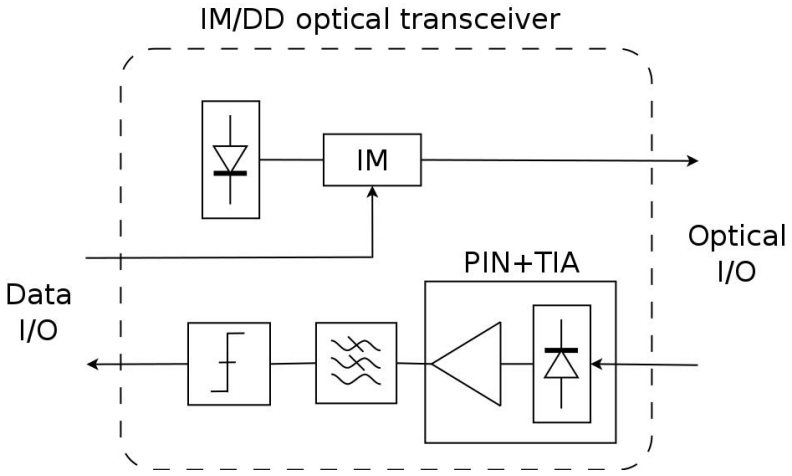

Figure 4.1: IM/DD OOK transceiver scheme. I/O: Input/Output, IM/DD: Intensity Modulation/Direct Detection.

4.2 Simulation analysis of standard OOK transmission and advanced transmission techniques based on OFDM technology

The architecture envisioned for the targeted use case was outlined in section 3.5 in Figure 3.3. There, an S-BVT is located at the BRAS premises, serving multiple low bit rates connections to the MTUs, each with the corresponding Transceiver (TRX) unit. The transmission schemes implemented at the S-BVT blocks are expected to be robust against transmission impairments, particularly against filter narrowing effect that is our case study. In this respect, we analyze two transmission schemes: simple OOK transmission with standard Intensity Modulation (IM)/DD scheme, and advanced transmission techniques based on OFDM technology.

The scheme of the OOK transceiver is shown in Figure 4.1. At the transmitter, input data is driven to an intensity modulator that is excited by a tuneable laser. At the receiver side a PIN+TIA module is used for DD, followed by an electrical low pass filter and the corresponding data decision block.

Figure 4.2 shows the OFDM-based transmitter block. At the transmitter side, the input data stream is first parallelized, mapped into a QPSK constellation and the TS are added. A CP is inserted after implementing the IFFT. After serialization, the resulting digital signal is converted into an analogue signal by a DAC. Next, the generated signal is upconverted to an intermediate frequency and modulated onto the optical carrier using a MZM biased near the null point. The output optical signal is then filtered by an optical band pass filter for implementing the SSB modulation. At the receiver, the incoming optical signal is photodetected, downconverted to baseband and further digitized by an

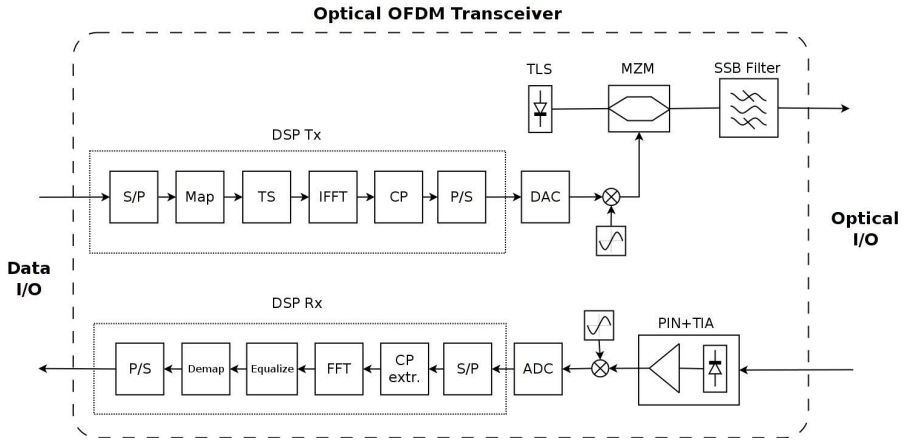

Figure 4.2: Optical OFDM transceiver scheme. TLS: Tunable Lightwave Source; MZM: Mach-Zehnder Modulator; S/P: Serial to Parallel, TS: Training Symbol insertion, CP: Cyclic Prefix, P/S: Parallel to Serial.

ADC. Afterwards, the data is OFDM demodulated following the modulation steps in the reverse order. After carrying out the FFT, training symbols are extracted in order to estimate the channel response and equalize the received symbols. Finally, data are detected after symbols de-mapping and serialization. Furthermore, for the DD-OFDM alternative the bit loading algorithm is applied. In fact, as it was introduced in section 2.3, one of the main features of OFDM is that its individual subcarriers can be set with different bit/power loads, enabling optical spectrum manipulation with sub-wavelength granularity. The different bits are loaded according to the channel state information [4]. In this case, we have implemented bit loading with a Levin–Campello MA algorithm, as in [8].

Please note that the IM/DD OOK system operates at a fixed 10 Gb/s data rate, with no DSP and legacy hardware. Along a different line, the OFDM transmitter is a low cost future-proven solution including DSP, enabling bit and power loading for optical spectrum manipulation [5].

4.2.1 Optical filters modelling

The optical filters used in the simulations are modeled according to [93]. To this extend, we carry out several spectral measurements of a commercial of-the-shelf programmable filter based on LCoS technology. Precisely, the filter is measured at a central wavelength of 1550 nm and different nominal values of the bandwidth: 12.5 GHz, 25 GHz and 50 GHz that corresponds to the ITU frequency slot, 25 GHz that correspond to two ITU elementary slots and 50 GHz that correspond to the typical fixed-grid frequency slot [10].

Results are shown in Figure 4.3. Note that the nominal values of the filter bandwidth correspond to the -6 dB bandwidth of the measurement. After carefully adjusting the

model of [93] to the measurements, the best fitting corresponds to a bandwidth of the optical transfer function of 11.77 GHz for all the measured nominal bandwidths. The results are also depicted in Figure 4.3 (a). There, we can observe that the model is perfectly matching all the measurements for relative magnitude values down to −20 dB. Accordingly, we calculate the transfer function, in terms of power, when concatenating up to 12 filters in steps of 2 filters (2 filters per node) for a filter of 50 GHz bandwidth. This is shown in Figure 4.3 (b). There, we can see that the −6 dB bandwidth of the initial filter is 50 GHz and, after concatenating 12 filters, the −6 dB bandwidth is 27.1 GHz due to the narrowing effect of the filter edges. Furthermore, in Figure 4.3 (c) the filter narrowing effect affecting the OFDM signal spectra is reflected after the concatenation of the filters.

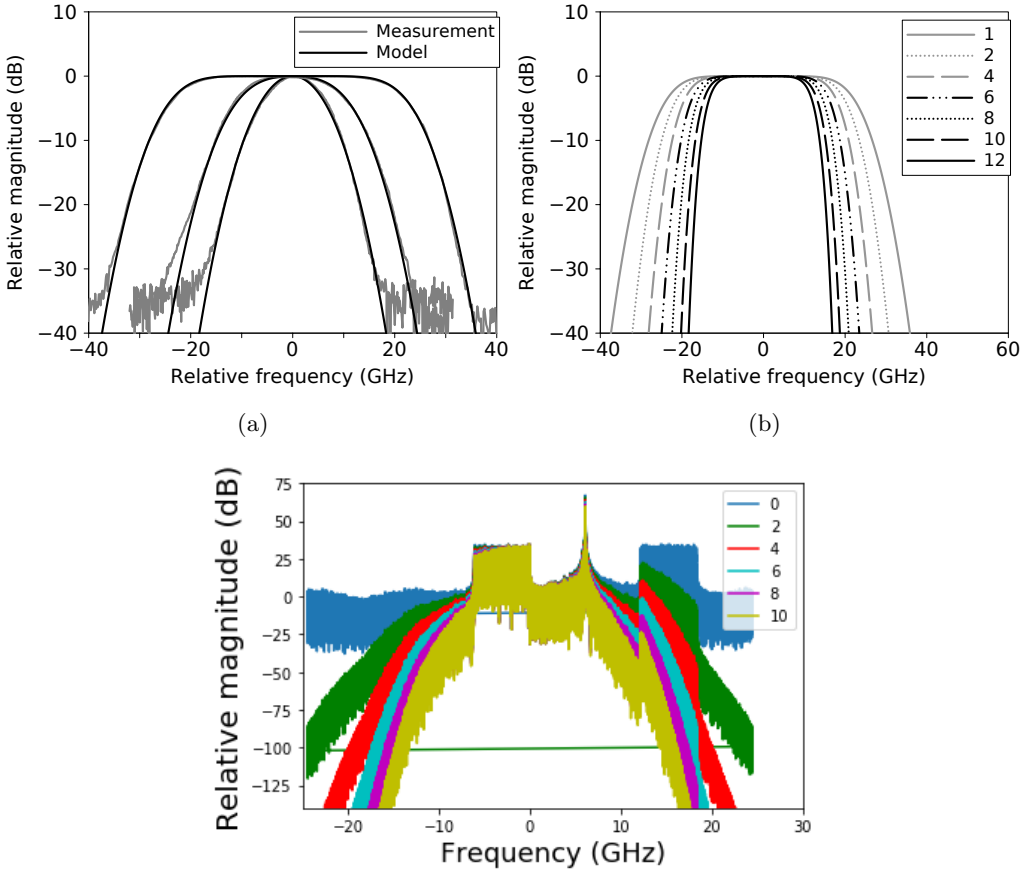

(a) (b)

(c)

Figure 4.3: (a) Model fitting of the filter for bandwidths of 12.5 GHz, 25 GHz and 50 GHz. (b) Transfer function when concatenating up to 12 times the transfer function of a 50 GHz filter. (c) Optical spectrum of the OFDM signal after being affected by several filter stages.

In Table 4.1 we can appreciate the decrease of the effective bandwidth whith the

increase of the number of filters in cascade. The reduction of the effective bandwidth when we consider 2 and 12 filters is 18.8 GHz when the nominal bandwidth of 50 GHz is considered, 9.38 GHz in the case of filter with nominal bandwidth of 25 GHz and 5.88 GHz if the nominal bandwidth of the filter is 12.5 GHz.

Nominal Bandwidth (GHz)	Number of filters in cascade	Bandwidth @ −6 dB (GHz)
50	2	45.9
	4	41.36
	6	37.52
	8	34.36
	10	30.86
	12	27.1
25	2	19.94
	4	16
	6	13.6
	8	12.34
	10	11.4
	12	10.56
12.5	2	10.2
	4	7.48
	6	6
	8	5.2
	10	4.68
	12	4.32

Table 4.1: Resulting bandwidths at −6 dB of the relative magnitude for the concatenation of 2, 4, 6, 8, 10 and 12 filters, considering filters with nominal bandwidths of 50 GHz, 25 GHz and 12.5 GHz.

4.2.2 Simulation assessment

The performance of the proposed system is assessed by means of numerical simulation using Matlab and Python software. Both approaches have been evaluated by means of Monte Carlo error counting, which provides the best estimation the system BER. In both cases, a target BER limit is set to 10^{-3} , assuming a HD-FEC coding scheme. In fact, a super FEC RS(1023,1007)/BCH(2047,1952) code can serve to this purpose, increasing the signal overhead up to 7% [94]. Additionally, a $2 \cdot 10^{-2}$ target BER is also taken into account for the OFDM alternative, as it is a more flexible solution with rate/distance adaptation capabilities and a SD-FEC scheme can be envisioned [95].

Regarding the IM/DD OOK system, a data set of 2^{17} pseudorandom bits is generated using a sequence of $2^{15} - 1$ running at 10.7 Gb/s, to consider the 7% HD-FEC overhead.

Next, data is transmitted at 1550 nm using intensity OOK with an extinction ratio of 10 dB and transmitter output power of +3 dBm.

The optical carrier is modelled as an ideal CW laser with 5 MHz linewidth. At the receiver side, after optical pre-amplification and filtering, the photodetector is modelled as standard PIN, featuring 0.7 A/W responsivity, dark current of 10 nA and thermal noise of 16 nA/sqrt(Hz). The photodetected current then traverses a 5^{th} order Bessel filter with 8.56 GHz bandwidth. Afterwards, data is downsampled and detected at the data decision stage.

For the OFDM, 2^{16} bits are randomly generated running at 10 Gb/s net data rate. Next, the bit sequence is parallelized, QPSK encoded and OFDM modulated to 512 subcarriers using the IFFT. The OFDM symbols are serialized and upsampled to emulate the DAC. The resulting signal is upconverted to an intermediate frequency of 9.17 GHz and injected to the MZM which is excited by a CW laser with 5 MHz linewidth. In order to achieve SSB transmission an optical bandpass filter of 25 GHz is placed after the MZM. At the receiver, the photodetector is modelled as PIN diode with the same parameters used for the OOK system. Intermediate frequency downconversion, filtering, OFDM decoding and data demodulation are performed after photodetection. The total signal overhead is 22.2%, in order to consider also a SD-FEC. Accordingly, the generated OFDM signal is operating at 6.11 Gbaud and, after SSB filtering, the optical bandwidth occupied is 12.2 GHz. The bandwidth of the SSB filter was selected after doing some simulations with different values of the filter bandwidth. Finally, we concluded that a bandwidth of 25 GHz was wide enough so as to not distort the signal spectrum. The SSB filter is centered on 6.11 GHz. Thus, the OFDM signal and the optical carrier are less affected by the SSB filter. This displacement of the SSB filter is fixed for the concatenation of the filters. The central frequency of the concatenation of filters remains constant for the different numbers of filters.

The performance of the proposed systems is assessed in terms of B2B OSNR requirement within 0.1 nm. Since typical broadcast and select architectures consider two filtering stages per node, we carry out the study considering the concatenation of up to 12 filters (6 hops). The filters are considered to have nominal bandwidth of 50 GHz, 25 GHz and 12.5 GHz, as it was mentioned above. Results are shown in Figure 4.4.

The 50 GHz case is depicted in Figure 4.4 (a) for OOK and (d) and (g) for OFDM. Neither the OOK nor the OFDM signals are affected by the filter narrowing effect. The required OSNR for the HD-FEC target BER is 10.7 dB for OOK, 12.0 dB for OFDM and 12.3 for adaptive OFDM at all the filter stages examined. 8.7 dB OSNR can also be a suitable requirement for OFDM, as it has the ability of switching the FEC coding scheme from HD-FEC to SD-FEC.

When considering 25 GHz filters, the required OSNR ranges from 10.7 dB up to 17.2 dB for the OOK case, whereas the OFDM system needs OSNR values within 12.0 dB

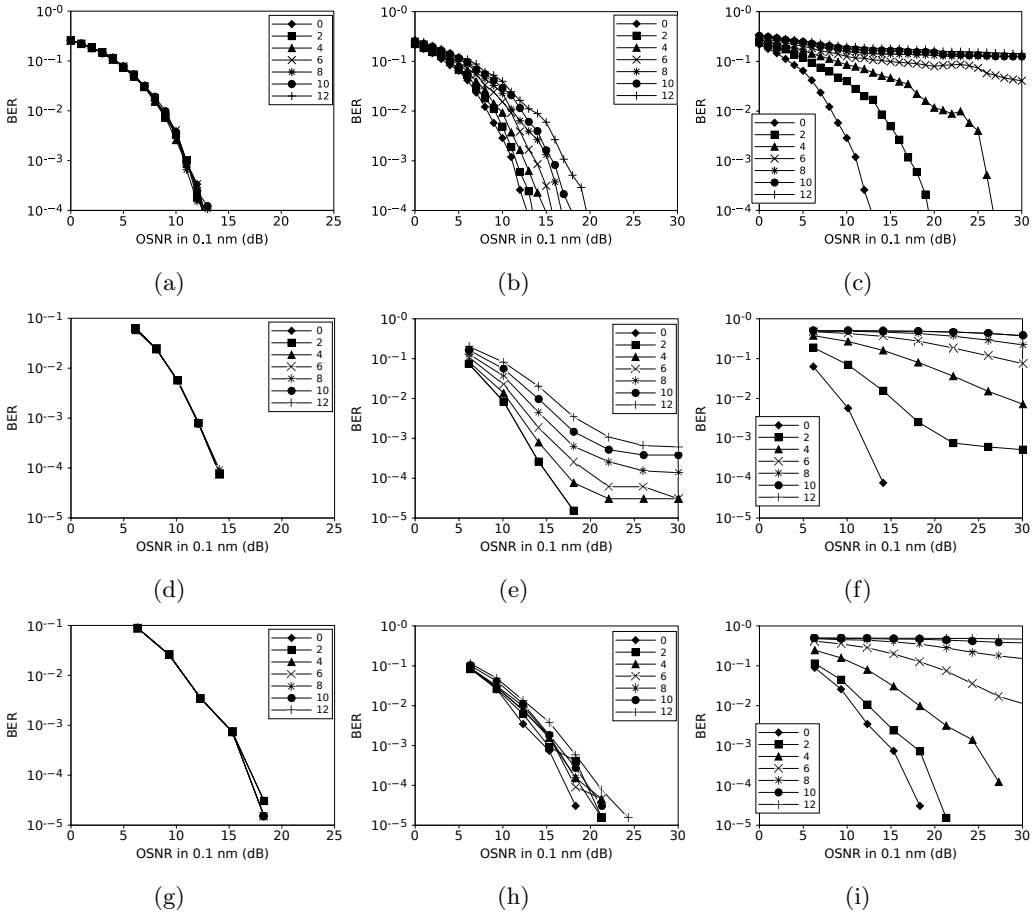

Figure 4.4: Simulation results for a standard IM/DD system (a, b, c), the OFDM SSB transceiver (d, e, f), the OFDM SSB transceiver using bit loading (g, h, i) after concatenation of different filters featuring bandwidths of 50 GHz (a, d, g), 25 GHz (b, e, h) and 12.5 GHz (c, f, i).

and 22.7 dB and adaptive OFDM 12.3 dB up to 15.0 dB to achieve the HD-FEC target BER. In case SD-FEC is used in OFDM, the OSNR requirement is relaxed to the range between 8.7 dB and 14.0 dB and within 10.1 dB y 11.8 dB for adaptive OFDM.

Finally, the case of filters with 12.5 GHz is analysed. As expected this is the worst examined case. Indeed, OOK can only meet the HD-FEC target BER after 2 and 4 filtering stages, with 17.2 dB and 25.7 dB OSNR, respectively. For the OFDM system, similar degradation is observed and it meets the proposed HD-FEC target BER after 2 filtering stages with 21.5 dB OSNR. For adaptive OFDM for 2 and 4 intermediate filtering stages the OSNR required is 14.6 dB and 20.7 dB, respectively.

In case the SD-FEC limit is used, OFDM can be suitable for 2 and 4 filtering stages requiring 14.1 dB and 25.9 dB OSNR, respectively. For the adaptive OFDM, the values are 9.7 dB and 11 dB respectively for 2 and 4 filtering stages.

4.3 Experimental analysis of standard OOK transmission and advanced transmission techniques based on OFDM technology

After the previously simulations analysis, in this section, we focus on the experimental analysis of the signal distortion due to the filter narrowing effect for low bandwidth connections. To this end, we first characterize the concatenation of 2 up to 12 filters (2 filters per node). After that, we analyze the filter narrowing effect for the OOK and the OFDM technology mentioned above.

The experimental setups for the OOK and OFDM transmission schemes are illustrated in Figure 4.5. The optical domain part of the experimental setups is common for both alternatives. Specifically, the OOK or OFDM electrical signal is converted to the optical domain by a MZM biased near to the null point for DD-OFDM or quadrature point for OOK. A laser centered at 1550.12 nm with 13.99 dBm output power is used. In order to achieve SSB transmission after the MZM and only for the DD-OFDM alternative, the signal is optically filtered with a filter of 25 GHz bandwidth resulting in an optical bandwidth of 12.22 GHz, including 6.11 GHz of guard band. Then, for both alternatives, the optical signal traverses the cascade of filters modeled by the programmable filter. After that, a Variable Optical Attenuator (VOA) and an Erbium Doped Fiber Amplifier (EDFA) are used to vary the OSNR at the receiver. Additionally, an Amplified Spontaneous Emission (ASE) filter of 50 GHz bandwidth and an OSA are added before the photodetection.

For the OOK case, the signal is generated by an arbitrary waveform generator as a pseudorandom binary sequence of $2^{15}-1$ bits at 10.7 Gb/s with 7% HD-FEC overhead. The total signal bandwidth is 10.7 GHz. At the receiver, the signal is converted into the electrical domain by means of a PIN and captured with a real-time oscilloscope, which is also used to analyze the eye pattern and estimate the BER. The received signal spectrum is shown in Figure 4.5 d).

For the DD-OFDM transmission setup, the DSP modules at the transmitter and at the receiver are the same as for the simulations previously presented. The main difference is that after the DSP at the transmitter, the signal is converted to analog by a DAC, but due to the limited bandwidth of the DAC, after the DSP transmitter, a pre-emphasis digital filter is included to compensate the system performance degradation. At the receiver, the signal is photodetected by a PIN and captured by a 100 GS/s real-time oscilloscope. The received signal spectrum is shown in Figure 4.5 e) and its bandwidth results in 6.11 GHz.

In addition, for the DD-OFDM system alternative we have also considered bit loading. Adaptive bit assignment is performed according to the channel state information estimated with a probe signal [4]. Bit loading is implemented with a Levin-Campello

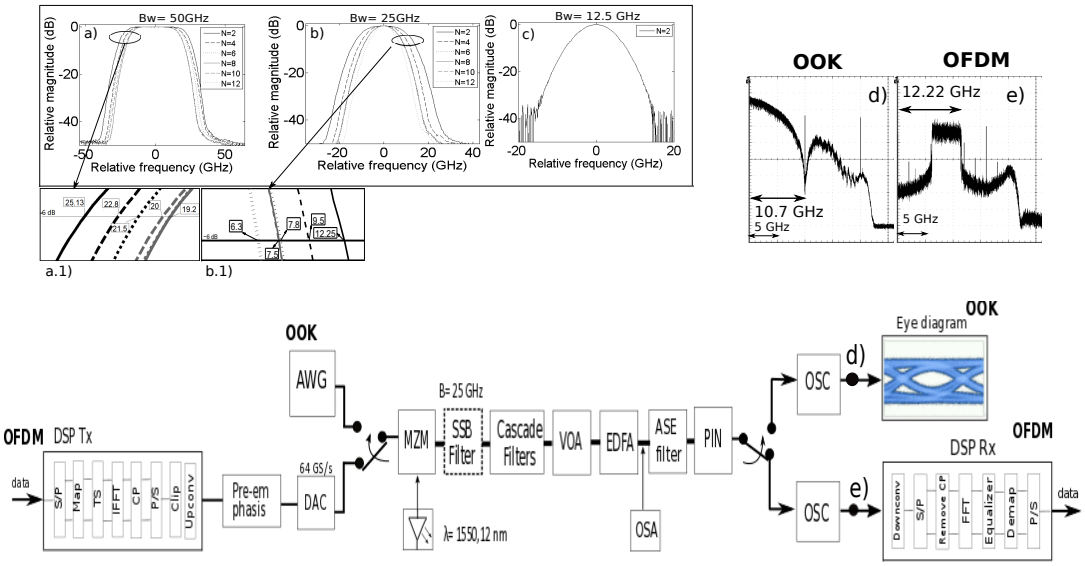

Figure 4.5: Experimental setup for OOK and DD-OFDM approach. Cascade filters characterized by the OSA for nominal bandwidths of 50 GHz a), 25 GHz b) and 12.5 GHz c). Received spectra after the oscilloscope for OOK d) and OFDM e) alternatives. A zoom of the area of interest of the 50 GHz filter nominal bandwidth a.1) and for the 25 GHz filter nominal bandwidth b.1). AWG: Arbitrary Waveform Generator, Bw: Bandwidth, OSC: OSCiloscope

MA algorithm, as in [13], set to operate at 10 Gb/s.

4.3.1 Filter transfer function characterization

Similarly to the simulation analysis, we study the case of filters with nominal bandwidths of 12.5 GHz, 25 GHz and 50 GHz, that correspond to the envisoned flexi-grid frequency slot [26], and a node architecture with two filters per node (up to 12 filters) [13].

To do this, we characterize the programmable filters with nominal bandwidths of 12.5 GHz, 25 GHz and 50 GHz according to the model of [93]. We concatenate the filters in steps of 2 filters up to 12 filters for each value of the nominal bandwidths. Then, we carry out the estimation of the filter concatenation by means of a high resolution OSA. Then, we set up the programmable filters with the obtained characterization.

Figure 4.6 (a) shows the transfer functions of the characterized filters and the modeled filters. There, we can observe that the model is perfectly matching all the experimental characterization for relative magnitudes values down to -25 dB. This is also reflected in Figure 4.6 (b) where the relative error between the model and the experimental filter characterization is illustrated. It can be observed that the maximum error is -0.37 dB for a frequency within ± 6.25 GHz for the 12.5 GHz nominal bandwidth filter. For the 25 GHz bandwidth filter, the maximum error is 0.33 dB within ± 12.5 GHz and,

similarly, for the 50 GHz bandwidth filter this error is 1.15 dB within ±25 GHz. We can also observe that the minimum frequency interval needed by the filter to achieve a −40 dB of relative magnitude is within −39 GHz and 35 GHz for a nominal bandwidth of 50GHz, within −26 GHz and 24 GHz for a nominal bandwidth of 25 GHz and within −18 GHz and 22 GHz for a nominal bandwidth of 12.5 GHz.

In Figure 4.5 [a-c] the transfer functions of the characterized filters for the above-mentioned nominal bandwidths in steps of 2 filters up to 12 are shown. It can be observed that at the increase of the number of concatenated filters, the narrowing of the filter bandwidth is more pronounced. In fact, the difference between the concatenation of 2 and 12 filters in terms of bandwidth reduction is 10 GHz (from 50 GHz to 40 GHz) for the 50 GHz nominal bandwidth filter and 12 GHz (from 24.5 GHz to 12.5 GHz) for the 25 GHz nominal bandwidth filter at −6 dB of the relative magnitude. A zoom of the area of interest of the 50 GHz and 25 GHz nominal bandwidth filters transfer function is illustrated in Figure 4.5 a.1) and b.1). In the case of the 12.5 GHz nominal bandwidth filter, where we only consider the concatenation of 2 filters, the resulting bandwidth is 5 GHz.

Nominal bandwidth (GHz)	Number of filters in cascade	Modeled bandwidth @ −6 dB (GHz)	Experimental bandwidth @ −6 dB (GHz)
50	2	45.9	50.26
	4	41.36	45.6
	6	37.52	43
	8	34.36	40
	10	30.86	38.4
	12	27.1	38.4
25	2	19.94	24.5
	4	16	19
	6	13.6	15.6
	8	12.34	15
	10	11.4	15
	12	10.56	12.6
12.5	2	10.2	5

Table 4.2: Comparison of the resulting bandwidths at −6 dB of the relative magnitude for the concatenation of 2, 4, 6, 8, 10 and 12 filters considering filters with nominal bandwidths of 50 GHz,25 GHz and 12.5 GHz for the modeled and the experimental filter characterization.

A comparison of the effective bandwidth is shown in Table 4.2 for the concatenation of 2, 4, 6, 8, 10 and 12 filters for the model and the experimental case. We can appreciate the decrease of the effective bandwidth with the increase of the number of filters in cascade, for both cases. This decrease of the effective bandwidth is more pronounced for the model than for the experimental filter characterization. However, if we consider the filter with nominal bandwidth of 12.5 GHz, the effective bandwidth of the experimental filter characterization is lower (5 GHz) than for the model (10.2 GHz). For this last nominal bandwidth it was not possible to obtain the characterization of more than 2 filters in cascade.

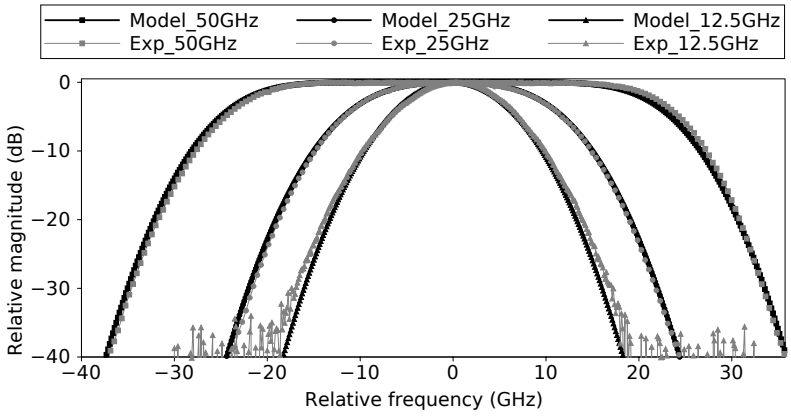

(a)

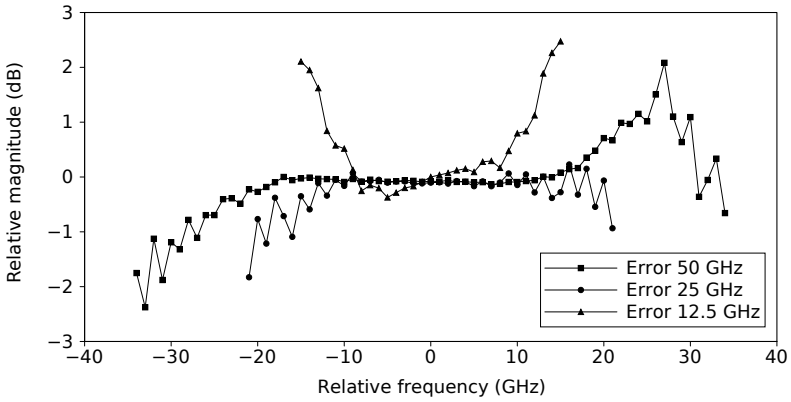

(b)

Figure 4.6: (a) Model fitting of the experimental filter characterization for bandwidths of 12.5 GHz, 25 GHz and 50 GHz. (b) Relative error between the model and the experimental filter characterization for bandwidths of 12.5 GHz, 25 GHz and 50 GHz.

As we will see in the upcoming sections, the BER characteristic will be affected by the nominal bandwidth of the filters, the filter narrowing effect due to the concatenation of the filters and hence the spectral characteristics of the signal.

4.3.2 Experimental assessment

The performance of the proposed system is assessed in terms of B2B OSNR requirements within 0.1 nm. The target BER is set to 10^{-3} assuming the HD-FEC coding scheme [13]. We also define the OSNR penalty as the difference between the OSNR required for the concatenation of 2 filters and 12 filters at target BER.

The 50 GHz case is depicted in Figure 4.7 (a), (b), (c) for the OOK and DD-OFDM schemes, this last using uniform loading and bit loading. The OOK signal is not affected by the filter narrowing effect for all the examined filtering stages, being 16.7 dB the required OSNR for the target BER. Nevertheless, for the DD-OFDM, the OSNR ranges

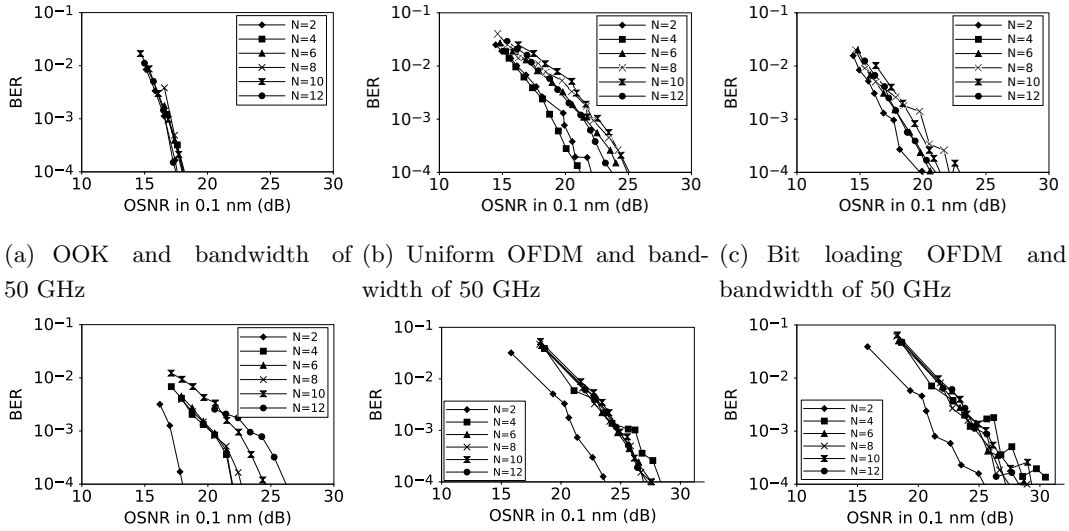

(a) OOK and bandwidth of 50 GHz

(b) Uniform OFDM and bandwidth of 50 GHz

(c) Bit loading OFDM and bandwidth of 50 GHz

(d) OOK and bandwidth of 25 GHz

(e) Uniform OFDM and bandwidth of 25 GHz

(f) Bit loading OFDM and bandwidth of 25 GHz

Figure 4.7: BER vs OSNR for the OOK approach (a and d), DD-OFDM approach using uniform loading (b and e) and bit loading (c and f) after cascade filters with bandwidths of 50 GHz (a, b, c) and 25 GHz (d, e, f).

between 18.7 dB and 22.5 dB for uniform loading and between 17.7 dB and 20 dB for bit loading. Therefore, the OSNR penalty results in 3.7 dB for uniform loading and for bit loading it decreases to 2.3 dB approaching to the performance characteristic of the OOK.

When we consider 25 GHz filter for the OOK scheme, the BER characteristics are more scattered than in the previous case, being the OSNR within 17 dB and 23.5 dB as it is shown in Figure 4.7 (d). The OSNR requirements for DD-OFDM with uniform loading and bit loading are around 21.1 dB for two filtering stages as it is shown in Figure 4.7 (e) and (f). However, it can be seen that, after two filtering stages up to 12 filters, the OSNR requirements remain concentrated around 26.5 dB for both. These last results are directly related to the transfer function of the filter concatenation shown in Figure 4.5 b) and in Figure 4.5 b.1). There, we can observe a significant reduction of the bandwidth between the concatenation of 2 filters and the concatenation after 4 up to 12 filters, leading the worsening of the performance characteristic in terms of OSNR. To be more precise, the value of the bandwidth after the concatenation of 2 filters is 24.5 GHz whereas after 4 up to 12 filters the corresponding bandwidth is within 19 GHz and 12.5 GHz. Therefore, it is noted that the OSNR is concentrated around 26.5 dB for an effective bandwidth smaller than 19 GHz.

Finally, the case of filter with 12.5 GHz of bandwidth is analyzed. The target BER of 10^{-3} can be achieved only after 2 filters. The experimental results are shown in

Figure 4.8. It can be seen that the OSNR at target BER is 19.3 dB for OOK and around 23 dB for DD-OFDM with uniform loading and bit loading.

As it was previously advanced, the bandwidth occupied by the signal is also of great relevance, in order to explain the performance degradation of the BER characteristic, when the effective bandwidth filter is reduced. The optical bandwidth of the signal, when we use the OOK system, is 10.7 GHz. The spectrum of the signal, can be seen in Figure 4.5 d). Considering the 50 GHz of filter nominal bandwidth, the minimum value of the effective bandwidth is near 40 GHz, and corresponds with the concatenation of 12 filters. Then, the bandwidth is wide enough with no effect in the system performance (Figure 4.7 (a)). However, using the 25 GHz of nominal bandwidth filter, we can see as the value of the effective bandwidth is close to the bandwidth of the signal, the performance decreases (Figure 4.7 (d)). It is the case of the concatenation of 12 filters that corresponds with a effective bandwidth of 12.5 GHz, which is very close to the 10.7 GHz and where the OSNR reaches its maximum value (23.5 dB at target BER).

Considering the OFDM alternative, the signal bandwidth is within 6.11 GHz and 12.22 GHz. The spectrum is shown in Figure 4.5 e). For the 50 GHz filter, there is a BER degradation after the concatenation of 4 filters as a consequence of the effective bandwidth reduction. This reduction can be appreciated in Figure 4.5 a.1). The degradation is also due to the spectral signal characteristic. In fact, the OFDM subcarriers loaded with data, are located at the edge of the occupied bandwidth, while the main data content of the OOK signal is located close to the optical carrier. As a result, the BER performance for the OFDM case is more affected. However, using the bit loading we can observe an improvement of the BER giving similar performance as OOK (Figure 4.7 (a),(b) and c)). For 25 GHz and 12.5 GHz of filter nominal bandwidth, the decrease of the effective bandwidth due to the similar values of the signal bandwidth, entails a further degradation of the BER performance (Figure 4.7 (e) and (f) and Figure 4.8). For example, if 2 filters are concatenated using the filter nominal bandwidth of 12.5 GHz, the resulting effective bandwidth is 5 GHz. This value is much smaller than the 12.22 GHz of the OFDM signal bandwidth. Therefore, the decrease of the effective bandwidth limits the benefit of applying bit loading.

4.4 Summary

Highly efficient and adaptive management of the optical spectrum is achieved by using flexi-grid technology [5]. Particularly, its applicability in metro/regional networks is appropriated and interesting also for low data rate envisioned, to provide for example the BRAS-MTU connectivity, as the use case mentioned in section 3.5. The flexi-grid paradigm involves that the signal traverses several nodes, so that the system performance can be affected. Thus, in this section, the filter narrowing effect is studied considering

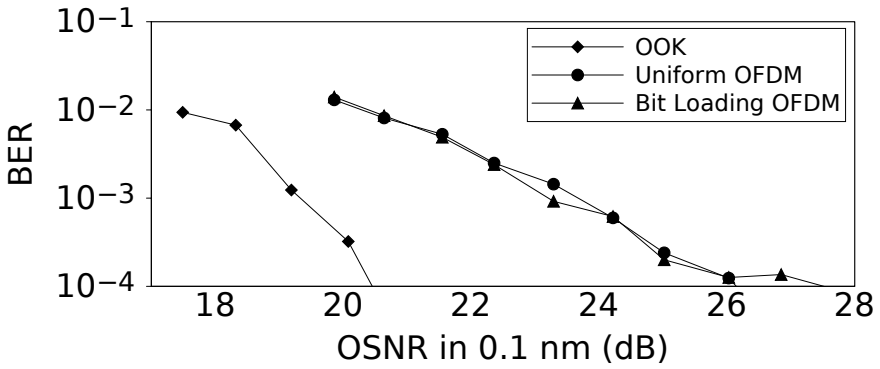

Figure 4.8: BER vs OSNR for the OOK approach, the DD-OFDM SSB approach using uniform loading and bit loading after 2 filters with bandwidths of 12.5 GHz.

two alternatives solutions: legacy OOK and advanced transmission techniques based on OFDM technologies with and without considering bit loading algorithms, trading cost and flexibility. We evaluate both alternatives taking into account that flexible and adaptive transceivers are a key element to cope with the future envisioned flexi-grid scenario.

First of all, the filter narrowing effect considering both solutions, have been analyzed by numerical simulations. Some of the results are here summarized:

- We have shown that advanced transmission techniques based on OFDM technologies are a feasible candidate, providing increased flexibility, thanks to its ability to set different performance target, when taking into account the filter narrowing effect.
- Severe filtering penalties are observed when employing single ITU-T elementary slot (12.5 GHz) for both transmission technologies, being the maximum number of intermediate nodes to traverse 2 (corresponding to the concatenation of 4 filters).
- In case of using two elementary slots (25 GHz), the filtering penalties are limited to 5.9 dB for OOK, 9.7 dB for SSB DD-OFDM and 2.7 dB for adaptive SSB DD-OFDM technology.
- Results show that adaptive SSB DD-OFDM provides increased flexibility and robustness to transmission impairments without dispersion compensation.

The filter narrowing effect has been also experimentally analyzed for legacy 10G OOK transmission system and advanced transmission systems based on OFDM technology. Some of the achieved results are summarized below:

- The impact on the system performance increases for the filters with nominal bandwidths of 12.5 GHz with respect to 25 GHz and 50 GHz for both solutions. The

performance degradation is more pronounced in DD-OFDM systems than in OOK systems. This performance degradation is due to the reduction of the effective bandwidth filter and also due to the bandwidth characteristics of the signal. Despite this, it is shown that OFDM is a feasible candidate since the creation of the generic flexi-grid mesh implies flexibility and adaptability, which fits with the essence of the OFDM principles, thanks, for example, to the manipulation capabilities at the subcarrier level.

- Furthermore, OFDM scheme avoids the need of dispersion compensation modules at the network nodes that in OOK systems are required.

As a general resume of this section, we can point out that advanced transmission techniques based on adaptive OFDM technology, unlike OOK, offer interesting features, such as flexibility and adaptability thanks to the ability of the individual control of its carriers. Thus, S-BVTs based on flexible transceivers using adaptive OFDM technology results in a cost-efficiency and robust solution against transmission impairments, meeting the needs of the envisioned metro/regional networks.

In the next chapter, we propose an advanced transmission technique based on DMT modulation, which is the simplest version of the OFDM technology, for a cost-effective BVT implementation. Particularly, the study analyzes the system performance of a programmable adaptive BVT adopting SOA-based switching nodes, in the context of optical metro networks.

Chapter 5

Adaptive BVT based on DMT modulation adopting SOA-based switching nodes

5.1 Introduction

Adaptive S-BVT are key enablers for future optical networks. Multiple parameters and S-BVT components can be suitably configured on demand by means of an integration of the transceiver in a SDN control plane, following the SDN principles [96]. As it was introduced in this thesis, in the context of optical metro networks requirements as cost-efficiency, reduced power consumption as well as high capacity and dynamicity can be dealt with the implementation of flexible, adaptive and programmable transmission and switching systems able to efficiently manage the available resources as well as the high peak of traffic and adaptive bit rates with cost- and power-efficient solutions [1,20]. In this section, we propose the analysis of a S-BVT architecture based on a DMT modulation as the simplest version of the OFDM implementation for a cost-effective design [4, 8].

In this context, Semiconductor Optical Amplifier (SOA) technology can be advantageously used, particularly for the metro segment, where the cost and power consumption are critical issues. In fact, the main advantages of using SOAs are the low power consumption, low cost, small size, and the possibility to be integrated with other optical components [97]. On the other hand, SOAs have high noise value compared to EDFA and have residual polarization-dependent operation < 1 dB [98]. There are some studies, such as in [99], focusing on the reduction of these impairments. SOAs can be designed to deploy building blocks for optical switching as well as a booster amplifier, inline amplifier, or preamplifier [100, 101]. By carefully adjusting the current injected into the SOA, it can be used as an optical amplifier; meanwhile, by turning on/off the electri-

cal current, the SOA can act as a fast optical gate. Furthermore, SOAs can be used for wavelength selective applications by combining them with wavelength-filtering technologies [97]. In this thesis, we focus on the role of SOAs as building blocks in optical switching technologies [100].

In particular, we consider an SOA-based switching node with and without filtering elements. In the last case, the switching functionalities are performed by the SOAs and can also find application in filterless optical networks [102]. Filterless optical networks are simple network architectures based on passive splitters and combiners avoiding optical filters. Thus, they are more cost-effective than networks adopting filters; however, some functionalities are limited, such as wavelength reuse or capacity at high utilization rates [13, 102]. In [102], a comparison between the filterless option and active switching, in terms of cost and performance, is provided. In the case where SOAs are combined with wavelength-filtering technologies, we consider SOA-based wavelength selectors as part of the Optical Add/Drop (OAD) nodes. These nodes have the capacity to insert or drop traffic to the optical network, by means of a SOA array with a splitter, a combiner and filtering elements based on WDM technology [100]. WDM technology allows the multiplexing of multiple signals with different optical carrier wavelengths. In visible light communications, the performance of WDM technology is limited due to transmission losses [103]. Some studies propose the design of a novel 1x4 optical demultiplexer based on multimode interference [103] to overcome this problem. In the range of C band for optical communications, an 8-channel wavelength multimode demultiplexer is demonstrated to work with low cross-talk [104]. WDM cross-connect switches combined with SOA technology have been assessed in [97,105]. The system is validated considering three different types of modulation formats, such as NRZ OOK, PAM and DMT. Potential lossless operation and low cross-talk (< -30 dB) has been demonstrated. Using BVTs, the bandwidth and bit rate can be dynamically adjusted by adopting a modulation format per each subcarrier. Therefore, more flexibility and adaptability can be obtained [106].

In this section, we present an analysis of a cost-effective S-BVT architecture based on DMT modulation in the context of elastic optical metro networks with switching nodes adopting SOA technology.

The contribution of this chapter can be summarized in several points:

- We analyze a cost-effective S-BVT architecture with programmable functions. Particularly, we propose a S-BVT based on DMT modulation with DD as a suitable solution to address the cost-efficiency requirements of optical metro networks.

- Furthermore, we propose the adoption of SOAs in the switching node architecture since it represents a cost-efficiency solution to compensate the attenuation due to passive elements and the transmission over the fiber links.

- Then, a BVT based on DMT modulation using bit loading and power loading algorithms implemented at the transceiver DSP module, [4, 8] is combined with SOA-based switching nodes to maximize the performance and the capacity as well as enhance the flexibility, adaptability of the system and the resilience towards transmission impairments. To analyze the performance of this approach two possible scenarios are proposed. One of them considers the use of simple SOAs in the switching node, while the second scenario considers the SOA as the key element of an OAD node. In both cases we use fiber spans of 25 km.

- As a preliminary assessment the impact of the SOAs as switching node element have been studied for different transmission distances. After that, both scenarios have been compared with and without considering filtering elements. The effects on the transmission performance caused by the filtering elements with respect to the case when no filtering elements are used, is analyzed.

5.2 Cost-effective (S)-BVT architecture based on DMT modulation

The S-BVT is a key element in EONs since it supports programmable functions and multi-adaptive, software-defined optical transmission. A general architecture proposed for future optical metro networks is shown in Figure 5.1. It is composed by N BVT modules. The multiple flows are aggregated/distributed at the output of the array of the N BVTs by an additional element, which can be implemented for example by a flexible WSS [4].

To design the optoelectronic front-ends for an S-BVT, we can consider simple architectures using DD receivers. For the experiments, we propose a cost-effective BVT solution, based on DMT using DD. Despite the simplicity of DMT, the CD can limit the system performance due to the transmission over the fiber [8]. At the increase of the fiber length, the impact of the CD is higher. As a result, various subcarriers, corresponding with certain frequencies, are highly attenuated. The frequencies were the attenuation peak appears, depends on the speed of light, the center wavelength, the fiber length, or the dispersion parameter. To mitigate this effect loading algorithms can be implemented to adapt the modulation format to the channel profile [8].

In DMT system, HS is forced on the input of the IFFT obtaining a real signal [8]. Thus, the complexity of the DSP module is reduced. The main building blocks of a DMT-based BVT are illustrated in Figure 5.1. At the transmitter, the input data is parallelized. After that, the signal is mapped adapting loading using BPSK and M-QAM or with uniform loading, using 4-QAM. According to the SNR profile, estimated at the receiver, with a uniform loaded probe signal, the DMT subcarriers are modulated at the transmitter side using bit loading and power loading algorithms. The algorithms have

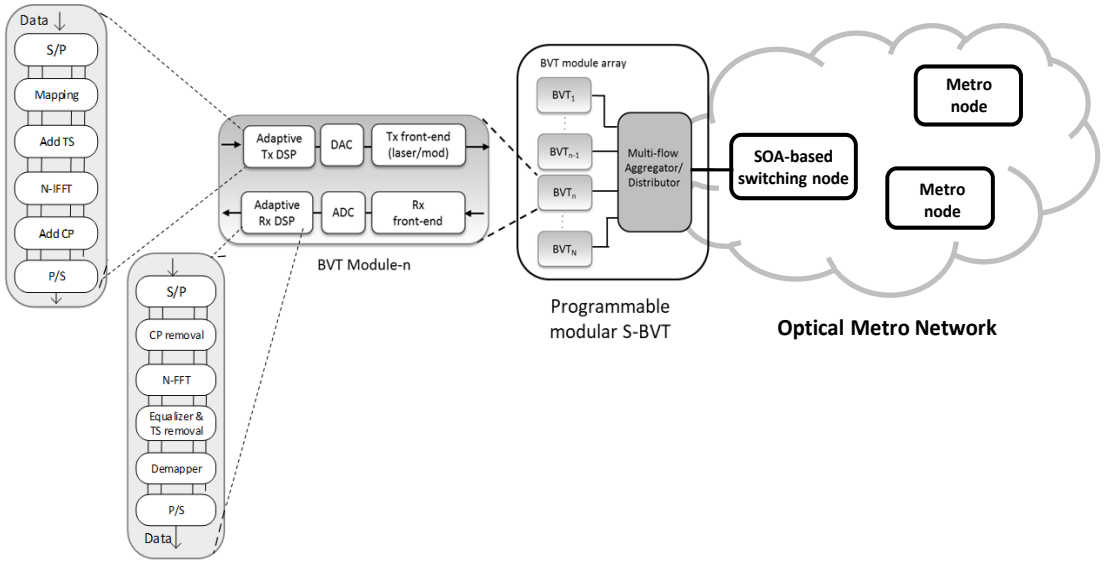

Figure 5.1: S-BVT architecture proposed and building blocks. S/P: Serial to Parallel, TS: Training Symbols, IFFT: Inverse Fast Fourier Transform, CP: Cyclic Prefix, P/S: Parallel to Serial, DSP: Digital Signal Processing, Tx: Transmitter, DAC: Digital to Analog Converter, ADC: Analog to Digital Converter, Rx: Receiver. BVT: Bandwidth Variable Transceiver.

been implemented under the Rate Adaptive (RA) and MA criteria [8,53]. Then, TS are added for zero-forcing equalization at the receiver side. The IFFT is performed forcing the HS, the CP is included, the signal is serialized (P/S) and finally it is symmetrically clipped [8]. After that, the digital signal is converted from digital to analog by means of a DAC. The transmitter optoelectronic front-end consists of an external modulator and a TLS, for arbitrary wavelength selection. At the receiver side, the signal is photo-detected by a DD optoelectronic front-end and converted from analog to digital by an ADC. Finally, the signal is processed by the receiver DSP module. Thereby, the signal is firstly parallelized (S/P), then the CP is removed. After that, the FFT is performed considering that the signal has HS, it is equalized and the TS are removed. Finally, the signal is demodulated and serialized to obtain the original data.

5.3 SOA technology for optical switching

Our analysis considers switching nodes based on SOAs. The general structure of a SOA is shown in Figure 5.2. The input signal is coupled through one of the two facets. Then it goes through the active region, which is pumped by external current injection. The output signal is coupled on the other facet. The main characteristic of these amplifiers is that the optical feedback of the laser is reduced compared to a semiconductor laser.

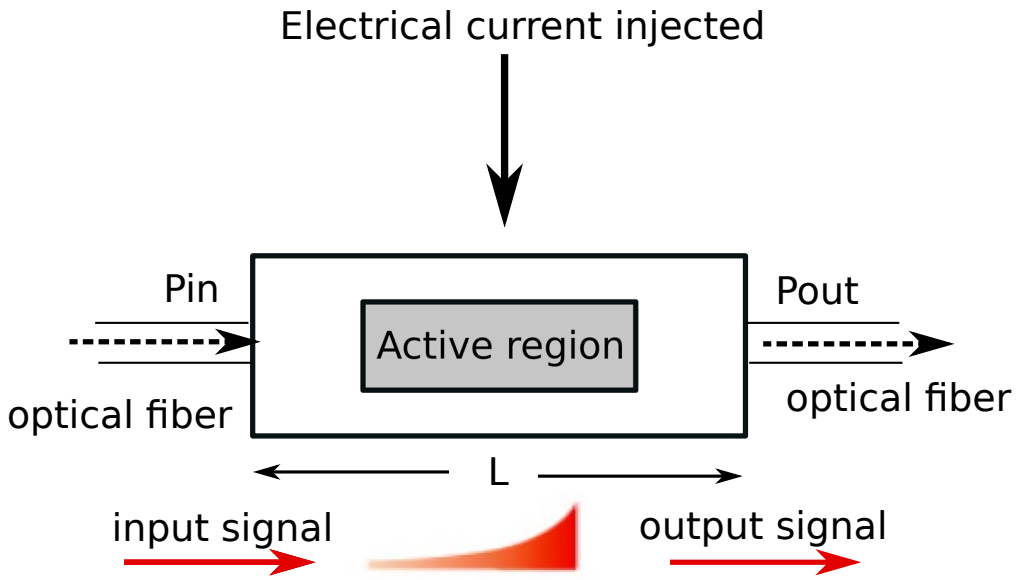

Figure 5.2: Semicondutor Optical Amplifier (SOA) structure. Pin: input power, Pout: output power, L: length.

There are two kinds of SOA amplifiers depending of the amount of light reflected. Fabry-Perot (FP) amplifiers have appreciable reflectivities and therefore the gain is not smooth. On the other hand, Traveling Wave (TW) amplifiers have no reflectivities and the gain is very smooth but the complexity on the fabrication is higher. For our experiments we consider FP SOAs.

SOA technology can be adopted for implementing switching devices. However, there are other optical switching technologies based on Electro-Optic, Acousto-Optic, Thermo-Optic or Opto-Mechanical switching. The main advantage of SOAs with respect to these other switching technologies is the scalability [100]. When several switches are in cascade, SOAs can control the gain with the injected current and, depending on the node architecture, overcome the limitation due to the power decay.

As losses due to the network elements can be compensated thanks to the presence of SOAs, this switching option can be envisioned also for applications in filterless optical networks. This would represent a cost-effective solution [102], as active reconfigurable components are eliminated or minimized using passive optical elements as combiners or/and splitters to interconnect the fiber links and to add or drop channel wavelengths at the nodes. Some advantages are expected for these networks such as simplified maintenance or reconfigurability. However, in a filterless optical network we must consider the related drawbacks and limitations. In this scenario, the use of SOA-based switching nodes combined with BVT technology can be advantageous. SOA-based switching nodes can be useful to compensate the attenuation, due to the passive elements and the transmission over the fiber, and BVT with loading capabilities, to combat the CD.

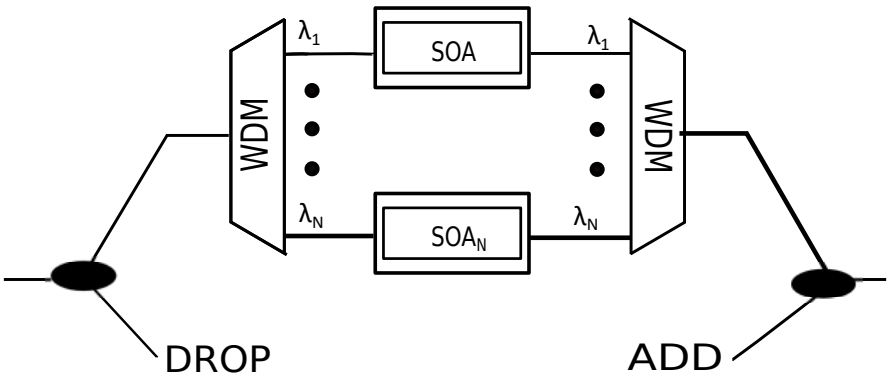

Figure 5.3: Estructure of an OAD node.SOA: Semiconductor Optical Amplifier, WDM: Wavelength Division Multiplexing.

On the other hand, a generic filtered optical mesh network is equipped with OAD multiplexer, placed at the nodes, enabling to dynamically configure the dropping or adding of different wavelengths through the fiber, remotely. Typically, the reconfigurable OAD nodes adopt WSS technology. Particularly, in the context of elastic optical networks, flexible WSS are needed to deploy a more flexible and bandwidth efficient network [13]. The main disadvantage of this solution is the penalties in signal degradation due to the filter narrowing effect caused by the crossing through a cascade of WSS [13], as it was analyzed in section 4. The use of S-BVT can flexibly adapt the transmission. Furthermore, we have considered the SOA-based wavelength selectors as the key element in OAD nodes to drop and add traffic in the network [100,107]. In fact, WDM optical cross-connect based on SOA has been presented in [97] for interconnecting network elements, computing, or storage resources in a metro network architecture. It has been experimentally demonstrated the potential lossless, low cross-talk or multicasting operation of these network elements.

In this section, we have analyzed the performance when the OAD nodes with SOA-based wavelength selectors are included, being the target the metro segment. The OAD node consists of one splitter, one combiner, the SOA array for gating one or more wavelengths and two wavelength selectors. One acting as a demultiplexer separating the incoming wavelengths and the other acting as a multiplexer combining the switching wavelengths. In the proposed system, the filter narrowing effect is also present due to the concatenation of the wavelength selectors [13]. The architecture of the SOA-based OAD node can be seen in Figure 5.3. In this case, losses are generated by the transmission over the fiber links and the filtering elements as well. Adjusting the SOA bias current, the filtering effects mainly due to the wavelength selectors and the losses due to the fiber, can be compensated.

5.4 Experimental setup for the S-BVT adopting SOA technology

For the experimental assessment we propose to use the S-BVT described in section 5.2 for optical metro networks adopting SOA-based switching nodes. In particular, the simplest S-BVT architecture using DMT and DD is considered attractive for a cost-effective implementation and, thus, it is envisioned to be used when SOA technology is adopted for the switching nodes. To analyze the performance of this approach, two scenarios are considered as shown in Figure 5.4. Both scenarios consider spans of 25 km of fiber and different cascading nodes; scenario a) envisions the use of a simple SOA acting as switching node, while scenario b) introduces OAD nodes based on SOA technology, as specified in Figure 5.3. As a reference, the case of multiple (up to 4) fiber spools of 25 km, without any SOA is analyzed as well. The scenario without considering filtering elements (filterless) is analyzed to study the impact on the system performance at different transmission distances with and without SOAs. Then, we analyze the case of SOA-based OAD nodes after each span of fiber. To evaluate the proposed system, the setup of Figure 5.3 has been considered. The WDM consists of 32 channels with a channel spacing of 100 GHz (0.8 nm), insertion loss of 2.98 dB and passband at 0.5 dB of ± 0.1 nm. However, for the experiments only the 1550.12 nm channel has been studied. It is marked by the red color in Figure 5.4. Thus, the signal traverses the first WDM, the SOA and finally the signal is multiplexed by the second WDM.

Related to the SOAs, it is also important to mention that the input power injected into SOA and the current applied to the SOA are relevant for the successfull functioning of the system transmission. The setup proposed for the characterization of the SOAs is illustrated in Figure 5.5. Firstly, we have varied the input power injected into SOA for a fixed current. The current was set to 65 mA [108]. Then, we have analyzed the BER and the maximum OSNR for different values of the input power. After that, we have analyzed the BER and the maximum OSNR versus the bias current for a fixed input power of -2 dBm. The results are presented in Figure 5.6 (a) and (b).

According to the results, we can conclude that for the successfull functioning of the SOA, the input power has to be around -2 dBm before the 25 km of fiber. Thus, the input power applied directly to the SOA is around -8 dBm due to the attenuation of the 25 km of fiber (0.2 dB/km of attenuation). Furthermore, in order to obtain the best performance in the experiments is convenient that the bias current is within 60 mA and 80 mA because is when the minimum BER is achieved and the maximum OSNR increases above 35 dB.

Then, the setup of Figure 5.4 has been experimentally analyze according to scenario (a) or scenario (b). To do that, Python software has been used at the DSP module. The IFFT with 512 subcarriers modulates the mapped sequence. Due to the HS, only half of

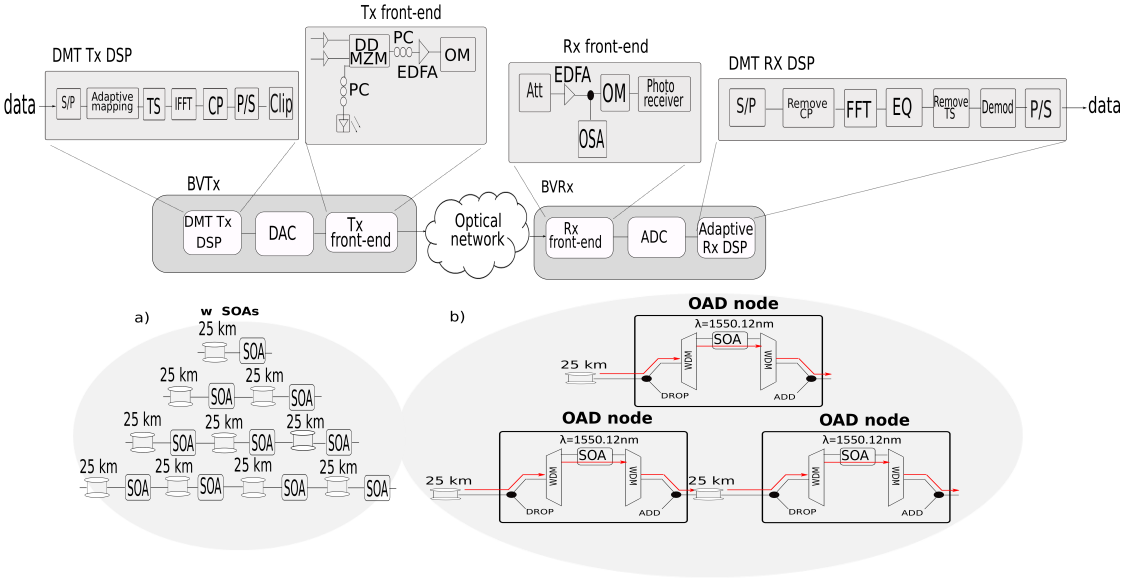

Figure 5.4: S-BVT architecture and experimental set-up. OM: optical power monitoring, Att: Attenuator, OSA: Optical Spectrum Analyzer, EQ: Equalizer. The different analyzed scenarios for the optical metro network are indicated: a) with SOAs and 25km SSMF spools, and b) with OAD nodes based on SOAs.

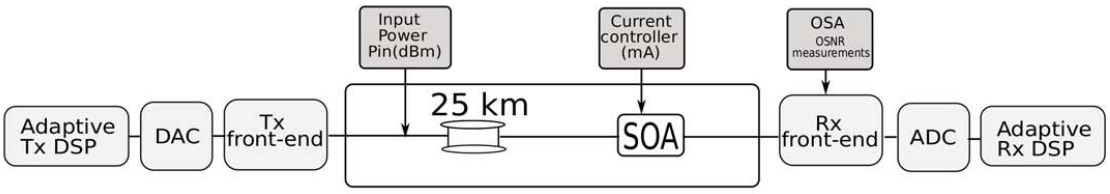

Figure 5.5: SOA characterization setup.

the IFFT subcarriers supports data. The total number of frames is 125 being 5 of them TS. The CP is 1.9% and the FEC considered is 7% . As it is well-known, the clipping factor can cause distortions and the degradation of the system performance. For this reason, the best clipping level should be selected according to the adopted constellation format. To estimate the channel profile, uniform loading is adopted, in particular 4-QAM. The clipping level recommended for this modulation format is 7 dB, which corresponds to a clipping factor of 2.24. When other modulation formats are used, 7 dB can be not enough. The clipping level must be selected according to the highest modulation format, when bit loading is used. In our case, the highest modulation format used in this experiment is 16-QAM. Accordingly, we have determined that the best clipping level is 8.5 dB giving a clipping factor of 2.6 . The sample rate of the DAC is 28 GS/s and a 3 dB bandwidth of 20 GHz. The obtained electrical signal is amplified by RF-amplifiers

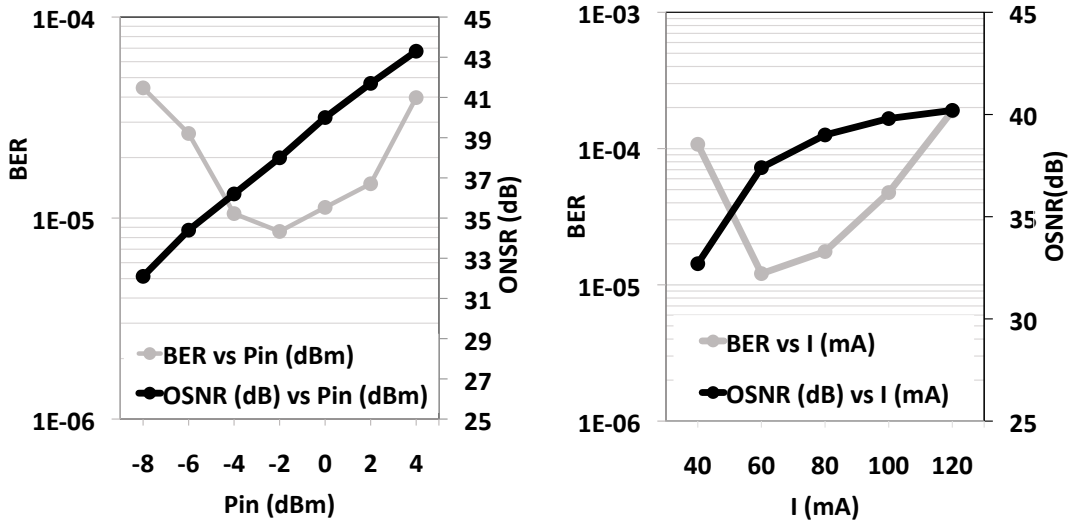

Figure 5.6: SOA characterization. (a) BER versus P_{in} (input power) and OSNR versus P_{in} for a fixed bias current of 65 mA. (b) BER versus I (SOA bias current) and OSNR versus I for a fixed P_{in} of -2 dBm.

with a bandwidth of 45 GHz. Then the signal is the input of a Dual Drive (DD)-MZM. The DD-MZM is working in the push-pull operation. The laser driving the DD-MZM is centered at 1550.12 nm with 13 dBm of output power. As the DD-MZM is polarization dependent, a Polarization Controller (PC) is needed in order to obtain the maximum power of the laser driving the DD-MZM. Another PC is at the output of the DD-MZM. With those PCs we can control the power at the input of the EDFA, obtaining a power value of 1.5 dBm at the input and 13 dBm at the output of the EDFA.

Then, the power launched to the network is measured by an Optical power Monitor (OM). At the receiver, an attenuator followed by an EDFA is used to vary the OSNR. After that, another OM is placed for being able to ensure a constant power at the input of the photodetector. The sample rate of the ADC is 80 GS/s. The OSNR is measured within 0.1 nm and the target BER is set to $3.8 \cdot 10^{-3}$. The fiber spans are SSMF of 25 km each, with 0.2 dB/km of attenuation.

A probe signal modulated with uniform loading (4-QAM) is sent to the channel in order to estimate the Signal-to-Noise Ratio (SNR) profile at the receiver side. Once we have calculated the SNR profile, we apply the sliding window method and analyze the impact of the window length on the BER performance. This method consist on the slicing of a window of a specified length over the SNR profile. Then, the SNR value for a specific subcarrier is computed as the mean over the data in the window. With this method the SNR profile is softened and the performance is optimized. We name the number of samples taken after or before the subcarrier considered, as Window Size (WS). The total number of the subcarriers considered for calculating the mean is given by

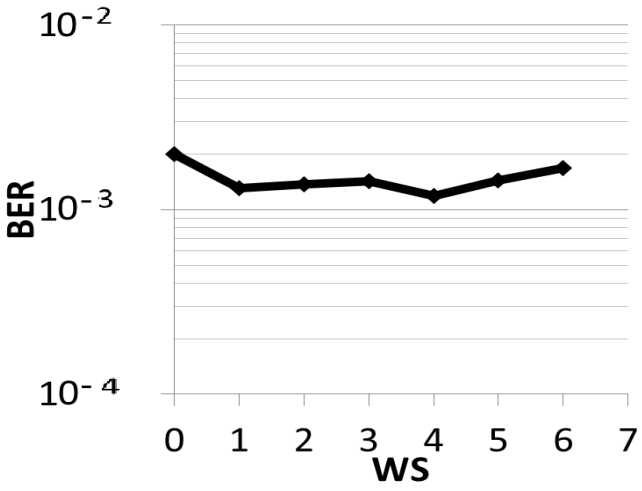

Figure 5.7: BER versus WS for 75 km of fiber and OSNR of 36 dB without considering SOAs placed inline. WS: Window Size.

$TSW = WS \cdot 2 + 1$ where TSW is the total size of the window. Thus, the minimum WS is 3 and the maximum WS is 13. Figure 5.7 shows the optimization for 75 km (3 spans of 25 km of SSMF). We can see that the minimum BER is achieved by a window size of 4 (meaning 4 subcarriers taken after and 4 subcarriers taken before the subcarrier considered) that corresponds to a TSW size of 9 .

As an example, the SNR estimation for the different scenarios with and without SOAs and with SOA-based OAD is shown in Figure 5.8 considering two spans of 25 km for a total of 50 km of fiber. There, it is possible to observe a degradation of the SNR around the 156th subcarrier, which is due to the CD. This attenuation depends on the fiber length and appears at certain frequencies that are given by the expression

$$f^n = \sqrt{\frac{\frac{c(2n-1)}{2\lambda^2}}{LD}}, \tag{5.1}$$

being c the speed of light, λ the center wavelength, L the fiber length, D the dispersion parameter and n the n-th attenuation peak (positive integer).

When the SOAs are included, this peak suffers a shift of around 10 subcarriers towards the lower frequencies. The maximum obtained SNR decreases 1 dB, but the SNR profile is similar. This frequency shift, with respect to the theoretical frequency, is due to the variation of the injected current of the SOAs to find the best working point. In our case study, the best conditions are achieved for a SOA input power of -8 dBm and an injected current within 60 mA and 80 mA as it was mentioned above. If the SNR profile is estimated when SOA-based OAD nodes are used, the maximum SNR decreases down to 14 dB, and the fading frequency peak is shifted to higher frequencies, where

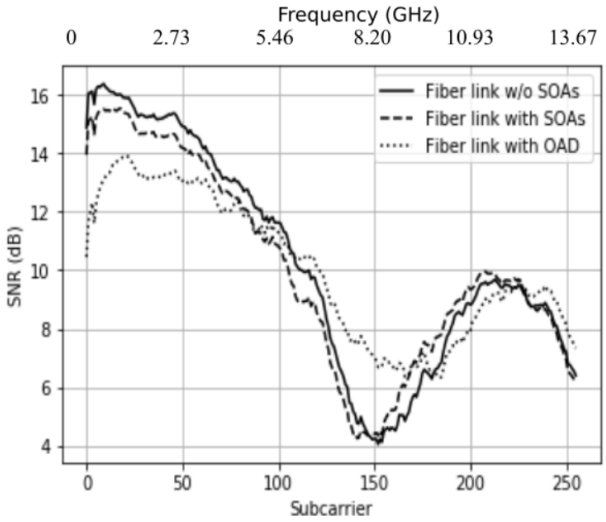

Figure 5.8: SNR profile considering MA at 28 Gb/s over two SSMF spans of 25 km, with and without SOAs and for SOAs-based OAD, at 34 dB of OSNR.

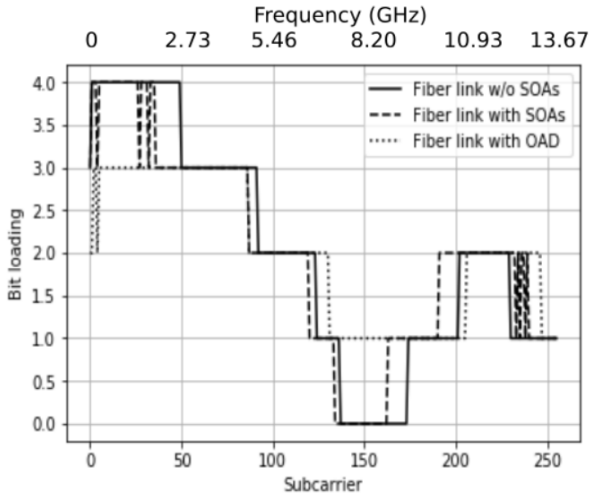

Figure 5.9: Bit loading assignment considering MA at 28 Gb/s over two SSMF spans of 25 km, with and without SOAs and for SOAs-based OAD, at 34 dB of OSNR.

the minimum SNR is about 6.5 dB. In this case, the cascading of network elements, in particular the presence of filtering elements, causes the reduction of the obtained SNR for all the subcarriers and the shift of the fading peak. Indeed, for this case, the peak fading is not so pronounced as in the case without filtering elements and it covers a greater number of subcarriers (from the 120 th to the 200 th approximately).

According to the SNR profile, the subcarriers for each scenario are modulated at the transmitter side using bit and power loading algorithms. Figure 5.9 shows the bit

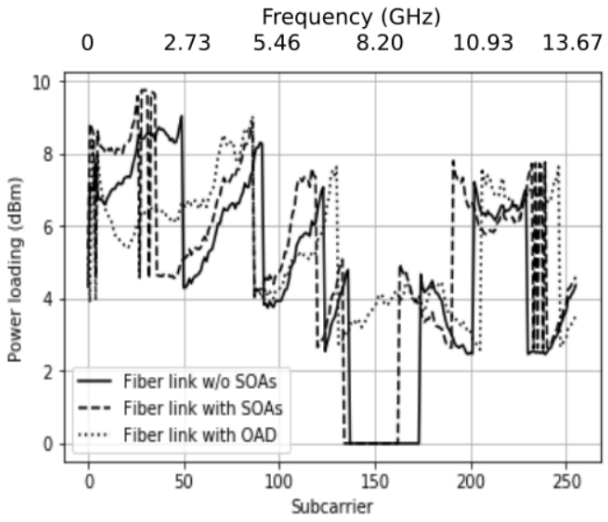

Figure 5.10: Power loading assignment considering MA at 28 Gb/s over two SSMF spans of 25 km, with and without SOAs and for SOAs-based OAD, at 34 dB of OSNR.

distribution according to the SNR estimation in Figure 5.8 and considering the MA criterion with a fixed gross bit rate of 28 Gb/s at 34 dB of OSNR. It can be seen that the modulation format order decreases with the reduction of the SNR values and increases with the increase of the SNR values. For the OAD scenario, since the SNR profile is more affected by the fiber impairments and the filtering elements, lower bits per symbol are loaded onto the subcarriers. In Figure 5.10, the power loading distribution according to the SNR profile is presented. It can be observed that the subcarriers corresponding to the lower SNR values for the case with SOAs, do not have power assigned. For the OAD scenario, all the subcarriers have power assigned and the power variation corresponds to the change from one modulation format to another. In Figure 5.11, the BER per subcarrier for the different analyzed cases is reported. We can observe that for the OAD scenario, the subcarriers affected by CD present high number of errors.

5.5 Experimental analysis

In this section, we firstly experimentally assess the impact of including simple SOAs acting as switching nodes without considering filtering elements as a key element for loss compensation. Furthermore, in order to overcome the SOA limitations outlined in section 5.3 and optimize the link-capacity, the advanced programmable BVT based on DMT modulation proposed in section 5.2, is also considered. Then, the transmission performance according to the RA criteria with filterless operation is experimentally assessed. Fiber spans of 25 km until a maximum of 4, for a total path of 100 km, are considered. In particular, to observe the impact of adopting the SOAs in the system, we

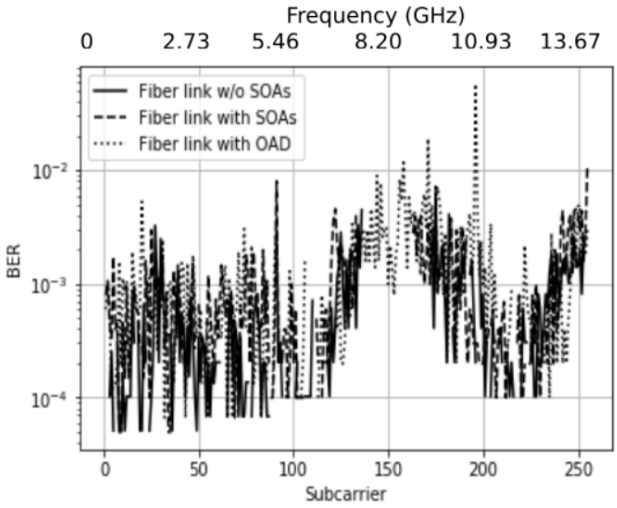

Figure 5.11: BER per DMT subcarrier considering MA at 28 Gb/s over two SSMF spans of 25 km, with and without SOAs and for SOAs-based OAD, at 34 dB of OSNR.

place an SOA after each span of fiber. The BVT technology and the experimental setup proposed, corresponds to the scenario (a) of Figure 5.4.

In Figure 5.12 (a) the net bit rate versus OSNR is presented for different transmission distances with and without SOAs acting as switching nodes for RA criterion. Here, we can see that as the optical elements increase (spans of fiber or/and SOA-based switching nodes), the OSNR is degraded due to the noise accumulation of the different components. As an example, for 25 km the maximum OSNR reached is 45 dB and including a SOA the maximum OSNR is 39 dB with the corresponding reduction of 3 Gb/s of net bit rate between both. However, the net bit rate performance behavior is maintained when the same links of fiber are compared with and without SOAs. In some cases even an improvement can be noticed. Indeed, in Figure 5.12 (b) we present the net bit rate improvement versus OSNR for different fiber links with and without SOAs. We can observe that for 25 km there are no improvements when the SOA is included. This means that the net bit rate performance is higher without the introduction of the SOA. However, for the rest of the use cases, these improvements are positive which means that, including the SOAs, the net bit rate performance enhances. This improvement is maximum and its value is 2.5 dB for 75 km of fiber and an OSNR of 30 dB.

Then, a comparison between the two scenarios detailed in section 5.4 shown in Figure 5.4 is presented. To analyze the second scenario, we consider SOA-based switching nodes based on the OAD node architecture of Figure 5.3. For both scenarios, the current injected into the SOA is properly varied to compensate the losses due to the fiber impairments or/and the different elements (splitters, combiners, filtering elements) of the OAD node.

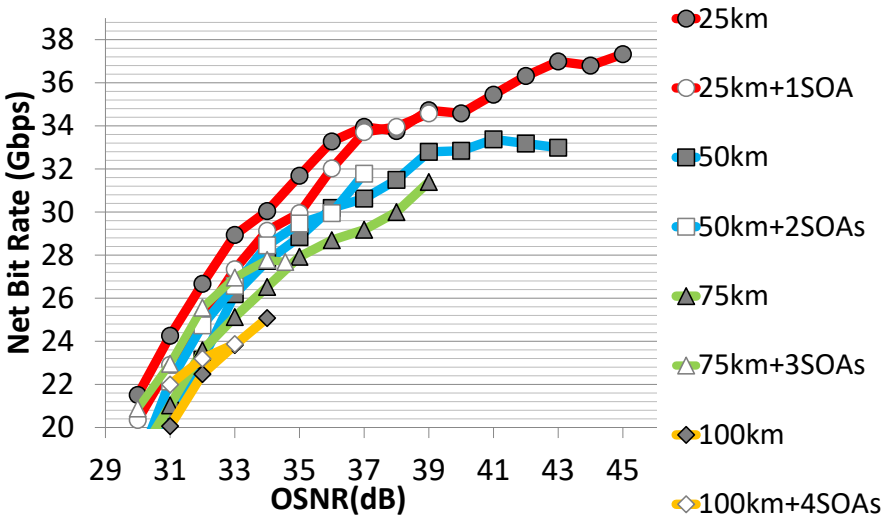

(a)

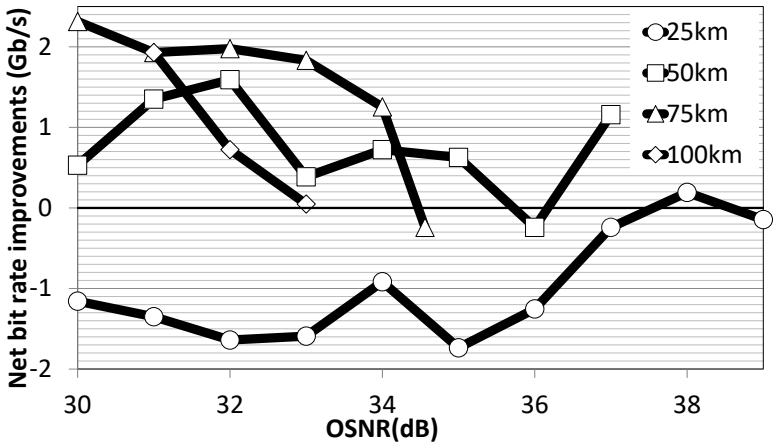

(b)

Figure 5.12: (a) Net bit rate performance versus OSNR for different fiber links with and without SOAs using RA criterion for a target BER of $3.8 \cdot 10^{-3}$. (b) Net bit rate improvements versus OSNR for different transmission distances.

First of all, we analyze the case at fixed bit rate (28 Gb/s) using the MA bit and power loading algorithm for maximizing the performance. The BER performance at the varying of the OSNR is presented in Figure 5.13. It is interesting to observe that a similar behavior is obtained for 75 km (3 spans) of fiber without SOAs, 50 km (2 spans) of fiber with an SOA after each span and one fiber span of 25 km with an OAD node, being the difference between these cases lower than 1 dB at the target BER of $3.8 \cdot 10^{-3}$. Similar results are obtained when we compare the BER curves for 100 km (4 spans) of fiber, 75 km (3 spans) of fiber with an SOA per each span and 50 km (2 spans) of fiber including 2 OAD nodes (one after each span), being as well the penalty less than 1 dB, at the target BER. Up to 100 km reach (4 fiber spans) can be achieved cascading 4

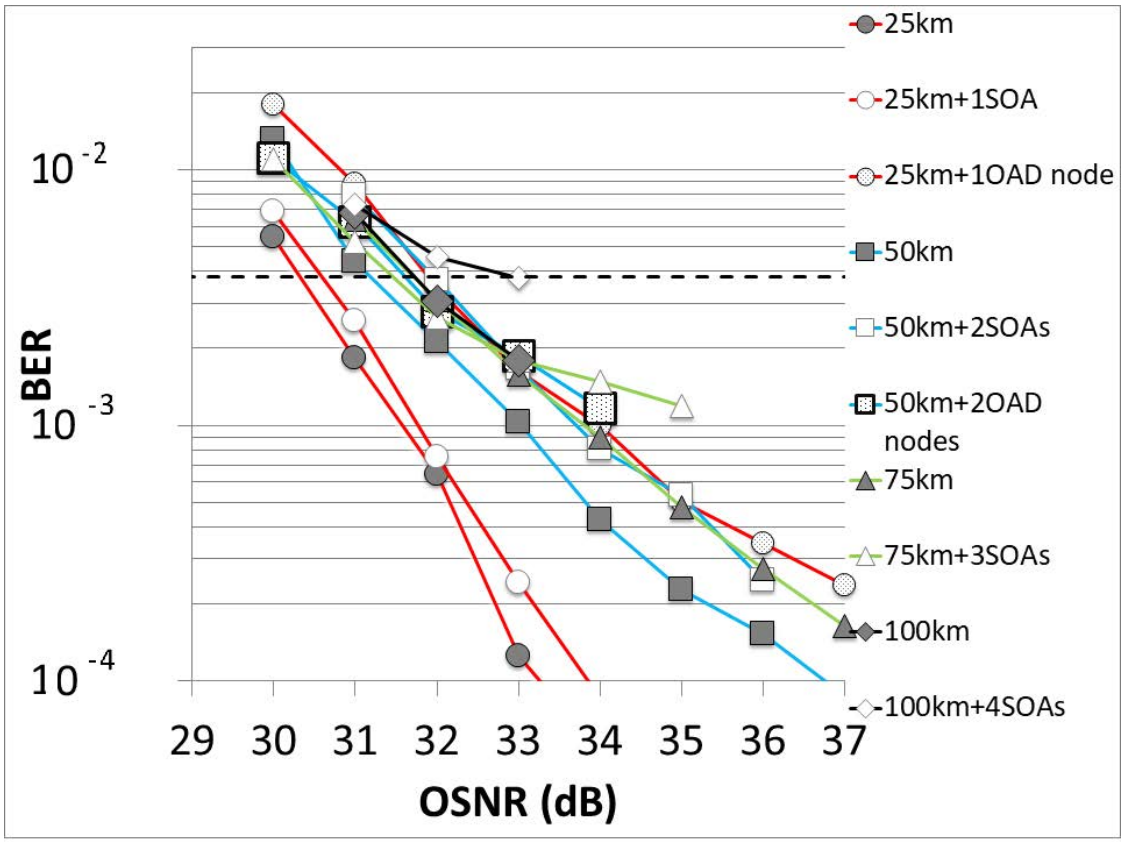

Figure 5.13: BER versus OSNR (with and without SOAs and including SOA-based OAD nodes) using bit and power loading algorithms under the MA criteria for a fixed gross bit rate of 28 Gb/s.

SOAs with an OSNR value of 33 dB. While, it was not possible to retrieve results after 75 km (3 spans) with the OAD nodes because of the losses accumulation, mainly due to the filtering elements, and the noise introduced by additional SOAs. Particularly, the introduction of the OAD nodes involves losses around 4 dBm per each WDM element and 1 dBm per each combiner/splitter.

Then, we have studied the maximum achievable net bit rate, adopting the RA bit and power loading algorithms, for different transmission distances and scenarios, considering at a fixed target BER of $3.8 \cdot 10^{-3}$. In Figure 5.14, the results at 33 dB of OSNR, are presented. We can see that, as the fiber length increases, the maximum net bit rate decreases, being this decreasing more pronounced for the case of fiber transmission without SOAs. In fact, for the 50 km (2 spans) of fiber, the maximum net bit rate is obtained when 2 SOAs or 2 SOA-based OAD nodes are included in the optical path, obtaining 26.5 Gb/s. The value of the net bit rate when only 2 spans of fiber are placed inline, is lower, being its value 26.1 Gb/s. Therefore, the introduction of the SOAs, as switching nodes themselves or either as part of the OAD node, improves the

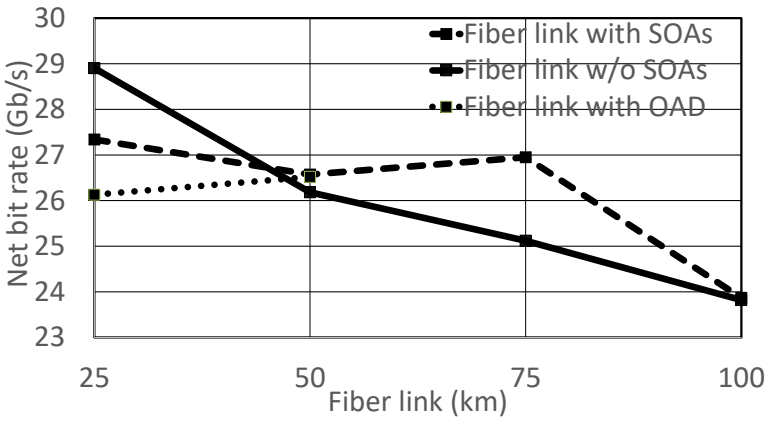

Figure 5.14: Net bit rate versus fiber link (with and without SOAs and including SOA-based OAD nodes), using RA bit and power loading algorithms, for an OSNR of 33 dB at target BER of $3.8 \cdot 10^{-3}$.

net bit rate performance at least for fiber links higher than 50 km. In fact, there is an improvement of 2 Gb/s when 75 km of fiber links and 3 SOAs are included, with respect to the case when the fiber links do not include the SOAs. This is due to the possibility of better optimizing the transmission by controlling the SOAs, in combination to the transceiver adaptability by means of the bit and power loading algorithms. According to the obtained results, a 26 Gb/s connection can be supported up to 50 km considering 2 cascading SOA-based OAD nodes and a maximum of 27 Gb/s for 75 km considering 3 cascading SOAs without filtering elements.

Table 5.1 shows the maximum achievable net data rate at different transmission distances for the considered scenarios adopting RA bit and power loading algorithms. Note that the maximum net bit rate of 37.32 Gb/s is achieved for 25 km of fiber when the SOAs are not included. On the other hand, the net bit rate penalty between the cases of 25 km of fiber and 100 km of fiber is greater (12.25 Gb/s of difference) when the SOAs are not included than when the SOAs are added (10.7 Gb/s of difference). Therefore, there is a reduction of the penalties, when SOAs are included. Thus, also in this case, the current injected into the SOAs is a key factor to control the penalties when multiple fiber links and SOAs are in cascade.

In case of considering SOA-based OAD nodes, the net bit rate decrease is greater than the case of using only SOAs. However, the maximum net bit rate achievable after 25 km of fiber is similar: 34.57 Gb/s and 34.77 Gb/s, with a simple additional SOA or including an OAD node, respectively.

When 2 OAD nodes and 50 km of fiber links are included, the maximum net bit rate is 27.97 Gb/s that is similar to the maximum net bit rate obtained for 75 km of fiber link and 3 SOAs (the difference is 0.29 dB)

	Fiber link w/o SOAs	**Fiber link with SOAs**	**Fiber link with OAD**
Reach (km)	**Net bit rate(Gb/s)**	**Net bit rate (Gb/s)**	**Net bit rate (Gb/s)**
25	37.32	34.57	34.77
50	33	31.78	27.97
75	31.4	27.68	-
100	25.07	23.87	-

Table 5.1: Achievable net bit rate and maximum OSNR for different transmission distances using the RA criterion bit and power loading algorithms, for different fiber links with and without SOAs and considering SOA-based OAD.

In Figure 5.15 (a) and (b) the net bit rate versus the OSNR for 25 km and 50 km of fiber are presented. It can be observed that the overlapping between the results of the different scenarios is higher when 2 spans (50 km) of fiber are considered. This is due to the increase of the number of elements in the optical network, either SOAs acting as switching nodes or AOD nodes. This enables the possibility to suitably manage (and carefully adjust) the SOAs bias current. Consequently, the system performance can be better optimized. In fact, when only one span of 25 km and one SOA is considered, the maximum OSNR achieved is 39 dB (6 dB lower than considering the span of 25 km and the OAD node) but the trend is similar than only using a span of 25 km (being 2.2 dB the maximum difference between them). For 50 km transmission distance, the penalties when the SOAs/OAD nodes are included, are minimum ($<$ 1 dB). Unfortunately, in this experiment, it has not been possible to further increase the cascading of more OAD nodes. Due to the different filtering elements and the associated noise accumulation, the maximum achievable OSNR was limited [109]. Thus, it was not possible to retrieve results after 75 km with the OAD nodes.

5.6 Summary

In this section, the use of S-BVTs, based on DMT modulation using DD, with adaptive loading capabilities adopting SOA-based switching nodes has been proposed as a flexible and adaptive cost-effective solution for optical metro networks. On one hand, the combination of BVT based on DMT offers a cost-efficient solution. Furthermore, including bit and power loading algorithms at the DSP modules, limitations due to transmission impairments (caused by the CD, DAC bandwidth or the network elements) can be mitigated enabling higher transmission rates and reach. On the other hand, the adoption of SOA-based switching nodes provides high scalability because of the possibility to control the injected current overcoming the power decay. The proposed implementation has been experimentally assessed considering two scenarios: with or without filtering elements.

The results obtained are summarized below:

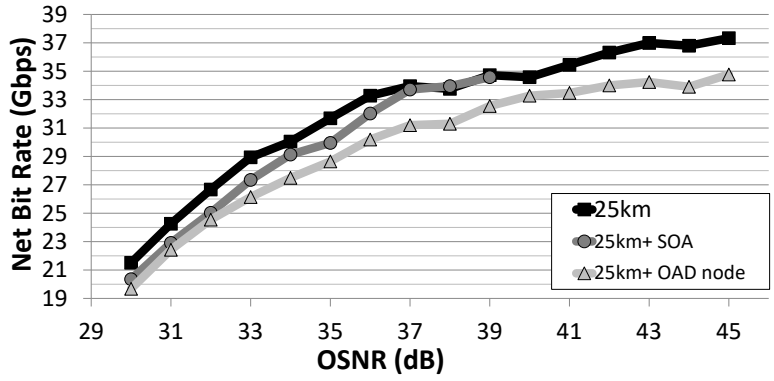

(a)

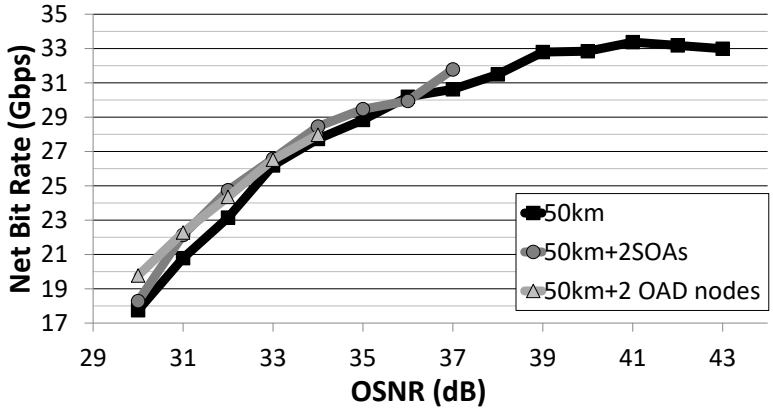

(b)

Figure 5.15: Net bit rate versus OSNR for (a) 25 km and (b) 50 km for the different scenarios at the target BER.

- The combination of adaptive BVT based on DMT modulation adopting SOAs acting as switching nodes, without considering filtering elements, improves the net bit rate for transmission distances higher than 25 km. This improvement is maximum and its value is 2.5 dB for 75 km of fiber.

- If we analyze both scenarios, meaning with and without filtering elements, when bit and power loading algorithms are implemented using the MA criterion, we can see that the BER performance obtained for a 25 km of fiber link with an SOA-based OAD node, has similar BER performance than the case of 50km (2 spans of 25 km) of fiber with 2 SOAs acting as switching nodes, or the case of 75 km (3 spans) of fiber. Thus, the introduction of the SOAs or the OAD node, in terms of BER performance, results as if an additional span of 25 km of fiber is included.

- Using the RA criterion, the net bit rate performance improves including SOA based OAD nodes or SOAs acting as switching nodes for 50 km of fiber links, compared to the case of simply adding fiber spans. This is due to the possibility of controlling

the SOA current to face the transmission impairments. These impairments include the losses due to the fiber links, the SOAs as well as the WDM elements or the splitter/combiners used in the experiments. These losses can be up to 4 dBm for each WDM element.

- Therefore, as the number of SOA-based switching nodes increases, more SOA elements can be controlled, to ensure a better optimization of the system and an improvement of the performance, overcoming the power losses due to the different elements in cascade. However, adding SOAs or/and filtering elements limits the maximum achievable OSNR and thus the number of cascading nodes that can be traversed by the adaptive signal generated by the S-BVT. In particular, 27 Gb/s connections can be supported up to 75 km including 3 SOAs acting as switching nodes without any filtering element, and while 26 Gb/s for 50 km is the maximum achievable reach including 2 OAD nodes.

- The experimental assessment demonstrates that thanks to the possibility of controlling the current injected into SOAs and the application of loading schemes at the adaptive transceivers, high flexibility, scalability and adaptability can be obtained. However, despite the possibility of compensating the losses thanks to the SOAs, the maximum transmission distance with 2 OAD nodes was 50 km, due to the introduction of the WDM elements and the splitters/combiners.

The combination of cost-effective implementation of programmable (SDN-enabled) BVT and SOA-based switching nodes, seems to be promising to be further investigated. However, different alternatives must be exploited in this direction to improve the proposed system and target future optical metro networks. For example, OFDM based on SSB or Vestigial Side Band (VSB) can be adopted with DD [55,106,109]. To enhance the impairment tolerance and the achievable distance, coherent detection can also be used as in [110,111]. In the following section, CO-OFDM systems based on multidimensional constellations are discussed.

Chapter 6

CO-OFDM systems based on multidimensional constellations

6.1 Introduction

Advanced transmission systems based on CO-OFDM systems have been proposed due to its robustness against CD and polarization dispersion at the expense of increasing the complexity in the transceiver design and cost [7]. In the context of flexi-grid paradigm, where different channels with different bandwidth or bit rates are expected to coexist, coherent detection is also considered for dealing high data rates or transmission reach. In fact, DMT transmission with CO detection has been proposed in [110] for MTU-BRAS connectivity covering up to 150 km. In [111] the authors propose two transceiver configurations, one of them based on intensity modulation with DD and the other on amplitude modulation with CO detection. The system is experimentally validated obtaining high robustness against accumulated dispersion by adopting CO detection.

CO-OFDM systems enable to recover the amplitude and the phase of the signal at the receiver, allowing to mitigate fiber effects and increase the attainable distance. Indeed, these systems are able to use both, quadrature and polarization components of the electromagnetic field, that naturally suit for using 4 dimensional constellations [39, 51]. One of the most known 4D constellation is DPQPSK [51]. This constellation takes advantage of the 4D signal space. It can be seen as four parallel and independent BPSK channels or as two independent QPSK in each polarization. Therefore, it uses 4 bits for each symbol giving 16 possible combinations. PSQPSK is another power efficient constellation. It also takes advantage of the 4D signal space but in this case it uses 3 bits per symbol. Thus, the number of levels is 8 instead of 16 which is the case of DPQPSK. In fact, PSQPSK can be seen as a subset with respect to the DPQPSK format, since the 8 levels of PSQPSK are contained withing the 16 possible combinations of DPQPSK. 6PQPSK constellation format is also presented in this section. It transmits 9 bits over 2

symbols. Depending on the configuration, these two symbols will be encoded as PSQPSK or DPQPSK constellation format as it is explained below.

In this section, we have estudied the performance of the mentioned constellations with respect to the BPSK constellation. BPSK is taken as the reference because it is the one that has the best sensitivity among all possible modulations [51, 112]. Additionaly, two advanced transmission systems based on CO detection have been proposed using DPQPSK constellation format for different fiber links.

The contributions of the section are listed below:

- First of all, we have made a preliminary study of different multidimensional constellation formats such as PSQPSK, DPQPSK and 6PQPSK. The BER performance for these constellation have been presented and compared according to our simulations.

- After that, we propose two advanced transmission schemes based on CO-OFDM technology adopting DPQPSK constellation. The first option uses the DPQPSK constellation and transmits the optical signal in time dimension, hence the name Time Diversity (TD)-DPQPSK. It enables avoiding the nonlinear interference for fiber propagation as it is demonstrated in [52]. The other transmission scheme, named as Polarization Diversity (PD)-DPQPSK, uses the polarization dimension in order to transmit the signal in the optical domain.

- Finally, the performance in terms of OSNR of the two transmission schemes based on DPQPSK constellation format, have been assessed by numerical simulations and compared with the conventional 4QAM CO-OFDM system for B2B configuration and after 1040 km and 2000 km fiber links.

6.2 Performance for 4D constellations

Coherent optical transmission technologies exploiting 4 dimensional signal space (two quadratures and two polarization) are in recent development. As it is well-known, the BPSK constellation is the most efficient because it is supposed to have the best sensitivity. However, we can use the 4D space using the real and imaginary parts of the electrical field in both polarizations in order to obtain a more efficient constellation [51]. In fact, the BER performance for DPQPSK is the same as BPSK as it was mentioned, but, in this case, each symbol is mapped by 4 bits. The DPQPSK can be expressed as the set $\{(\pm 1, \pm 1, \pm 1, \pm 1)\}$. Thus, it can be also seen as 2QAM, one per each polarization. The Spectral Efficiency (SE) is defined as the number of bits per symbol per polarization. The SE for DPQPSK is 2 but for BPSK its value is 1. There are other modulation formats that improves the sensitivity with respect to the BPSK constellation format but decreasing the SE with respect to the DPQPSK constellation format.

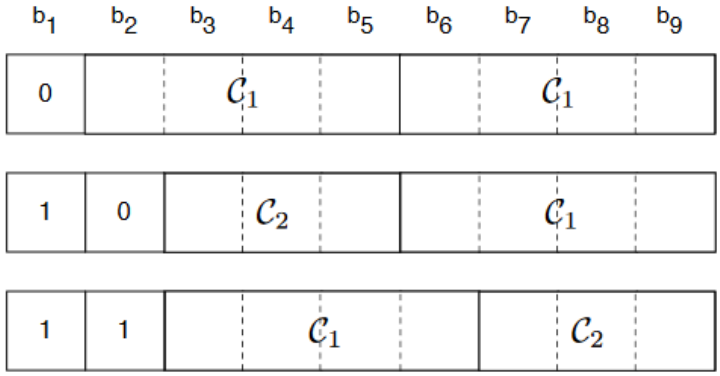

Figure 6.1: Bit-to-symbol mapping for 6PQPSK. C_1 corresponds to the DPQPSK constellation format and C_2 corresponds to PSQPSK format.

This is the case of the PSQPSK format, which has a SE of 1.5. So, this constellation maps 1.5 bits per symbol per polarization. It can be implemented in different ways. It can be seen as blocks of 3 bits, where one of them decides the polarization whereby the signal is transmitted and the other 2 bits are used to map the QPSK format. Other representation considers a subset of the DPQPSK by using two XOR gates forcing the bits to have even parity. In our analysis, we have chosen the following mapping of the bits $\{(0,0,0),(0,0,1),(0,1,1),(0,1,0),(1,1,0),(1,1,1),(1,0,1),(1,0,0)\}$ as $\{(2,0,0,0),(0,2,0,0),(0,0,2,0),(0,0,0,2),(-2,0,0,0),(0,-2,0,0),(0,0,-2,0),(0,0,0,-2)\}$.

Finally, the 6PQPSK constellation format, has been evaluated as it is specified in [51]. In this case, there are 9 bits to be mapped. The first bit gives information of the constellation format of the rest of the bits. If b_1 is 0 the rest of 8 bits are DPQPSK mapped (in blocks of 4 bits). If b_1 is 1 the sequence of the mapping depends on the second bit b_2 using DPQPSK or PSQPSK constellation formats in blocks of 4 or 3 bits, respectively. The bit to symbol mapping can be seen in Figure 6.1 (source: [51]), where C_1 corresponds to the DPQPSK constellation format and C_2 corresponds to PSQPSK format. Thus, in this case the SE is 2.25.

The BER performance over an Additive White Gaussian Noise (AWGN) channel have been studied for these 3 constellation formats and compared with the BPSK constellation. The results are illustrated in Figure 6.2. It can be seen that the DPQPSK has the same BER performance as BPSK as it was expected. On the other hand, at the target value of 10^{-3} , the BER performance improves for PSQPSK in 1 dB with respet to the BPSK format that is also expected due to its higher power efficiency, as theoretically demonstrated in [51]. Finally, the performance for 6PQPSK is also presented. We can observe that at the target BER, the E_b/N_0 is 0.6 dB higher than BPSK performance, which is also in line with the theoretical analysis presented in [51].

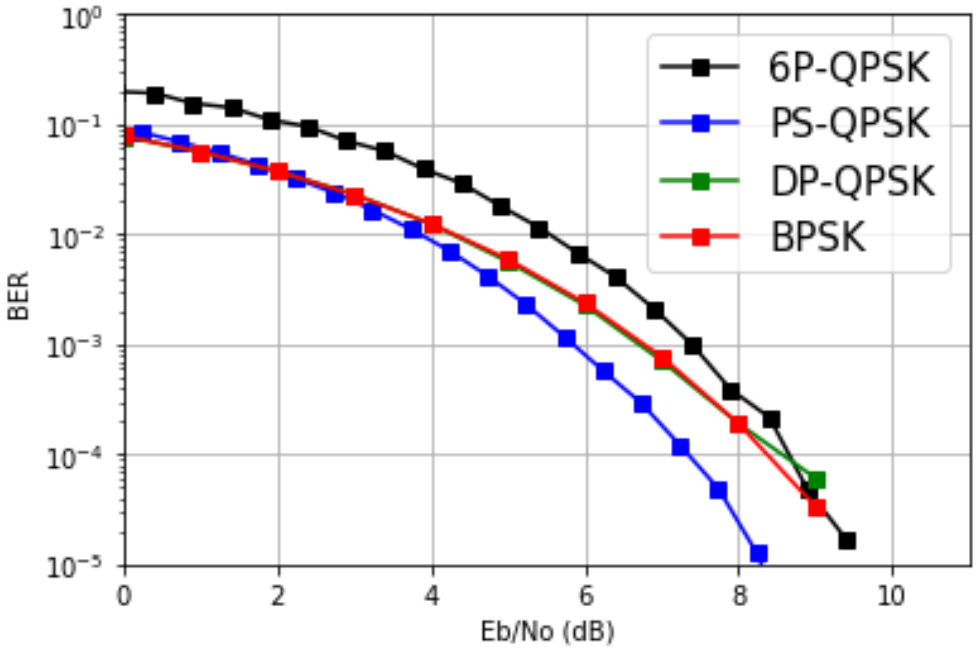

Figure 6.2: BER performance versus E_b/N_0 for DPQPSK, PSQPSK, 6PQPSK and BPSK constellation formats.

6.3 CO-OFDM transmission schemes based on DPQPSK constellation format

We propose two transmission schemes taking advantage of the DPQPSK constellation in a CO-OFDM system, one of them based on TD and the second option based on PD. In Figure 6.3 the block diagram for both transmission schemes is illustrated. At the transmitter, the input data is mapped onto the DPQPSK constellation [51]. As a result, we obtain two signals, one for each polarization. For each one, the TS are inserted. As it is well-known, phase noise has an important impact on the system performance. There are different methods to combat the phase noise. For our simulations we implement the RF algorithm [113] as it is explained below in section 6.4. Thus, after the TS, we include the Spectral Gap (SG) around the RF and the Zero Padding (ZP). After that, the digital time domain signal is obtained by using the IFFT in 2 Dimensions (IFFT2D) [114]. Next, the CP is added for both polarizations and the signals are serialized and clipped. At this point, we propose two alternatives in order to transmit the signal though the optical channel.

For TD-DPQPSK scheme, the transmission is done over the time dimension, as it is shown in Figure 6.3. As it can be observed, at the output of the clipping, two different complex signals are obtained, corresponding to the two orthogonal polarization states. We interleave the in-phase component of both polarizations in the time domain

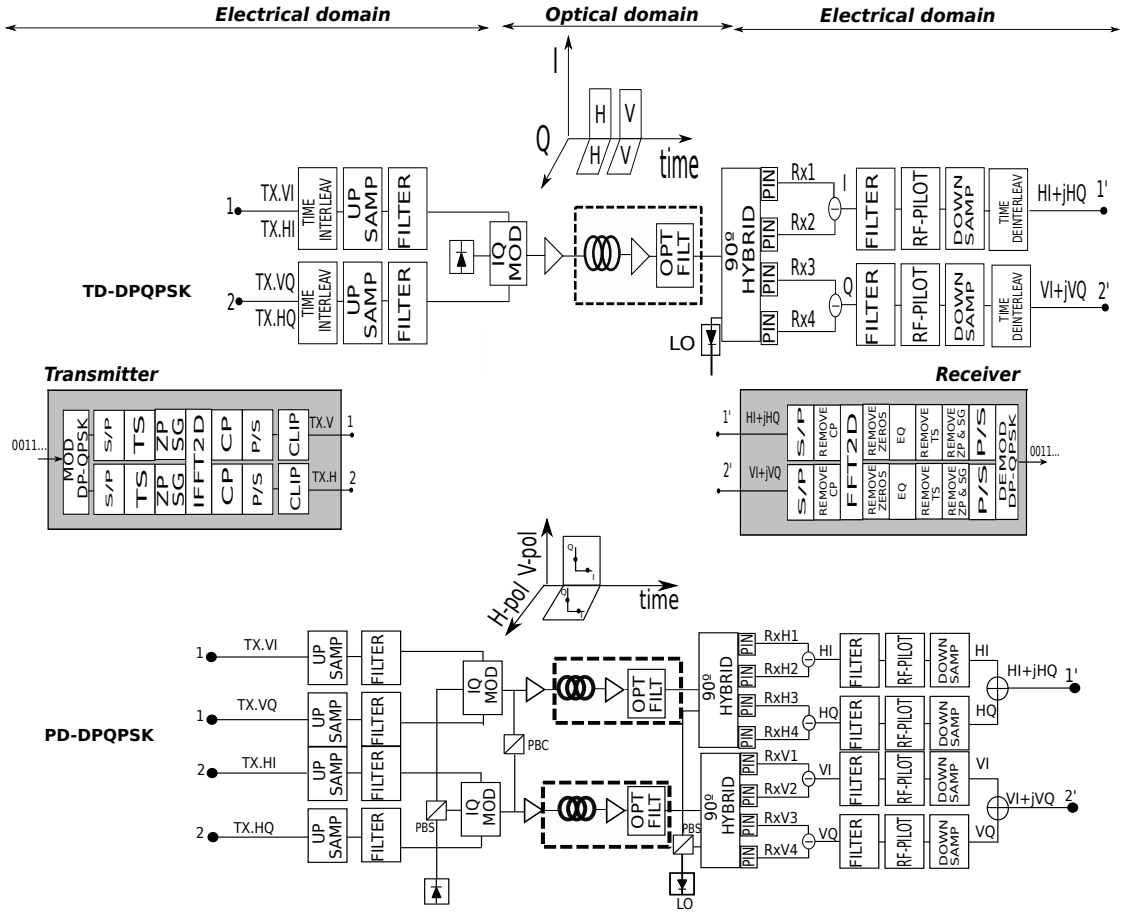

Figure 6.3: Block diagram for the TD-DPQPSK and PD-DPQPSK transmission schemes. MOD: Modulator, S/P: Serial to parallel, TS: Training Symbols, ZP: Zero Padding, SG: Spectral Gap, IQ: Inphase Quadrature, OPT FILT: Optical Filter, RF: Radio Frequency, FFT2D: Fast Fourier Transform 2 Dimensions, IFFT2D: Inverse Fast Fourier Transform 2 Dimensions.

in consecutive time slots. The same process is repeated for the quadrature component of both polarizations. Consequently, we obtain two signals as shown in Figure 6.4. Next, the two signals are upsampled and filtered in order to simulate the DAC. The resulting signals are converted onto the optical domain using an I/Q modulator biased near to the null point. The output signal is amplified and transmitted through the fiber. To convert the signal from optical to electrical domain, we use homodyne detection. It is realized with a 90^{o} optical hybrid and two pairs of balanced photo detectors resulting in an electrical in-phase and quadrature signals. Then the signals are filtered and a RF pilot algorithm is applied to compensate the phase noise. After that, the signals are downsampled in order to simulate the ADC. At this point, the time domain signals are time deinterleaved obtaining two complex signals, one for each polarization, with their corresponding in-phase and quadrature components.

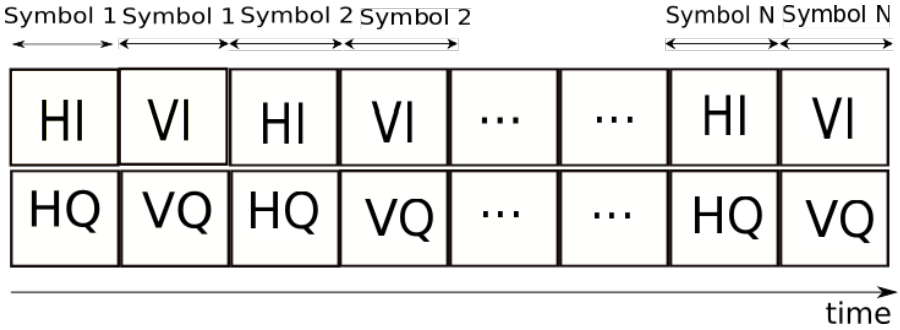

Figure 6.4: Interleaving of the polarization signals in time dimension. HI: Horizontal Inphase, HQ: Horizontal quadrature, VI: Vertical Inphase, VQ: Vertical Quadrature.

The other option to transmit the signals is using the polarization dimension referred to PD-DPQPSK in Figure 6.3. After the clipping, the in-phase and quadrature components of both polarizations are upsampled and filtered. The resulting signals are injected into the corresponding nested I/Q modulator that consists of two I/Q modulators each one for each polarization. The laser in this case is splitted in order to obtain two optical (Horizontal (H) and Vertical (V)) signals, one for each I/Q modulator. Thus, the Jones vector of the laser signal is given by: $E_{laser} = \binom{E_H}{E_V} = \binom{\frac{E_{laser}}{\sqrt{2}}}{\frac{E_{laser}}{\sqrt{2}}}$. The resulting optical signals traverse several fiber spans and, at the receiver, they are detected by two homodyne detectors, such as the one previously described. The main difference is that, in this case, the LO is 45º linearly polarized. After that, the corresponding in phase and quadrature signals for both polarizations are filtered, the RF pilot algorithm is applied for phase compensation and the signals are downsampled emulating the conversion from analog to digital domain. The outputs are composed of two signals, each one with their corresponding in-phase and quadrature components as for the TD-DPQPSK scheme. Hence, the following DSP stage is common for both transmission schemes as can be observed in Figure 6.3. This final stage consists on the parallelization of the signals, the removal of the CP and the FFT in 2 Dimensions (FFT2D) performance. Next, the equalization and the removal of the SG, the ZP and the TS. Finally, the serialization and the demodulation of the signals in order to obtain the original bit stream.

Please note that the TD-DPQPSK transmission scheme uses only one I/Q modulator and one homodyne detector, whereas the PD-DPQPSK scheme doubles these optical resources. However, the DSP module associated to TD-DPQPSK scheme involves higher complexity. Another interesting aspect to be considered for the TD-DPQPSK transmission scheme, is the expected reduction of the fiber nonlinearities impact on the system performance, as it has been recently demonstrated in [52], with respect to the PD-DPQPSK.

6.4 Simulation analysis

The proposed systems have been assessed by means of numerical simulations done by Python software. The performance evaluation is done by the BER. We have considered the SD-FEC that entails the 20% of overhead in data transmission and a target BER of $2 \cdot 10^{-2}$.

A pseudorandom data sequence with 2^{17} bits is generated running at net symbol rate of 10 Gbaud and gross symbol rate of 14.31 Gbaud. The overhead consist of the aforementioned FEC, 1.9% of CP, 5.88% of TS, 9.37% of SG around the RF and 1.17% of ZP. At the transmitter, the bit sequence is DPQPSK encoded and OFDM modulated with 512 subcarriers. The frame structure for the total number of the subcarriers can be observed in Figure 6.5 a) and the corresponding frequency mapping in Figure 6.5 b). The DPQPSK constellation uses 4 bits per symbol, 2 per each polarization. The clipping level is fixed to an optimal value of 9.5 dB. The optical carrier is modelled as an ideal CW laser with 150 kHz linewidth for the transmitter and for the Local Oscillator (LO) at the receiver. The EDFA has 4 dB of noise figure. The optical channel consists on spans of SSMF of 80 km of fiber, each followed by an EDFA and an optical filter with 100 GHz of bandwidth. The split-step Fourier method is used to model the propagation over the SSMF. We assume an effective core area of the fiber is 80 pm2, nonlinear index of $2.4\dot{1}0^{-20}$ m2/W, dispersion of $16.24\dot{1}0^{-6}$ s/m2, dispersion slope of $0.057\dot{1}0^{3}$ s/m2 and average loss of $0.2\dot{1}0^{-3}$ dB/m. At the receiver, the photo detectors are modelled as ideal PIN diodes with responsivity of 0.7 A/W, dark current of 10 nA and thermal noise of 16 nA/sqrt(Hz). Once the signal has been photodetected the phase noise has to be compensated. This phase noise is caused by the transmitter and the LO receiver lasers. The larger the laser linewidth, the greater the effect is. Thus, in order to compensate the phase noise, we implement the RF pilot algorithm [113]. The RF SG inserted around the RF at the transmitter is distorted as the same way that the rest of the OFDM signal. Hence, the received RF SG can be used to compensate these distortions. To do this, the optical carrier is filtered with a digital Low Pass Filter (LPF) with 100 MHz bandwidth and then is conjugated in order to obtain the phase error. The resulting signal is multiplied by the photodetected OFDM signal for phase compensation.

Firstly, we analyze the optical fiber launch power considering the TD-DPQPSK and PD-DPQPSK transmission schemes. For this purpose, the BER as a function of the fiber launch after 1040 km of fiber is calculated and it is presented in Figure 6.6. We can observe that the minimum BER is reached around -3 dBm. Thus, we select this value of the fiber launch power for both transmission schemes. This value of the fiber launch keeps constant for all the measurements for both transmission schemes. Additionally, we evaluate the BER performance for both transmission schemes and we compare them with the conventional 4 QAM CO-OFDM for B2B transmission and after different transmission distances. It is important to note that all the analysed schemes are running at

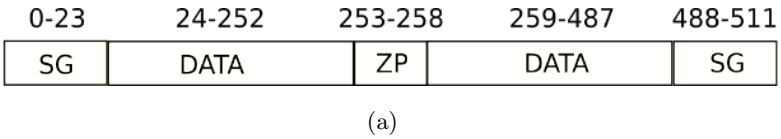

(a)

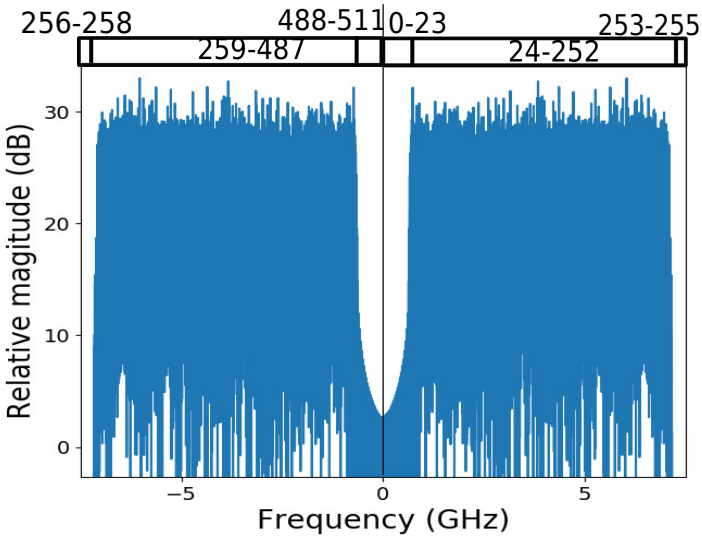

(b)

Figure 6.5: a) Frame structure for 512 subcarriers and b) its corresponding mapping in frequency domain. ZP: Zero padding, SG: Spectral Gap.

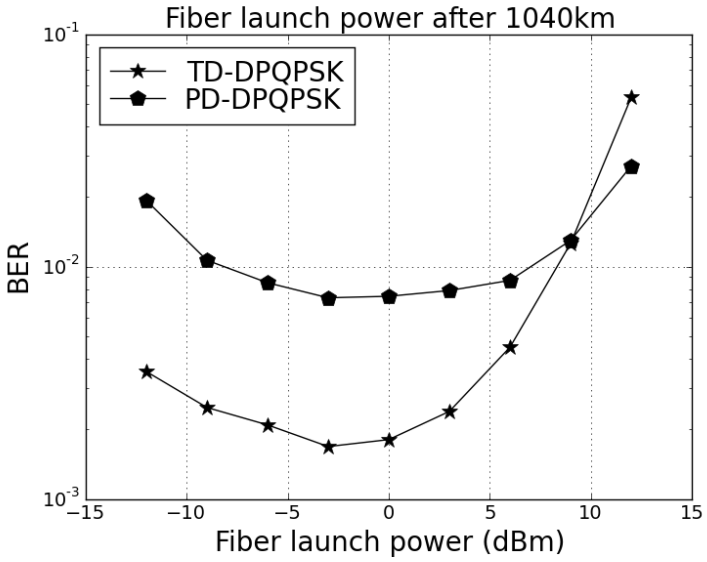

Figure 6.6: BER versus fiber launch power after 1040km of fiber for TD-DPQPSK and PD-DPQPSK transmission schemes.

the same net symbol rate of 10 Gbaud. The OSNR is defined in a 12.5 GHz bandwidth.

Figure 6.7 shows the BER characteristic for a B2B system and transmission after

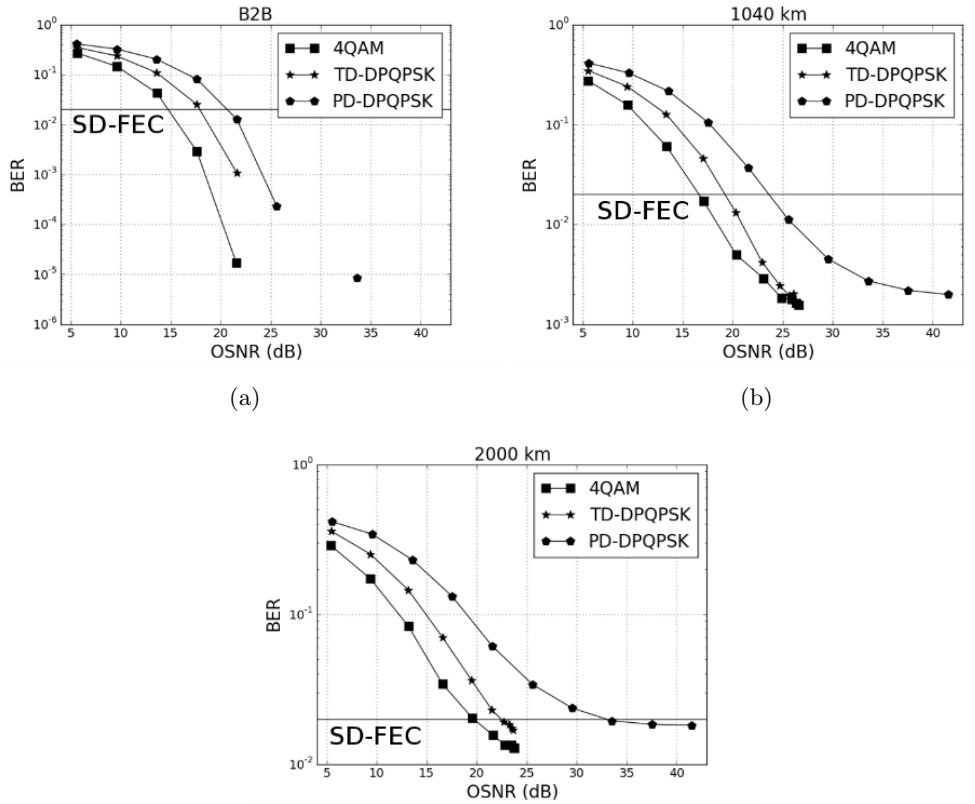

Figure 6.7: BER vs OSNR for 4QAM, TD-DPQPSK and PD-DPQPSK for a) B2B, and after b)1040 km and c)2000 km of fiber.

1040 km and 2000 km of fiber. In Figure 6.7 a) it can be observed that using the 4 QAM conventional scheme, the OSNR at the target BER is 14.7 dB for B2B. In case of using TD-DPQPSK and PD-DPQPSK, the OSNR required is 17.8 dB and 20.6 dB, respectively. When the signal traverses 1040 km of fiber (13 spans of 80 km), the achieved OSNR is 16.6 dB, 19 dB and 23.6 dB for 4 QAM, TD-DPQPSK and PS-DPQPSK transmission schemes, respectively, as it can be seen on Figure 6.7 b). Finally, in Figure 6.7 c), after 2000 km of fiber (25 spans of 80 km), the OSNR increases reaching values of 19.6 dB for 4 QAM, 22.4 dB for TD-DPQPSK and 33 dB for PD-DPQPSK. It can be observed that the scheme more affected by the increase of the fiber length is PD-DPQPSK. However for TD-DPQPSK the trend is similar than 4 QAM system (within 2 and 3 dB of OSNR difference between both at the target BER), but TD-DPQPSK doubles the bit rate. If we compare these results with the obtained in Section 3.5, we can observe that the OSNR needed to fulfill the target BER, using DD, is whithin 7 dB and 10 dB. This is because the DD-OFDM scheme seen in Section 3.5 uses the I/Q mixer to upconvert the signal to an intermediate frequency avoiding the mixing of the OFDM signal with the mixing products, improving the sensitivity.

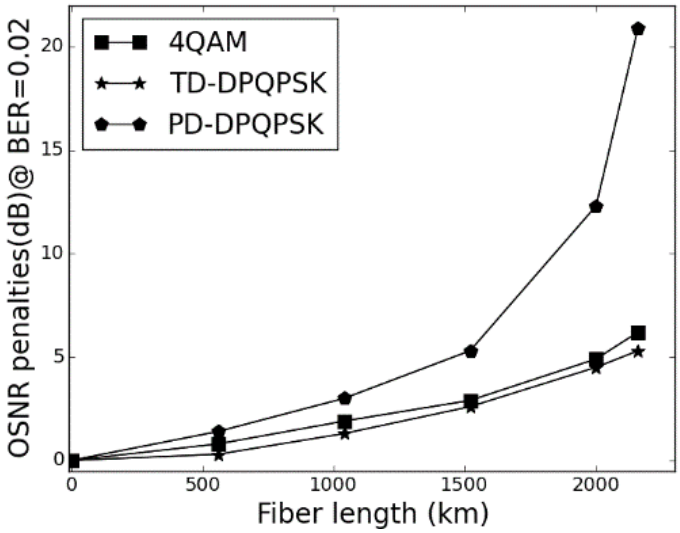

Figure 6.8: OSNR penalties at a target BER for different fiber lengths considering the transmission schemes of 4QAM, TD-DPQPSK and PD-DPQPSK.

In Figure 6.8 the OSNR penalties at the target BER versus the fiber length with respect to the B2B configuration is illustrated. In general terms, these penalties increase with the length of the fiber. We can observe that the conventional 4QAM system and the TD-DPQPSK have a similar behaviour, with the difference that the penalties are lower for TD-DPQPSK than for 4QAM. For a distance of 2160 km this difference is 0.9 dB. In the case of PD-DPQPSK the penalties increase steeply after 1000 km reaching an OSNR penalty of 20.9 dB at 2160 km of fiber. This steep increase of the penalty after 1500 km may be due to the increase of fiber length and also by the nonlinear interferences for fiber propagation.

6.5 Summary

In this section, multi-adaptive transceivers using multidimensional constellations are introduced. They allow a more efficient exploitation of all the resources of the electromagnetic field propagating through the optical link optimizing the network capacity. Advanced transmission systems, based on CO-OFDM technology, enabling to use both quadratures and polarization components of the electromagnetic field for data transmission have been proposed [51].

Fist of all, we have studied and compared different multidimensional constellations formats. Then, we have assessed two advanced transmission systems based on CO-OFDM technology using DPQPSK constellation. One of them uses the polarization dimension to transmit the signal in the optical domain and the other uses the time dimension. Both

schemes have been simulated covering different transmission distances. The robustness of these schemes have been studied and compared with conventional 4QAM constellation.

The results are summarized below:

- The DPQPSK constellation format has the same BER performance as BPSK with the difference that with DPQPSK the transmitted bits are doubled with respect to BPSK. An improvement of 1 dB in the BER performance can be obtained at the target BER using PSQPSK. In this case, the bits transmitted are 3. On the other hand, 9 bits we can transmit thanks to the 6PQPSK constellation format with only a decrease of 0.6 dB of sensitivity at the target BER with respect to the BPSK constellation.

- Furthermore, considering the two proposed transmission schemes, the system adopting CO-OFDM transmission with PD-DPQPSK is the one more affected by fiber nonlinearities generated through the fiber. Results have shown that the OSNR penalties increases steeply for more than 1000 km. Besides, the optical resources are doubled in this transmission scheme with respect to TD-DPQPSK scheme.

- In contrast, TD-DPQPSK scheme is less affected by the transmission distance than PD-DPQPSK. This difference is maximum for 2160 km and its value is 0.9 dB. On the other hand, TD-DPQPSK behavior is similar to the 4QAM conventional system but TD-DPQPSK transmit the double of the bit rate with respect to 4QAM conventional scheme for the same net symbol rate (10 Gbaud).

- In general terms, the results show that TD-DPQPSK transmission scheme is a promising solution for an efficient use of the network resources. Furthermore, considering the analysis previously done for PSQPSK and 6PQPSK constellation formats, it can be interesting to integrate them in a transmission scheme in order to compare with the proposed DPQPSK schemes.

Chapter 7

Conclusions and future work

This section presents the main contributions of the thesis and the possible future work according to the research carried out. First of all, in section 7.1 we present the general conclusions of the thesis followed by the main conclusions obtained for each section. After that, section 7.2 future work presents the main open investigation lines related to the presented results.

7.1 Conclusions

In this thesis, we have proposed multi-adaptive transceivers based on advanced transmission systems adopting OFDM technologies for the envisioned EONs, following the SDN paradigm. Particularly, programmable cost-effective S-BVTs based on DD-OFDM systems have been analyzed as a solution to cope with the requirements envisioned for flexi-grid in optical metro/regional networks. The problematic of the filter narrowing effect, that is a concern in the context of the flexi-grid scenario, have been also analyzed. We have studied this effect by numerical simulations and experimentally considering two approaches, one based on legacy OOK and the other based on advanced transmission systems adopting DD-OFDM with adaptive modulation algorithms implemented at the DSP modules.

On the other hand, we have experimentally validated the combination of DMT modulation, as a simplest version of DD system with adaptive capabilities, with SOA-based switching nodes. Thus, the transmission impairments due to the fiber and filtering elements have been compensated and the cost-effectiveness requirements of metropolitan/regional optical networks have been maintained. In order to enhance the transmission reach and the data rate, we have also proposed the implementation of CO-OFDM systems based on multidimensional constellations.

In the following, we provide a summary of the main contributions for each section.

It is envisioned that the future metro networks connections with different capacities

should be accomodated, increasing the network flexibility at reduced cost and complexity. In **chapter 3**, multi-band OFDM systems using DD have been proposed to face with these requirements. To do that, we have adapted a theoretical model of the resulting photodetected signal for a multi-band DD-OFDM system. Attending to this model, we have identified the mixing products due to the inter-bands effects. According to the numerical simulations, we have confirmed that the inter-band effects are concentrated at the guard band and its relevance depends on the MZM bias point. These effects have increased when the MZM was biased near the null point and they have been more pronounced for the bands placed close to the optical carrier.

Furthermore, this model has been assessed in a realistic metro/regional network. To this end, an S-BVT architecture based on multi-band cost-effective DD-OFDM technology have been proposed and validated by simulations. We concluded that with the increase of the hops number (6 hops in total corresponding to a maximum length of 545 km considered), the impairments due to the fiber nonlinearities have been, in general, more relevant. These effects have been more pronounced for the bands closer to the optical carrier. Thus, multi-band DD-OFDM systems have tourned out to be a promising solution for flexi-metro/regional networks to reduce the number of optoelectronic resources and support the multiple low bit-rate connections.

In **chapter 4**, we have introduced the filter narrowing effect in the context of flexi-grid optical aggregation networks. The filter narrowing effect has been analyzed for different systems: legacy OOK and advanced transmission technique based on DD-OFDM technologies with adaptive capabilities. As a first step the filter narrowing effect has been studied by simulations. We have analyzed the concatenation of 2 up to 12 filters (2 filters per node) considering slots of 50 GHz and 25 GHz and the concatenation of 2 up to 4 filters considering slots of 12.5 GHz. We have demonstrated that OFDM has been a feasible candidate for transceiver implementation, in the context of flexi-grid networks. The highest penalties have been observed for a filter bandwidth of 12.5 GHz. For two elementary slots (filter bandwidth of 25 GHz) the penalties were limited obtaining the best results for adaptive DD-OFDM technology.

This effect has also been evaluated experimentally. To this end, we have characterized the programmable filters and set up the programmable filters with the obtained characterization to emulate the filter concatenation of 2 up to 12 filters (considering 2 filters per node). The experimental setups for the OOK and the advanced transmission technique based on DD-OFDM technology with adaptive capabilities have been presented for the concatenation of filters with nominal bandwidths of 50 GHz, 25 GHz and 12.5 GHz. The performance degradation has been more pronounced for the DD-OFDM case but, unlike to OOK, it offered flexibility, adaptability and programmability that were important requirements for the envisioned optical networks. Furthermore, OFDM avoided the need of dispersion compensation modules at the networks nodes that in OOK systems

were required.

According to the simulations and the experimental results we concluded that adaptive DD-OFDM system has proved to be a feasible candidate to cope with the flexible and adaptive requirements that a flexi-grid mesh involves.

In **chapter 5**, requirements envisioned for future optical metro networks such as cost-efficiency and reduced power consumption have been addressed with flexible, adaptive and programmable transmission and switching systems to efficiently manage the available resources. Particularly, we have proposed the combination of programmable adaptive BVT based on OFDM using DMT modulation adopting SOA-based switching nodes. We have experimentally assessed the system considering two scenarios: with and without considering filtering elements. The maximum transmission distance was 75 km considering 27 Gb/s connections including 3 SOAs without filtering elements and 50 km for a bit rate of 26 Gb/s including 2 OAD nodes.

We concluded that SOA technology has resulted in a suitable solution for optical switching thanks to the possibility of controlling the current injected allowing to face transmission impairments. Further capacity, adaptability and resilience towards transmission impairments were obtained when the SOAs were combined with bit and power loading algorithms implemented in the transceiver DSP module. However, despite the possibility to compensate the losses, the introduction of WDM elements, splitters/combiners or SOAs degraded the OSNR due to the noise accumulation of the different components, limiting the maximum transmission reach. In order to increase the attainable distance, different setup could be exploited using either, DD with SSB or CO detection.

In **chapter 6**, multidimensional constellation implementations at the BVT DSP modules combined with CO detection have been considered to increase the data rate and transmission reach with respect to the DD option. Two advanced transmission systems based on CO-OFDM technology and DPQPSK constellation format have been analysed. One of them used the time dimension in order to transmit the signal in the optical domain, which was called TD-DPQPSK, and in the polarization domain named PD-DPQPSK.

We concluded that TD-DPQPSK constellation format have tourned out to be an appropriate solution for an efficient use of the network resources, since it was less affected by the fiber nonlinearities than PD-DPQPSK and its behavior was similar to conventional 4QAM for the same net symbol rate of 10 Gbaud/s. Hence, multidimensional constellation combined with CO detection could be a promising solution for flexi-grid scenario in order to overcome the impairments due to the fiber nonlinearities, increasing the attainable distance and the data rate.

7.2 Future work

The main lines of investigation to continue the work performed in this dissertation are summarized in the following points:

- In order to further optimize the multi-band system and take advantage of the deployed infrastructure, we can propose the transmission over the polarization domain. Thus, the multi-band signal can be transmitted through the horizontal and the vertical polarization doubling the capacity of the system.

- PSQPSK and 6P-QPSK constellations could be implemented at the DSP modules for advanced transmission systems based on CO-OFDM. Both systems could be evaluated and compared with CO-OFDM based on DPQPSK and/or conventional 4-QAM for the transmission over the time or the polarization dimensions. Comparative results could be achieved in terms of transmission reach and supported data rate.

- Future investigations could include loading algorithms considering the multidimensional constellations mentioned above to further increase the CO-OFDM system performance. Furthemore, CO-OFDM transmission systems with loading functionalities could be assessed combined with SOA technology with and without filtering elements in order to compare with the DMT with DD transmission scheme proposed. Promising solutions could be obtained in terms of flexibility, programmability, cost-efficiency, capacity and scalability for the future challenges in optical networks. In this case, the complexity of the DSP modules and the cost of the optoelectronic front-ends will increase. In contrast, the transmission distance, the exploitation of the deployed resources and the system capacity will be enhanced.

- An alternative investigation line is based on space dimension, providing high data rate transmission using several fiber modes or cores. However, the infrastructure currently deployed would have to be replaced, with the consequent cost increase. DD-OFDM or CO-OFDM transmission systems considering the polarization dimension, loading algorithms or multidimensional constellation formats could be also implemented for these MCF or FMF in order to increase the spectral efficiency, flexibility and transmission distances.

- Finally, as the target scenario is flexi-grid metro/regional network, the multi-adaptive optical transceivers based on OFDM technology, proposed in this thesis, could be experimentally validated (e. g. in the CTTC ADRENALINE testbed).

Bibliography

[1] CISCO, "The zettabyte era: Trends and analysis," June 2017.

[2] K. Schuh, F. Buchali, W. Idler, T. A. Eriksson, L. Schmalen, W. Templ, L. Altenhain, U. Dümler, R. Schmid, M. Müller, and K. Engenhardt, "Single carrier 1.2 Tbit/s transmission over 300 km with PM-64 QAM at 100 GBaud," in *Optical Fiber Communications Conference and Exhibition (OFC)*, March 2017, pp. 1–3.

[3] V. López and L. Velasco, *Elastic Optical Networks: Architectures, Technologies, and Control*, 1st ed., ser. Optical Networks. Springer International Publishing, 2016.

[4] M. S. Moreolo, J. M. Fàbrega, L. Nadal, F. J. Vílchez, A. Mayoral, R. Vilalta, R. Munoz, R. Casellas, R. Martínez, M. Nishihara, T. Tanaka, T. Takahara, J. C. Rasmussen, C. Kottke, M. Schlosser, R. Freund, F. Meng, S. Yan, G. Zervas, D. Simeonidou, Y. Yoshida, and K. I. Kitayama, "SDN-enabled sliceable BVT based on multicarrier technology for multiflow rate/distance and grid adaptation," *Journal of Lightwave Technology*, vol. 34, no. 6, pp. 1516–1522, March 2016.

[5] N. Sambo, P. Castoldi, A. D'Errico, E. Riccardi, A. Pagano, M. S. Moreolo, J. M. Fàbrega, D. Rafique, A. Napoli, S. Frigerio, E. H. Salas, G. Zervas, M. Nolle, J. K. Fischer, A. Lord, and J. P. F. P. Giménez, "Next generation sliceable bandwidth variable transponders," *IEEE Communications Magazine*, vol. 53, no. 2, pp. 163–171, Feb 2015.

[6] B. A. A. Nunes, M. Mendonca, X. N. Nguyen, K. Obraczka, and T. Turletti, "A survey of software-defined networking: past, present, and future of programmable networks," *IEEE Communications Surveys Tutorials*, vol. 16, no. 3, pp. 1617–1634, Feb, 2014.

[7] W. Shieh and I. Djordjevic, *OFDM for Optical Communications*. USA: Elsevier, 2010.

[8] L. Nadal, M. S. Moreolo, J. M. Fàbrega, A. Dochhan, H. Grieber, M. Eiselt, and J. P. Elbers, "DMT modulation with adaptive loading for high bit rate transmission over directly detected optical channels," *Journal of Lightwave Technology*, vol. 32, no. 21, pp. 4143–4153, Nov 2014.

[9] M. S. Moreolo, J. M. Fàbrega, L. Nadal, F. J. Vílchez, V. López, and J. P. Fernández-Palacios, "Cost-effective data plane solutions based on OFDM technology for flexi-grid metro networks using sliceable bandwidth variable transponders," in *2014 International Conference on Optical Network Design and Modeling*, May 2014, pp. 281–286.

[10] "Spectral grids for WDM applications: DWDM frequency grid, ITU-T Recommendation G.694.1," Feb 2012.

[11] A. Morea, J. Renaudier, T. Zami, A. Ghazisaeidi, and O. Bertran-Pardo, "Throughput comparison between 50-GHz and 37.5-GHz grid transparent networks [Invited]," *IEEE/OSA Journal of Optical Communications and Networking*, vol. 7, no. 2, pp. A293–A300, Feb 2015.

[12] T. Zami, "Current and future flexible wavelength routing cross-connects," *Bell Labs Technical Journal*, vol. 18, no. 3, pp. 23–38, Dec 2013.

[13] J. M. Fàbrega, M. S. Moreolo, L. Martín, A. C. Piat, E. Riccardi, D. Roccato, N. Sambo, F. Cugini, L. Potì, S. Yan, E. Hugues-Salas, D. Simeonidou, M. Gunkel, R. Palmer, S. Fedderwitz, D. Rafique, T. Rahman, H. de Waardt, and A. Napoli, "On the filter narrowing issues in elastic optical networks," *Journal of Optical Communication Networks*, vol. 8, no. 7, pp. A23–A33, Jul 2016.

[14] P. Winzer, "Spatial multiplexing in fiber optics: the 10X scaling of metro/core capacities," *Bell Labs Technical Journal*, vol. 19, pp. 22–30, 2014.

[15] R. Essiambre, G. Kramer, P. Winzer, G. Foschini, and B. Goebel, "Capacity limits of optical fiber networks," *Journal of Lightwave Technology*, vol. 28, no. 4, pp. 662–701, Feb 2010.

[16] D. Donald and B. K. Corning, "Optical fiber spans 30 years," 2000.

[17] "Charles kao nobel prize," 1999.

[18] M. Al-Amri, M. El-Gomati, and M. Zubairy, *Optics in Our Time*. Springer International Publishing, 2016.

[19] G. P. Agrawal, *Fiber-optic communication systems*. The Institute of Optics University of Rochester Rochester: NY: Wiley-Interscience John Wiley and Sons, Inc., 2002.

[20] A. Napoli, M. Bohn, D. Rafique, A. Stavdas, N. Sambo, L. Poti, M. Nolle, J. K. Fischer, E. Riccardi, A. Pagano, A. D. Giglio, M. S. Moreolo, J. M. Fàbrega, E. Hugues-Salas, G. Zervas, D. Simeonidou, P. Layec, A. D'Errico, T. Rahman, and J. P. F. P. Giménez, "Next generation elastic optical networks: The vision of the European research project IDEALIST," *IEEE Communications Magazine*, vol. 53, no. 2, pp. 152–162, Feb 2015.

[21] S. Sezer, S. Scott-Hayward, P. K. Chouhan, B. Fraser, D. Lake, J. Finnegan, N. Viljoen, M. Miller, and N. Rao, "Are we ready for SDN? Implementation challenges for software-defined networks," *IEEE Communications Magazine*, vol. 51, no. 7, pp. 36–43, July 2013.

[22] D. Kreutz, F. M. V. Ramos, P. E. Veríssimo, C. E. Rothenberg, S. Azodolmolky, and S. Uhlig, "Software-defined networking: a comprehensive survey," *Proceedings of the IEEE*, vol. 103, no. 1, pp. 14–76, Jan 2015.

[23] O. N. Fundation, "Software-defined networking: the new norm for networks, white paper ," 2012. [Online]. Available: https://www.opennetworking.org

[24] G. Bosco, A. Carena, V. Curri, P. Poggiolini, and F. Forghieri, "Performance limits of Nyquist-WDM and CO-OFDM in high-speed PM-QPSK systems," *IEEE Photonics Technology Letters*, vol. 22, no. 15, pp. 1129–1131, Aug 2010.

[25] A. Barbieri, D. Fertonani, and G. Colavolpe, "Time-frequency packing for linear modulations: spectral efficiency and practical detection schemes," *IEEE Transactions on Communications*, vol. 57, no. 10, pp. 2951–2959, Oct 2009.

[26] "ITU-T Recommendation G.975.1," 2004.

[27] S. Poole, S. Frisken, M. Roelens, and C. Cameron, "Bandwidth-flexible ROADMs as network elements," in *2011 Optical Fiber Communication Conference and Exposition and the National Fiber Optic Engineers Conference*, March 2011, pp. 1–3.

[28] M. Doelz, E. Heald, and D. Martin, "Binary data transmission techniques for linear systems," *Proceedings of the IRE*, vol. 45, no. 5, pp. 656–661, May 1957.

[29] J. Bingham, "Multicarrier modulation for data transmission: an idea whose time has come," *IEEE Communications Magazine*, vol. 28, no. 5, pp. 5–14, May 1990.

[30] R. W. Chang, "Synthesis of band-limited orthogonal signals multichannel data transmission," *The Bell System Technical Journal*, pp. 1775–1796, Dec 1966.

[31] J. Leonard, J.Cimini, "Analysis and simulation of a digital mobile channel using orthogonal frequency division multiplexing," *IEEE Transactions Communications*, vol. 33, no. 7, pp. 665–675, Jul 1985.

[32] J. Armstrong, "OFDM for optical communications," *Journal of Lightwave Technology*, pp. 189–204, Feb 2009.

[33] U. Reimers, "Digital video broadcasting," *IEEE Communications Magazine*, vol. 36, no. 6, pp. 104–110, Jun 1998.

[34] Q. Pan and R. J. Green, "Bit-Error-Rate performance of ligthwave hybrid AM/OFDM systems with comparison with AM/QAM systems in presence of clipping impulse noise," *IEEE Communications Magazine*, vol. 8, pp. 278–280, Jun 1998.

[35] B. Dixon, R. D. Pollard, and S. Iezekiel, "Orthogonal frequency division multiplexing in wireless communication systems with multimode fibre feeds," *IEEE Radio and Wireless Conference, RAWCON*, pp. 79–82, 2000.

[36] L. Nadal, M. Svaluto Moreolo, J. M. Fàbrega, and G. Junyent, "Comparison of peak power reduction techniques in optical OFDM systems based on FFT and FHT," *International Conference on Transparent Optical Networks, (ICTON)*, pp. 1–4, June 2011.

[37] L. Nadal, M. Svaluto Moreolo, J. M. Fàbrega and G. Junyent, "Clipping and quantization noise mitigation in intensity-modulated direct detection O-OFDM systems based on the FHT," *International Conference on Transparent Optical Networks, (ICTON)*, pp. 1–4, July 2012.

[38] E. Vanin, "Performance evaluation of intensity modulated optical OFDM system with digital baseband distortion," *Optics Express*, vol. 19, no. 5, pp. 4280–4293, Feb 2011.

[39] S. L. Jansen, I. Morita, T. C. W. Schenk, N. Takeda, and H. Tanaka, "Coherent optical 25.8-Gb/s OFDM transmission over 4160-km SSMF," *Journal of Lightwave Technology*, vol. 26, no. 1, pp. 6–15, Jan 2008.

[40] J. Leibrich, A. Ali, H. Paul, W. Rosenkranz, and K. Kammeyer, "Impact of modulator bias on the OSNR requirement of direct-detection optical OFDM," *IEEE Photonics Technology Letters*, vol. 21, no. 15, pp. 1033–1035, Aug 2009.

[41] B. Schmidt, A. Lowery, and J. Armstrong, "Experimental demonstrations of electronic dispersion compensation for long-haul transmission using direct-detection optical OFDM," *Journal of Lightwave Technology*, vol. 26, no. 1, pp. 196–203, Jan 2008.

[42] M. Moreolo, R. Munoz, and G. Junyent, "Novel power efficient optical OFDM based on Hartley transform for intensity-modulated direct-detection systems," *Journal of Lightwave Technology*, vol. 28, no. 5, pp. 798–805, March 2010.

[43] M. Svaluto Moreolo, "Performance analysis of DHT-based optical OFDM using large-size constellations in AWGN," *IEEE Communications Letters*, vol. 15, no. 5, pp. 572–574, May 2011.

[44] R. Shieh and C. Athaudage, "Coherent optical orthogonal frequency division multiplexing," *Electronics Letters*, vol. 42, pp. 587–589, 2006.

[45] W. Shieh, X. Yi, Y. Ma, and Y. Tang, "Theoretical and experimental study on PMD-supported transmission using polarization diversity in coherent optical OFDM systems," *Opt. Express*, vol. 15, no. 16, pp. 9936–9947, Aug 2007.

[46] S. Okamoto, K. Toyoda, T. Omiya, K. Kasai, M. Yoshida, and M. Nakazawa, "512 QAM (54 Gbit/s) coherent optical transmission over 150 km with an optical bandwidth of 4.1 GHz," *2010 36th European Conference and Exhibition on Optical Communication (ECOC)*, pp. 1–3, Sept 2010.

[47] M. Nakazawa, S. Okamoto, T. Omiya, K. Kasai, and M. Yoshida, "256-QAM (64 Gb/s) coherent optical transmission over 160 km with an optical bandwidth of 5.4 GHz," *IEEE Photonics Technology Letters*, vol. 22, no. 3, pp. 185–187, Feb 2010.

[48] A. Gnauck, P. Winzer, A. Konczykowska, F. Jorge, J. Dupuy, M. Riet, G. Charlet, B. Zhu, and D. Peckham, "Generation and transmission of 21.4-Gbaud PDM 64-QAM using a novel high-power DAC driving a single I/Q modulator," *Journal of Lightwave Technology*, vol. 30, no. 4, pp. 532–536, Feb 2012.

[49] G. Raybon, S. Randel, A. Adamiecki, P. Winzer, L. Salamanca, R. Urbanke, S. Chandrasekhar, A. Konczykowska, F. Jorge, J. Dupuy, L. Buhl, S. Draving, M. Grove, and K. Rush, "1-Tb/s dual-carrier 80-GBaud PDM-16QAM WDM transmission at 5.2 b/s/Hz over 3200 km," *IEEE Photonics Conference (IPC)*, pp. 1–2, Sept 2012.

[50] G. Raybon, A. Adamiecki, P. Winzer, S. Randel, L. Salamanca, A. Konczykowska, F. Jorge, J.-Y. Dupuy, L. Buhl, S. Chandrashekhar, C. Xie, S. Draving, M. Grove, K. Rush, and R. Urbanke, "High symbol rate coherent optical transmission systems: 80 and 107 Gbaud," *Journal of Lightwave Technology*, vol. 32, no. 4, pp. 824–831, Feb 2014.

[51] E. Agrell and M. Karlsson, "Power-efficient modulation formats in coherent transmission systems," *Journal of Lightwave Technology*, vol. 27, no. 22, pp. 5115–5126, Nov 2009.

[52] A. D. Shiner, M. Reimer, A. Borowiec, S. O. Gharan, J. Gaudette, P. Mehta, D. Charlton, K. Roberts, and M. O'Sullivan, "Demonstration of an 8-dimensional

modulation format with reduced inter-channel nonlinearities in a polarization multiplexed coherent system," *Opt. Express*, vol. 22, no. 17, pp. 20 366–20 374, Aug 2014.

[53] J. Cioffi. Data transmission theory. (in Course Text for EE379A-B and EE479, Stanford, CA, USA: Stanford Univ., ch. 4. (2013)). [Online]. Available: www.stanford.edu/group/cioffi/book/

[54] R. Hui, B. Zhu, R. Huang, C. T. Allen, K. R. Demarest, and D. Richards, "Subcarrier multiplexing for high-speed optical transmission," *Journal of Lightwave Technology*, vol. 20, no. 3, pp. 417–427, Mar 2002.

[55] M. S. Moreolo, J. M. Fàbrega, L. Martín, K. Christodoulopoulos, E. Varvarigos, and J. P. Fernández-Palacios, "Flexgrid technologies enabling BRAS centralization in MANs," *IEEE/OSA Journal of Optical Communications and Networking*, vol. 8, no. 7, pp. A64–A75, July 2016.

[56] S. L. Jansen, I. Morita, T. W. Schenk, and H. Tanaka, "121.9-Gb/s PDM-OFDM transmission with 2-b/s/Hz spectral efficiency over 1000 km of SSMF," *Journal of Lightwave Technology*, vol. 27, no. 3, pp. 177–188, Feb 2009.

[57] E. Pincemin, M. Song, J. Karaki, O. Zia-Chahabi, T. Guillossou, D. Grot, G. Thouenon, C. Betoule, R. Clavier, A. Poudoulec, M. V. der Keur, Y. Jaoeen, R. L. Bidan, T. L. Gall, P. Gravey, M. Morvan, B. Dumas-Feris, M. L. Moulinard, and G. Froc, "Multi-band OFDM transmission at 100 Gbps with sub-band optical switching," *Journal of Lightwave Technology*, vol. 32, no. 12, pp. 2202–2219, June 2014.

[58] W. R. Peng, I. Morita, H. Takahashi, and T. Tsuritani, "Transmission of high-speed (100 Gb/s) direct-detection optical OFDM superchannel," *Journal of Lightwave Technology*, vol. 30, no. 12, pp. 2025–2034, Jun 2012.

[59] K. M. Feng, J. H. Yan, Y. W. Chang, and F. L. Cheng, "A novel double-sided multiband direct-detection optical OFDM system with single laser source," in *Conference on Lasers and Electro-Optics, (CLEO)*, May 2012, p. CF1F.5.

[60] L. Nadal, M. S. Moreolo, J. M. Fàbrega, and F. J. Vílchez, "Meeting the future metro network challenges and requirements by adopting programmable S-BVT with direct-detection and PDM functionality," *Optical Fiber Technology*, vol. 36, pp. 344 – 352, 2017.

[61] D. van den Borne, N. Hecker-Denschlag, G. Khoe, and H. de Waardt, "PMD-induced transmission penalties in polarization-multiplexed transmission," *Journal of Lightwave Technology*, vol. 23, no. 12, pp. 4004–4015, Dec 2005.

[62] N. Cvijetic, N. Prasad, M. Cvijetic, and T. Wang, "Efficient and robust MIMO DSP equalization in POLMUX OFDM transmission with direct detection," in *37th European Conference and Exhibition on Optical Communication*, Sept 2011, pp. 1–3.

[63] X. Zhou, K. Zhong, Y. Gao, Q. Sui, Z. Dong, J. Yuan, L. Wang, K. Long, A. P. T. Lau, and C. Lu, "Polarization-interleave-multiplexed discrete multi-tone modulation with direct detection utilizing MIMO equalization," *Opt. Express*, vol. 23, no. 7, pp. 8409–8421, Apr 2015.

[64] M. Yagi, S. Satomi, and S. Ryu, "Field trial of 160-Gbit/s, polarization-division multiplexed RZ-DQPSK transmission system using automatic polarization control," in *OFC/NFOEC Conference on Optical Fiber Communication/National Fiber Optic Engineers Conference*, Feb 2008, pp. 1–3.

[65] D. Qian, N. Cvijetic, J. Hu, and T. Wang, "40-Gb/s MIMO-OFDM-PON using polarization multiplexing and direct-detection," pp. 1–3, March 2009.

[66] B. Lin, J. Li, Y. He, and Z. Chen, "Performance study of 40-Gb/s OFDM-PON based on polarization interleaving," *Opto-Electronics and Communications Conference, (OECC)*, pp. 136–137, July 2012.

[67] D. v. d. Borne, T. Duthel, C. R. S. Fludger, E. D. Schmidt, T. Wuth, C. Schulien, E. Gottwald, G. D. Khoe, and H. d. Waardt, "Electrical PMD compensation in 43-Gb/s POLMUX-NRZ-DQPSK enabled by coherent detection and equalization," *European Conference and Ehxibition of Optical Communication, (ECOC)*, pp. 1–4, Sept 2007.

[68] H. Weber, S. Ferber, M. Kroh, C. Schmidt-Langhorst, R. Ludwig, V. Marembert, C. Boerner, F. Futami, S. Watanabe, and C. Schubert, "Single channel 1.28 Tbit/s and 2.56 Tbit/s DQPSK transmission," *European Conference on Optical Communication, (ECOC)*, vol. 6, pp. 3–4, Sept 2005.

[69] H. C. H. Mulvad, M. Galili, L. K. Oxenløwe, H. Hu, A. T. Clausen, J. B. Jensen, C. Peucheret, and P. Jeppesen, "Demonstration of 5.1 Tbit/s data capacity on a single-wavelength channel," *Optical Express*, vol. 18, no. 2, pp. 1438–1443, Jan 2010.

[70] E. Lach and K. Schuh, "Recent advances in ultrahigh bit rate ETDM transmission systems," *Journal of Lightwave Technology*, vol. 24, no. 12, pp. 4455–4467, Dec 2006.

[71] W. Lee, V. Filsinger, L. Klapproth, H. Bach, and A. Beling, "Implementation of an 80 Gbit/s full ETDM multi-format ASK optical transmitter," *European Conference on Optical Communication,(ECOC)*, vol. 3, pp. 383–384 vol.3, Sept 2005.

[72] G. Raybon, P. Winzer, and C. Doerr, "1-Tb/s (10 times;107 Gb/s) Electronically multiplexed optical signal generation and WDM transmission," *Journal of Lightwave Technology*, vol. 25, no. 1, pp. 233–238, Jan 2007.

[73] P. Winzer, G. Raybon, C. Doerr, M. Duelk, and C. Dorrer, "107-gb/s optical signal generation using electronic time-division multiplexing," *Journal of Lightwave Technology*, vol. 24, no. 8, pp. 3107–3113, Aug 2006.

[74] A. Lowery, L. B. Du, and J. Armstrong, "Performance of optical OFDM in ultralong-haul WDM lightwave systems," *Journal of Lightwave Technology*, vol. 25, no. 1, pp. 131–138, Jan 2007.

[75] A. Lowery, L. Du, and J. Armstrong, "Orthogonal Frequency Division Multiplexing for adaptive dispersion compensation in long haul WDM systems," pp. 1–3, March 2006.

[76] J. Richardson, J. M. Fini, and L. E. Nelson, "Space-division multiplexing in optical fibres," *Nature Photonics*, vol. 7, pp. 354–362, May 2013.

[77] A. Sano, H. Takara, T. Kobayashi, and Y. Miyamoto, "Crosstalk-managed high capacity long haul multicore fiber transmission with propagation-direction interleaving," *Journal of Lightwave Technology*, vol. 32, no. 16, pp. 2771–2779, Aug 2014.

[78] J. Sakaguchi, B. Puttnam, W. Klaus, Y. Awaji, N. Wada, A. Kanno, T. Kawanishi, K. Imamura, H. Inaba, K. Mukasa, R. Sugizaki, T. Kobayashi, and M. Watanabe, "19-core fiber transmission of 19x100x172-GB/s SDM-WDM-PDM-QPSK signals at 305Tb/s," pp. 1–3, March 2012.

[79] S. Randel, R. Ryf, A. Gnauck, M. Mestre, C. Schmidt, R. Essiambre, P. Winzer, R. Delbue, P. Pupalaikis, A. Sureka, Y. Sun, X. Jiang, and R. Lingle, "Mode-multiplexed 6x20-GBd QPSK transmission over 1200-km DGD-compensated few-mode fiber," *Optical Fiber Communication Conference and Exhibition/National Fiber Optic Engineers Conference, (OFC/NFOEC)*, pp. 1–3, March 2012.

[80] Y. Sasaki, K. Takenaga, S. Matsuo, K. Aikawa, and K. Saitoh, "Few-mode multi-core fibers for long-haul transmission line," *Optical Fiber Technology*, vol. 35, pp. 19 – 27, 2017.

[81] A. Al Amin, H. Takahashi, I. Morita, and H. Tanaka, "100-Gb/s Direct-Detection OFDM transmission on independent polarization tributaries," *IEEE Photonics Technology Letters*, vol. 22, no. 7, pp. 468–470, April 2010.

[82] T. Alves and A. Cartaxo, "Transmission of multiband OFDM-UWB signals along LR-PONs employing a mach-zehnder modulator biased at the quasi-minimum

power transmission point," *Journal of Lightwave Technology*, vol. 30, no. 11, pp. 1587–1594, June 2012.

[83] P. E. D. Cruz, T. M. F. Alves, and A. V. T. Cartaxo, "Theoretical analysis of the four-wave mixing effect in virtual carrier-assisted DD MB-OFDM ultradense WDM metropolitan networks," *Journal of Lightwave Technology*, vol. 34, no. 23, pp. 5401–5411, Dec 2016.

[84] T. M. F. Alves, L. M. M. Mendes, and A. V. T. Cartaxo, "High granularity multi-band OFDM virtual carrier-assisted direct-detection metro networks," *Journal of Lightwave Technology*, vol. 33, no. 1, pp. 42–54, Jan 2015.

[85] M. Svaluto Moreolo, J. Fàbrega, F. Vílchez, K. Christodoulopoulos, E. Varvarigos, V. López, and J. Fernández-Palacios, "Assessment of flexgrid technologies in the MAN for centralized BRAS architecture using S-BVT," in *2014 European Conference on Optical Communication, (ECOC)*, Sept 2014, p. P.6.9.

[86] M. Svaluto Moreolo, J. Fàbrega, F. Vílchez, L. Nadal, V. López, and G. Junyent, "Experimental validation of an elastic low-complex OFDM-based BVT for flexi-grid metro networks," in *39th European Conference and Exhibition on Optical Communication, (ECOC 2013)*, Sept 2013, p. We.1.E.5.

[87] C.-T. Lin, J. J. Chen, S.-P. Dai, P.-C. Peng, and S. Chi, "Impact of nonlinear transfer function and imperfect splitting ratio of MZM on optical up-conversion employing double sideband with carrier suppression modulation," *Journal of Lightwave Technology*, vol. 26, no. 15, pp. 2449–2459, 2008.

[88] A. Ali, J. Leibrich, and W. Rosenkranz, "Spectral efficiency and receiver sensitivity in direct detection optical-OFDM," in *Conference on Optical Fiber Communication, (OFC)*, March 2009, p. OMT7.

[89] Thor labs. 10 GHz Intensity Modulators, 2012. [Online]. Available: https://www.thorlabs.com/catalogpages/V21/1203.PDF

[90] S. Jansen, "OFDM for Optical Communications," in *Optical Fiber Communications Conference*, April 2012.

[91] I. A. S. M. Abramowitz, *Handbook of Mathematical Functions.* USA: Dover publications, 1972.

[92] J. D. Downie, I. Tomkos, N. Antoniades, and A. Boskovic, "Effects of filter concatenation for directly modulated transmission lasers at 2.5 and 10 Gb/s," *Journal of Lightwave Technology*, vol. 20, no. 2, pp. 218–228, Feb 2002.

[93] C. Pulikkaseril, L. A. Stewart, M. A. F. Roelens, G. W. Baxter, S. Poole, and S. Frisken, "Spectral modeling of channel band shapes in wavelength selective switches," *Optical Express*, vol. 19, no. 9, pp. 8458–8470, Apr 2011.

[94] "ITU-T Rec. G.975:Forward error Correction," 2006.

[95] K. Onohara, T. Sugihara, Y. Miyata, K. Sugihara, K. Kubo, H. Yoshida, K. Koguchi, and T. Mizuochi, "Soft-decision forward error correction for 100Gb/s digital coherent systems," *Optical Fiber Technology*, vol. 17, no. 5, pp. 452 – 455, 2011, 100G and Beyond.

[96] R. Casellas, J. M. Fàbrega, R. Munoz, L. N. Reixats, R. Vilalta, M. S. Moreolo, and R. Martinez, "On-demand allocation of control plane functions via SDN/NFV for monitoring-enabled flexi-grid optical networks with programmable BVTs," in *ECOC 2016; 42nd European Conference on Optical Communication*, Sept 2016, pp. 1–3.

[97] N. Calabretta, W. Miao, K. Mekonnen, and K. Prifti, "SOA based photonic integrated WDM cross-connects for optical metro-access networks," *Applied Sciences*, vol. 9, no. 7, p. 865, 2017.

[98] S. Singh, A. Singh, and R. Kaler, "Performance evaluation of EDFA, RAMAN and SOA optical amplifier for WDM systems," *Optik - international journal for light and electron optics*, vol. 124, no. 2, pp. 95–101, 2013.

[99] J. Renaudier, A. C. Meseguer, A. Ghazisaeidi, P. Tran, R. R. Muller, R. Brenot, A. Verdier, F. Blache, K. Mekhazni, B. Duval, H. Debregeas, M. Achouche, A. Boutin, F. Morin, L. Letteron, N. Fontaine, Y. Frignac, and G. Charlet, "First 100-nm continuous-band WDM transmission system with 115Tb/s transport over 100km using novel ultra-wideband semiconductor optical amplifiers," in *2017 European Conference on Optical Communication (ECOC)*, Sept 2017, pp. 1–3.

[100] T. S. E. Bawab, *Optical switching*. USA: Springer, 2010.

[101] K. E. Stubkjaer, "Semiconductor optical amplifier-based all-optical gates for high-speed optical processing," *IEEE Journal of Selected Topics in Quantum Electronics*, vol. 6, no. 6, pp. 1428–1435, Nov 2000.

[102] C. Tremblay, É. Archambault, M. P. Bélanger, J.-P. Savoie, F. Gagnon, and D. V. Plant, "Passive filterless core networks based on advanced modulation and electrical compensation technologies," *Telecommunication Systems*, vol. 54, no. 2, pp. 167–181, Oct 2013.

[103] T. Shoresh, N. Katanov, and D. Malka, "1X4 MMI visible light wavelength demultiplexer based on a GaN slot-waveguide structure," *Photonics and Nanostructures - Fundamentals and Applications*, vol. 30, pp. 45–49, 2018.

[104] B. B. Ben Zaken, T. Zanzury, and D. Malka, "An 8 channel wavelength MMI demultiplexer in slot waveguide structures," *Materials*, vol. 9, no. 11, 2016.

[105] N. Calabretta, W. Miao, K. Prifti, and K. Williams, "System performance assessment of a monolithically integrated WDM cross-connect switch for optical data centre networks," in *ECOC 2016; 42nd European Conference on Optical Communication*, Sept 2016, pp. 1–3.

[106] M. S. Moreolo, J. M. Fàbrega, and L. N. Reixats, "S-BVT for next-generation optical metro networks: benefits, design and key enabling technologies," Jan. 2017. [Online]. Available: https://doi.org/10.1117/12.2250326

[107] W. Miao, H. de Waardt, and N. Calabretta, "Optical label switching add-drop multiplexer for high-performance metro networks," *IEEE Photonics Technology Letters*, vol. 28, no. 10, pp. 1065–1068, May 2016.

[108] K. Morito, "Output-level control of semiconductor optical amplifier by external light injection," *Journal of Lightwave Technology*, vol. 23, no. 12, pp. 4332–4341, Dec 2005.

[109] D. Pilori, C. Fludger, and R. Gaudino, "Comparing DMT variants in medium-reach 100G optically amplified systems," *Journal of Lightwave Technology*, vol. 34, no. 14, pp. 3389–3399, July 2016.

[110] J. M. Fàbrega, P. Sevillano, M. S. Moreolo, A. Villafranca, F. J. Vìlchez, and J. M. Subìas, "OFDM subcarrier monitoring using high resolution optical spectrum analysis," *Optics Communications*, vol. 342, pp. 144 – 151, 2015.

[111] L. Nadal, M. S. Moreolo, J. M. Fàbrega, R. Casellas, F. J. Vílchez, R. Martínez, R. Vilalta, and R. Munoz, "Programmable SDN-enabled S-BVT based on hybrid electro-optical MCM," *IEEE/OSA Journal of Optical Communications and Networking*, vol. 10, no. 6, pp. 593–602, June 2018.

[112] M. Karlsson and E. Agrell, "Which is the most power-efficient modulation format in optical links?" *Opt. Express*, vol. 17, no. 13, pp. 10 814–10 819, Jun 2009.

[113] S. Hussin, K. Puntsri, and R. Noé, "Performance analysis of RF-pilot phase noise compensation techniques in coherent optical OFDM systems," pp. 1–5, June 2012.

[114] J. M. Fàbrega and M. S. Moreolo, "Multidimensional OFDM for programmable optical transceivers," in *2016 18th International Conference on Transparent Optical Networks (ICTON)*, July 2016, pp. 1–4.